Reports and Technical Reports	All Technical Reports Collection

1987-10-31

The analysis of multichannel two-dimensional random signals

Therrien, Charles W.

Monterey, California. Naval Postgraduate School

http://hdl.handle.net/10945/28851

NAVAL POSTGRADUATE SCHOOL
Monterey, California

TECHNICAL REPORT

THE ANALYSIS OF MULTICHANNEL
TWO-DIMENSIONAL RANDOM SIGNALS

Charles W. Therrien
31 October 1986

Approved for public release; distribution unlimited.

Naval Postgraduate School
Monterey, California

Rear Admiral R. C. Austin
Superintendent

D. A. Schrady
Provost

Reproduction of all or part of this report is authorized.

This report was prepared by:

REPORT DOCUMENTATION PAGE

1a REPORT SECURITY CLASSIFICATION Unclassified		1b RESTRICTIVE MARKINGS			
2a. SECURITY CLASSIFICATION AUTHORITY		3 DISTRIBUTION / AVAILABILITY OF REPORT Approved for public release; distribution unlimited			
2b DECLASSIFICATION / DOWNGRADING SCHEDULE					
4 PERFORMING ORGANIZATION REPORT NUMBER(S) NPS62-87-002		5 MONITORING ORGANIZATION REPORT NUMBER(S)			
6a NAME OF PERFORMING ORGANIZATION Naval Postgraduate School	6b OFFICE SYMBOL (If applicable)	7a NAME OF MONITORING ORGANIZATION			
6c. ADDRESS (City, State, and ZIP Code) Monterey, CA 93943		7b ADDRESS (City, State, and ZIP Code)			
8a NAME OF FUNDING / SPONSORING ORGANIZATION Chief of Naval Research	8b OFFICE SYMBOL (If applicable)	9 PROCUREMENT INSTRUMENT IDENTIFICATION NUMBER N0001486WR4E001			
8c ADDRESS (City, State, and ZIP Code) Arlington, VA 22217		10 SOURCE OF FUNDING NUMBERS			
		PROGRAM ELEMENT NO 61152N	PROJECT NO RR	TASK NO	WORK UNIT ACCESSION NO 000-01

11 TITLE (Include Security Classification)

The Analysis of Multichannel Two-Dimensional Random Signals

12 PERSONAL AUTHOR(S)
Charles W. Therrien

13a TYPE OF REPORT	13b TIME COVERED FROM 10/85 TO 10/86	14 DATE OF REPORT (Year, Month, Day) 1986, 10, 31	15 PAGE COUNT 98

16 SUPPLEMENTARY NOTATION

17 COSATI CODES			18 SUBJECT TERMS (Continue on reverse if necessary and identify by block number)
FIELD	GROUP	SUB-GROUP	Multi-dimensional signal processing, multichannel image processing, 2-D spectral analysis, two-dimensional linear prediction, 2-D AR Modeling.

19 ABSTRACT (Continue on reverse if necessary and identify by block number)
The analysis of multiple correlated two-dimensional (2D) random signals or multichannel 2-D signals is described. The emphasis is on estimation (linear prediction) and modeling of the 2-D random signals. Applications to spectrum analysis and image processing are considered.

20 DISTRIBUTION / AVAILABILITY OF ABSTRACT ☒ UNCLASSIFIED/UNLIMITED ☐ SAME AS RPT ☐ DTIC USERS	21 ABSTRACT SECURITY CLASSIFICATION Unclassified	
22a NAME OF RESPONSIBLE INDIVIDUAL C.W. Therrien	22b TELEPHONE (Include Area Code) (408) 646-3347	22c OFFICE SYMBOL

DD FORM 1473, 84 MAR
83 APR edition may be used until exhausted
All other editions are obsolete

SECURITY CLASSIFICATION OF THIS PAGE
Unclassified

Table of Contents

List of Figures

ABSTRACT

The analysis of multiple correlated two-dimensional (2-D) random signals or multichannel 2-D signals is described. The emphasis is on estimation (linear prediction) and modeling of the 2-D random signals. Applications to spectrum analysis and image processing are considered.

Acknowledgement

The author wishes to thank the people who contributed to this report. I especially want to thank my graduate students Hamdy El Shaer whose extensive work on spectrum estimation appears in Chapter IV and Mr. Timur Kupeli whose results on color image segmentation are given in Chapter V.

This report was prepared in T$_E$X. I want to thank our department secretary Mrs. Pat Allen for bringing the knowledge of T$_E$X into our office and for an excellent job in typing a difficult manuscript. I hope that someday we may all learn this document preparation language as well.

I. Introduction

This report deals with the analysis of multichannel two-dimensional (2-D) random signals. The signals are two-dimensional in that the signal is a function of two independent variables (n_1, n_2). We say the signals are multichannel since there are possibly *several* correlated 2-D signals, perhaps received on different communication channels that are processed and analyzed together.

One example of a multichannel 2-D signal is the set of images received from a satellite multispectral scanner. The satellite forms several images of the ground in pixel registration but corresponding to different frequency bands in the visible and infrared. One can have four, seven, or even more such channels comprising the multichannel data.

A more common example of a multichannel 2-D signal is a color image. The signal is inherently two-dimensional but consists of three registered components representing red, green and blue intensities or other tristimulus values such as those used in the NTSC video standard.

Other examples of multichannel 2-D signals can be found in linear arrays when the sensor measurements are inherently separated along certain channels (for example in-phase and quadrature, principal and orthogonal returns of a radar, and in the measurement of dual polarized radar cross section as a function of space and time for extended targets. In these examples one can easily imagine multichannel signals that are higher than two- dimensional.

Although the image processing community has long dealt with multiple correlated images, [see e.g. Ref. 1], this community has for the most part not approached the analysis from a signal processing point of view. A notable exception is the work by Hunt and Kubler [2] who seem to have been the first to apply signal-processing methods to multichannel image restoration. The signal processing community on the other hand has dealt with the analysis of multidimensional signals but has also largely ignored the analysis of *multiple* multidimensional signals. While multichannel 2-D signals can be regarded as a special case of 3-D signals, multichannel signals have their own special properties that makes their analysis distinct and in many cases more tractible than the analysis of 3-D signals in general. Therefore we have chosen to concentrate on these special signals and study their properties explicitly.

This report is primarily concerned with random multichannel 2-D signals and their applications. These signals will have properties sometimes similar to multichannel 1-D signals and sometimes more like 2-D signals. We will be concerned here mostly with topics related to filtering and estimation of these signals; and in particular linear prediction and its applications.

The remainder of this report is organized as follows. Chapter II deals with the rep-

resentation of multichannel 2-D signals and their statistical characterization. Chapter III focuses on linear prediction and autoregressive (AR) modeling. This forms a basis for the remainder of the material. Chapter IV discusses spectrum estimation. Model-based methods for estimating the entire spectral matrix are presented. The estimate includes the 2-D autospectrum for each channel and the magnitude and phase of the cross- spectra. Chapter V describes applications of the theory to image processing. Chapter IV provides a summary and conclusion. Areas for future work are cited there.

II. Statistical Characterization of Multichannel 2-D Random Processes

2.1 Representation of Multichannel 2-D Signals and Systems

2.1.1 Signal Domain Representation

Discrete multichannel 2-D signals (or sequences) will be represented by a vector quantity $\mathbf{x}(n_1, n_2)$ as illustrated in Fig. 2.1. Each component $x_\kappa(n_1, n_2)$ of the vector represents a 2-D signal existing in one of the channels. Note that the vector-valued nature of the <u>function</u> relates to the fact that the signal is <u>multichannel</u> while the vector nature of the argument $\underline{n} = (n_1, n_2)$ relates to the fact that the signal is <u>multidimensional</u>*

The processing of these signals is analogous to that for other discrete signals. We will be primarily concerned with linear shift-invariant (LSI) operations that can be represented by 2-D vector difference equations. In particular an M-Channel 2-D signal $\mathbf{x}(n_1, n_2)$ is transformed to another M-channel 2-D signal by an LSI system represented by the difference equation

$$\mathbf{y}(n_1, n_2) = -\sum_{\substack{(i_1,i_2)\in\alpha \\ (i_1,i_2)\neq(0,0)}} A_{i_1 i_2}\mathbf{y}(n_1 - i_1, n_2 - i_2) + \sum_{(\ell_1,\ell_2)\in\beta} B_{\ell_1 \ell_2}\mathbf{x}(n_1 - \ell_1, n_2 - \ell_2)$$

$$(2.1)$$

where the $A_{i_1 i_2}$ and $B_{\ell_1 \ell_2}$ are $M \times M$ matrix coefficients and α and β define their (fixed) regions of support. The system will be <u>recursively computable</u> if there exists an ordering for processing of the points such that values of the signal $\mathbf{y}$ needed to compute the signal's current value at the point (n_1, n_2) are always available. Whether such an ordering exists depends on the shape of the output region α.

The output for a multichannel 2-D system can be equivalently represented by the 2-D convolution operation in either of the forms

$$\mathbf{y}(n_1, n_2) = \sum_{\ell_1,\ell_2=-\infty,-\infty}^{\infty,\infty} H(\ell_1, \ell_2)\mathbf{x}(n_1, -\ell_1, n_2 - \ell_2) \qquad (2.2a)$$

$$\mathbf{y}(n_1, n_2) = \sum_{\ell_1 \ell_2=-\infty,-\infty}^{\infty,\infty} H(n_1 - \ell_1, n_2 - \ell_2)\mathbf{x}(\ell_1, \ell_2) \qquad (2.2b)$$

where $H(\cdot, \cdot)$ is a matrix function representing the 2-D multichannel impulse response. (Each term $H(\ell_1, \ell_2)$ in Eq. (2.2) is an $M \times M$ matrix.) A 2-D multichannel system

---

* Although it is tempting to use vector notation for the arguments, this tends to hide the essential 2-D nature of the signals. Therefore we use the longer but more explicit notation involving the two indices n_1 and n_2.
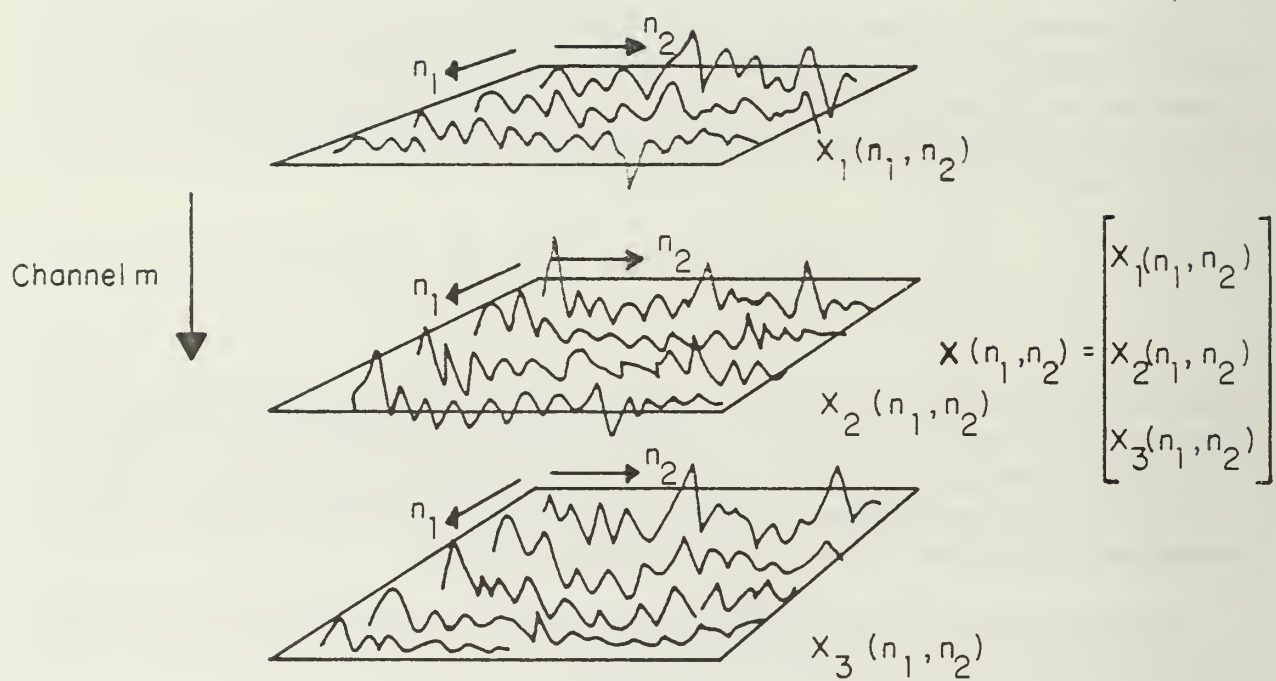
Figure 2.1   Discrete Multichannel 2-D Signal.

will be called a Finite Impulse Response (FIR) system if the support of $H(\ell, m)$ is finite and an Infinite Impulse Response (IIR) system otherwise. Clearly for an FIR system all of the $A_{i_1 i_2}$ in Eq. (2.1) are zero and $H(\ell_1, \ell_2) = B_{\ell_1 \ell_2}$ for $(\ell_1, \ell_2) \in \beta$.

For purposes of this report, we will be dealing with statistical properties of random signals. Thus the mean of a signal $\mathbf{x}(n_1, n_2)$ is a vector quantity defined by

$$\mathbf{m}_x(n_1, n_2) = E[\mathbf{x}(n_1, n_2)] \tag{2.3}$$

and the correlation and covariance are $M \times M$ matrix functions defined (respectively) by

$$R(n_1, n_2 \; ; \; m_1, m_2) = E\left[\mathbf{x}(n_1, n_2)\mathbf{x}^T(m_1, m_2)\right] \tag{2.4a}$$

$$C(n_1, n_2; m_1, m_2) = E\left[(\mathbf{x}(n_1, n_2) - \mathbf{m}_x(n_1, n_2))(\mathbf{x}(m_1, m_2) - \mathbf{m}_x(m_1, m_2))^T\right] \tag{2.4b}$$

When the random process representing the signal is homogenous or stationary the mean is constant and the correlation and covariance are functions only of the vector distance between the points (n_1, n_2) and (m_1, m_2). In this case Eqs. (2.3) and (2.4) become

$$\mathbf{m}_x = E\left[\mathbf{x}(n_1, n_2)\right] \tag{2.5}$$

and

$$R(k_1, k_2) = E\left[\mathbf{x}(n_1, n_2)\mathbf{x}^T(n_1 - k_1, n_2 - k_2)\right] \tag{2.6a}$$

$$C(k_1, k_2) = E\left[(\mathbf{x}(n_1, n_2) - \mathbf{m}_x)(\mathbf{x}(n_1 - k_1, n_2 - k_2) - \mathbf{m}_x)^T\right] \tag{2.6b}$$

It can be seen from their definition that the correlation and covariance functions have the following symmetry properties

$$R(k_1, k_2) = R^T(-k_1, -k_2) \tag{2.7a}$$

$$C(k_1, k_2) = C^T(-k_1, -k_2) \tag{2.7b}$$

When a stationary random signal is transformed by a linear shift-invariant system, the statistical characteristics of the output can be expressed in terms of those of the input by using Eqs. (2.1) and (2.2) and taking expectations. Thus, from (2.1) the mean satisfies

$$\mathbf{m}_y = - \sum_{\substack{(i_1, i_2) \in \alpha \\ (i_1, i_2) \neq (0,0)}} A_{i_1 i_2} \mathbf{m}_y + \sum_{(l_1, l_2) \in \beta} B_{l_1, l_2} \mathbf{m}_x$$

or

$$\mathbf{m}_y = \left(\sum_{(i_1, i_2) \in \alpha} A_{i_1 i_2}\right)^{-1} \left(\sum_{(\ell_1, \ell_2) \in \beta} B_{\ell_1, \ell_2}\right) \mathbf{m}_x \tag{2.8}$$

where

$$A_{oo} = I \tag{2.9}$$

The correlation function satisfies the pair of equations

$$R_y(k_1, k_2) = - \sum_{\substack{(i_1, i_2) \in \alpha \\ (i_1, i_2) \neq (0,0)}} A_{i_1 i_2} R_y(k_1 - i_1, k_2 - i_2) + \sum_{(\ell_1, \ell_2) \in \beta} B_{\ell_1 \ell_2} R_{xy}(k_1 - \ell_1, k_2 - \ell_2)$$

$$\tag{2.10a}$$

$$R_{yx}(k_1, k_2) = - \sum_{\substack{(i_1, i_2) \in \alpha \\ (i_1, i_2) \neq (0,0)}} A_{i_1 i_2} R_{yx}(k_1 - i_1, k_2 - i_2) + \sum_{(\ell_1, \ell_2) \in \beta} B_{\ell_1 \ell_2} R_x(k_1 - \ell_1, k_2 - \ell_2)$$

$$\tag{2.10b}$$

where the cross correlation is defined by

$$R_{xy}(k_1, k_2) = R_{yx}^T(-k_1, -k_2) = E\left[(\mathbf{x}(n_1, n_2) - \mathbf{m}_x)(\mathbf{y}(n_1, n_2) - \mathbf{m}_y)^T\right] \tag{2.11}$$

Alternate relations, in terms of the impulse response are, from (2.2)

$$\mathbf{m}_y = \left(\sum_{\ell_1, \ell_2 = -\infty, -\infty}^{\infty, \infty} H(\ell_1, \ell_2) \right) \mathbf{m}_x \tag{2.12}$$

and

$$R_y(k_1, k_2) = \sum_{\ell_1, \ell_2 = -\infty, -\infty}^{\infty, \infty} \sum_{p_1, p_2 = -\infty, -\infty}^{\infty, \infty} H(\ell_1, \ell_2) R_x(k_1 + p_1 - \ell_1, k_2 + p_2 - \ell_2) H^T(p_1, p_2)$$

$$\tag{2.13}$$

The relation between the correlation and the cross correlation can also be expressed in terms of the impulse response as

$$R_{yx}(k_1, k_2) = \sum_{(\ell_1, \ell_2) = -\infty, -\infty}^{\infty, \infty} H(\ell_1, \ell_2) R_x(k_1 - \ell_1, k_2 - \ell_2) \tag{2.14a}$$

and

$$R_y(k_1, k_2) = \sum_{\ell_1, \ell_2 = -\infty, -\infty}^{\infty, \infty} H(\ell_1, \ell_2) R_{xy}(k_1 - \ell_1, k_2 - \ell_2) \tag{2.14b}$$

which forms a connection between Eqs. (2.10) and (2.13). Relations analogous to Eqs. (2.10), (2.11), (2.13), and (2.14) clearly apply to the covariance and are easily derived.

2.1.2 Frequency Domain Representation

When a (deterministic) signal of the form

$$\mathbf{x}(n_1, n_2) = \mathbf{c} z_1^{n_1} z_2^{n_2} \tag{2.15}$$

is applied to an LSI system, the output (from Eq. 2.2) is given by

$$\mathbf{y}(n_1, n_2) = H_z(z_1, z_2)\mathbf{c}z_1^{n_1}z_2^{n_2} \tag{2.16}$$

where

$$H_z(z_1, z_2) = \sum_{\ell_1, \ell_2 = -\infty, -\infty}^{\infty, \infty} H(l_1, l_2)z_1^{-\ell_1}z_2^{-\ell_2} \tag{2.17}$$

is the z transform of the impulse response and is called the <u>system</u> <u>function</u>. If one applies Eqs. (2.15) and (2.16) to Eq. (2.1) it can be seen that

$$H_z(z_1, z_2) = \left(\sum_{(i_1, i_2) \in \alpha} A_{i_1 i_2}^T z_1^{-i_1} z_2^{-i_2}\right)^{-1} \left(\sum_{\ell_1, \ell_2 \in \beta} B_{\ell_1, \ell_2}^T z_1^{-\ell_1} z_2^{-\ell_2}\right) \tag{2.18}$$

The <u>frequency</u> <u>response</u> of the system is the system function evaluated on the two unit circles

$$H_v(\omega_1, \omega_2) = H_z\left(e^{j\omega_1}, e^{j\omega_2}\right) \tag{2.19}$$

Stability of the 2-D multichannel system corresponds to convergence of H_z on the unit circles. Stability thus implies that the frequency response exists for all values of ω_1 and ω_2.

Random signals are characterized in the frequency domain by the power spectral density matrix. This is defined as the 2-D Fourier transform of the correlation function

$$S_x(\omega_1, \omega_2) = \sum_{k_1, k_2 = -\infty, -\infty}^{\infty, \infty} R_x(k_1, k_2)e^{-j\omega_1 k_1}e^{-j\omega_2 k_2} \tag{2.20}$$

The spectral matrix is positive semi-definite and Hermitian. Its off-diagonal terms represent cross spectra between <u>components</u> of the signal and need not be real. For the case of a two-channel 2-D signal the matrix can be written as

$$S_x(\omega_1, \omega_2) = \begin{bmatrix} S_{11}(\omega_1, \omega_2) & S_{12}(\omega_1, \omega_2) \\ S_{21}(\omega_1, \omega_2) & S_{22}(\omega_1, \omega_2) \end{bmatrix} \tag{2.21}$$

The terms S_{11} and S_{22} are real and nonnegative and represent the 2-D power spectrum or autospectrum for each channel while the terms S_{12} and S_{21} represent cross spectra. Because of the Hermitian symmetry the cross spectra have identical magnitude and opposite phase. The normalized quantity

$$\kappa^2(\omega_1, \omega_2) = \frac{|S_{12}(\omega_1, \omega_2)|^2}{S_{11}(\omega_1, \omega_2)S_{22}(\omega_1, \omega_2)} \tag{2.22}$$

is the 2-D <u>magnitude</u> <u>squared</u> <u>coherency</u> (MSC) and is frequently used instead of $|S_{12}|$ to represent the magnitude of the 2-D cross spectrum. Further treatment of the MSC is given in Appendix A.

A <u>cross-spectral</u> <u>matrix</u> $S_{xy}(\omega_1,\omega_2)$ can also be defined as the Fourier transform of the cross correlation function

$$S_{xy}(\omega_1,\omega_2) = \sum_{k_1,k_2=-\infty,-\infty}^{\infty,\infty} R_{xy}(k_1,k_2)e^{-j\omega_1 k_1}e^{-j\omega_2 k_2} \qquad (2.23)$$

Its components represent cross spectra between components of the signal $\mathbf{x}$ and components of $\mathbf{y}$. This matrix is neither positive definite nor Hermitian. However it shares a symmetry property with S_{yx} in that

$$S_{xy}(\omega_1,\omega_2) = S_{yx}^{*T}(\omega_1,\omega_2) \qquad (2.24)$$

When a signal is transformed by an LSI system, frequency domain expressions for the output power spectrum and the cross spectrum between input and output can be obtained. These are derived by taking Fourier transforms of Eqs. (2.13) and (2.14). The output power spectral matrix has the form

$$S_y(\omega_1,\omega_2) = H_w(\omega_1,\omega_2)S_x(\omega_1,\omega_2)H_w^{*T}(\omega_1,\omega_2) \qquad (2.25)$$

while the cross spectral matrices relate to S_x and S_y through the expression

$$S_{yx}(\omega_1,\omega_2) = H_w(\omega_1,\omega_2)S_x(\omega_1,\omega_2) \qquad (2.26a)$$

$$S_y(\omega_1,\omega_2) = H_w(\omega_1,\omega_2)S_{xy}(\omega_1,\omega_2) \qquad (2.26b)$$

and the symmetry relation (2.24).

2.2 Vector Representation of Multichannel 2-D Signals
2.2.1 Signal Vector Representation

Frequently, a multichannel signal is defined over some finite rectangular region of support. That is, the signal is considered only for $0 \le n_1 < N_1$, and $0 \le n_2 < N_2$. In this case it can be useful to represent the signal as an $N_1 N_2 M$-dimensional vector of the signal values. Two such representations are most useful. In the first, the vector valued signals at points (n_1,n_2) are lexicographically organized first by row and then by column into the larger vector. That is, the multichannel 2-D signal is represented by

$$\underline{x} = \begin{bmatrix} \underline{x}_0 \\ \underline{x}_1 \\ \vdots \\ \underline{x}_{N_1-1} \end{bmatrix} \qquad (2.27a)$$

where

$$\underline{x}_{n_1} = \begin{bmatrix} \mathbf{x}(n_1,0) \\ \mathbf{x}(n_1,1) \\ \vdots \\ \mathbf{x}(n_1,N_2-1) \end{bmatrix} \qquad (2.27b)$$

– 8–

This representation will be called <u>index</u> <u>ordering</u>.

A second type of representation organizes signal component within each channel by rows and columns and then stacks the components. This representation has the form

$$\underline{x}' = \begin{bmatrix} \underline{x}^1 \\ \underline{x}^2 \\ \vdots \\ \underline{x}^M \end{bmatrix} \tag{2.28a}$$

where

$$\underline{x}^m = \begin{bmatrix} \underline{x}_0^m \\ \underline{x}_1^m \\ \vdots \\ \underline{x}_{N_1-1}^m \end{bmatrix} \qquad m = 1, 2, \ldots, m \tag{2.28b}$$

where

$$\underline{x}_{n_1}^m = \begin{bmatrix} x_m(n_1, 0) \\ x_m(n_1, 1) \\ \vdots \\ x_m(n_1, N_2 - 1) \end{bmatrix} \qquad n_1 = 0, 1, \ldots, N_1 - 1 \tag{2.28c}$$

This representation will be called <u>component</u> <u>ordering</u>.

Index and component orderings are related by permutation transformations

$$\underline{x}' = P\underline{x} \tag{2.29a}$$
$$\underline{x} = P^T \underline{x}' \tag{2.29b}$$

The form of the permutation matrix is illustrated in Fig. 2.2 for $N_1 = 3$, $N_2 = 4$, and $M = 2$.

2.2.2 <u>Statistical Characterization of Signal Vectors</u>

The signal vectors previously defined can be characterized by mean vectors and correlation or covariance <u>matrices</u>. These quantities are defined for index-ordered vectors by

$$\underline{m} = E[\underline{x}] \tag{2.30a}$$
$$\mathbf{R} = E[\underline{x}\underline{x}^T] \tag{2.30b}$$
$$\mathbf{K} = E[(\underline{x} - \underline{m})(\underline{x} - \underline{m})^T] \tag{2.30c}$$

and for component-ordered vectors by similar expressions with primed variables. From Eqs (2.29) and (2.30) it can be seen that the index-ordered and component-ordered
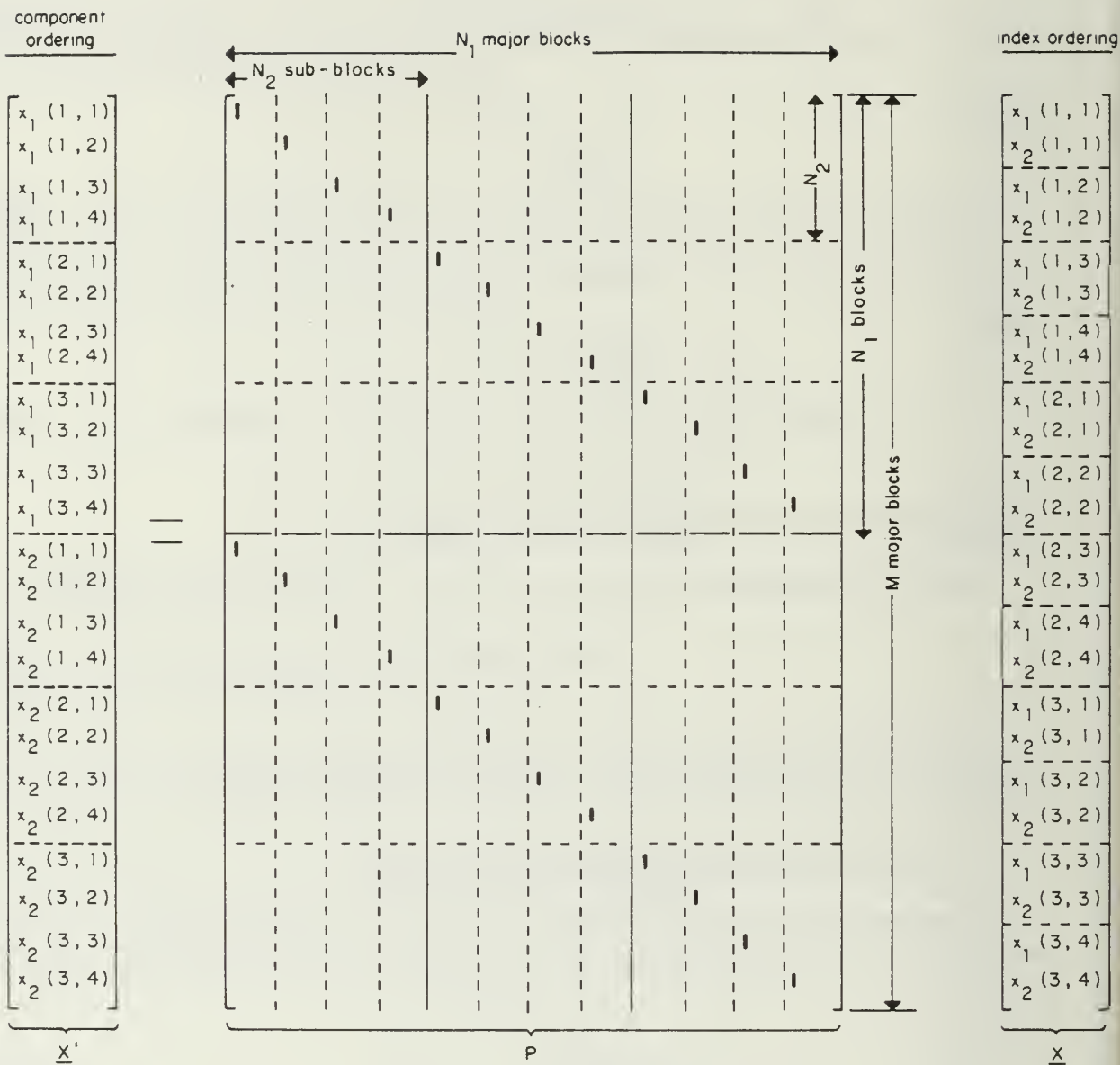
Figure 2.2   Permutation matrix for $N_1 = 3$, $N_2 = 4$, $M = 2$.

statistics are related by

$$\underline{m}' = P\underline{m} \tag{2.31a}$$

$$\mathbf{R}' = PRP^T \tag{2.31b}$$

$$\mathbf{K}' = PKP^T \tag{2.31c}$$

Note that for a stationary random process the vector $\underline{m}$ will consist of $N_1 N_2$ M-dimensional subvectors equal to the signal mean (see Eq. 2.5). The vector $\underline{m}'$ will consist of $M N_1$ N_2-dimensional subvectors. Each subvector has elements that are all identical and equal to the mean of the signal in the corresponding channel.

The correlation and covariance matrices for a stationary 2-D random process have specific structure and symmetry at their various levels of partitioning. These properties are illustrated in Figs. 2.3 and 2.4. An example showing detailed structure of these matrices is given in Appendix B.

2.2.3 Linear Transformation of Signal Vectors

Linear transformations on signal vectors can be represented by matrix equation

$$\underline{y} = A\underline{x} \tag{2.32}$$

We will consider only index-ordered transformations here since index ordering is more extensively used in this report. The equivalent matrix for component-ordered transformation is given by

$$A' = PAP^T \tag{2.33}$$

General linear transformations such as this may operate upon the rows, columns, or channel dimensions of the signal.

Linear transformations corresponding to a LSI filtering operations are represented by a matrix of the form

$$\tilde{\tilde{\mathbf{H}}} = \begin{bmatrix} \tilde{\mathbf{H}}(0) & \tilde{\mathbf{H}}(-1)\ldots & \tilde{\mathbf{H}}(-N_1+1) \\ \tilde{\mathbf{H}}(1) & \tilde{\mathbf{H}}(0)\ldots & \tilde{\mathbf{H}}(-N_1+2) \\ \vdots & & \\ \tilde{\mathbf{H}}(N_1-1) & \tilde{\mathbf{H}}(N_1-2)\ldots & \tilde{\mathbf{H}}(0) \end{bmatrix} \tag{2.34a}$$

where

$$\tilde{\mathbf{H}}(n_1) = \begin{bmatrix} H(n_1,0) & H(n_1,-1) & \ldots & H(n_1,-N_2+1) \\ H(n_1,1) & H(n_1,0) & \ldots & H(n_1,-N_2+2) \\ \vdots & & & \\ H(n_1,N_2-1) & H(n_1,N_2-2) & \ldots & H(n_1,0) \end{bmatrix} \tag{2.34b}$$

Signal Vector

$$\underline{x} = \begin{bmatrix} \underline{x}_0 \\ \underline{x}_1 \\ . \\ . \\ \underline{x}_{N_1-1} \end{bmatrix} \qquad \text{where} \qquad \underline{x}_{n_1} = \begin{bmatrix} x(n_1,0) \\ x(n_1,1) \\ . \\ . \\ . \\ x(n_1,N_2-1) \end{bmatrix}$$

Correlation Matrix

$$\mathbf{R} = E\underline{x}\underline{x}^T = \begin{bmatrix} \mathbf{R}(0) & \mathbf{R}(1) & \ldots & \mathbf{R}(N_1-1) \\ \mathbf{R}(-1) & \mathbf{R}(0) & \ldots & \mathbf{R}(N_1-2) \\ . & & & . \\ . & & & . \\ . & . & & . \\ \mathbf{R}(-N_1+1) & \mathbf{R}(-N_1+2) & \ldots & \mathbf{R}(0) \end{bmatrix} \qquad \begin{array}{c} (BLOCK\ TOEPLITZ\ WITH \\ N_2 M \times N_2 M\ BLOCKS) \end{array}$$

where

$$\mathbf{R}(k) = E\,\underline{x}_n\underline{x}_{n-k}^T = \begin{bmatrix} R(k,0) & R(k,1) & \ldots & R(k,N_2-1) \\ R(k,-1) & R(k,0) & \ldots & R(k,N_2-2) \\ . & . & & . \\ . & . & & . \\ . & . & & . \\ R(k,-N_2-1) & R(k,-N_2-2) & \ldots & R(k,0) \end{bmatrix} \qquad \begin{array}{c} (BLOCK\ TOEPLITZ\ WITH \\ M \times M\ BLOCKS) \end{array}$$

where

$$R(k_1,k_2) = R^T(-k_1,-k_2) = E\,x(n_1,n_2)x^T(n_1-k_1,n_2-k_2) \qquad (NOT\ TOEPLITZ)$$

Fig. 2.3 Correlation matrix for index ordering.

Signal Vector

$$\underline{x}' = \begin{bmatrix} \underline{x}^1 \\ \underline{x}^2 \\ \cdot \\ \cdot \\ \cdot \\ \underline{x}^M \end{bmatrix} \quad \text{where} \quad \underline{x}^m = \begin{bmatrix} \underline{x}_0^m \\ \underline{x}_1^m \\ \cdot \\ \cdot \\ \cdot \\ \underline{x}_{N_1-1}^m \end{bmatrix} \quad \text{where} \quad \underline{x}_{n_1}^m = \begin{bmatrix} x_m(n_1,0) \\ x_m(n_1,1) \\ \cdot \\ \cdot \\ \cdot \\ x_m(n_1,N_2-1) \end{bmatrix}$$

Correlation Matrix

$$\mathbf{R}' = E'\underline{x}'\underline{x}'^T = \begin{bmatrix} \mathbf{R}_{11} & \mathbf{R}_{12} & \cdot & \cdot & \cdot & \mathbf{R}_{1M} \\ \mathbf{R}_{21} & \mathbf{R}_{22} & \cdot & \cdot & \cdot & \mathbf{R}_{2M} \\ \cdot & & & & & \cdot \\ \cdot & & & & & \cdot \\ \cdot & & & & & \cdot \\ \mathbf{R}_{M1} & \mathbf{R}_{M2} & \cdot & \cdot & \cdot & \mathbf{R}_{MM} \end{bmatrix} \quad (N_1 N_2 \times N_1 N_2 \ BLOCKS)$$

where

$$\mathbf{R}_{lk} = E\,\underline{x}^l\underline{x}^{k^T} = \begin{bmatrix} R_0^{lk} & R_1^{lk} & \cdot & \cdot & \cdot & R_{N_1-1}^{lk} \\ R_{-1}^{lk} & R_0^{lk} & \cdot & \cdot & \cdot & R_{N_1-2}^{lk} \\ \cdot & & & & & \cdot \\ \cdot & & & & & \cdot \\ \cdot & & & & & \cdot \\ R_{-N_1+1}^{lk} & R_{-N_1-2}^{lk} & \cdot & \cdot & \cdot & R_0^{lk} \end{bmatrix} \quad \begin{array}{l}(BLOCK \ \ TOEPLITZ \\ WITH \ \ N_2 \times N_2 \ \ BLOCKS)\end{array}$$

where

$$R_{n_1}^{lk} = E'\underline{x}_n^l\underline{x}_{n-n_1}^{k^T} \quad (TOEPLITZ)$$

Fig. 2.4 Correlation matrix for component ordering.

(The $\sim$ notation has special meaning that will be explained shortly.) When the transformation corresponds to an FIR filter many of the blocks and subblocks in Eq. (2.34) will be zero; the specific arrangement will depend on the shape of the support region for the impulse response.

For a system described by a linear difference equation (2.1), one can write

$$\widetilde{\widetilde{\mathbf{A}}}\underline{y} = \widetilde{\widetilde{\mathbf{B}}}\underline{x} \tag{2.35}$$

where the matrices $\widetilde{\widetilde{\mathbf{A}}}$ and $\widetilde{\widetilde{\mathbf{B}}}$ are defined in terms of the coefficient matrices $A^T_{i_1 i_2}$ and $B^T_{\ell_1,\ell_2}$ analogously to Eqs. (2.34). The output $\underline{y}$ can then be expressed directly as

$$\underline{y} = \left(\widetilde{\widetilde{\mathbf{A}}}\right)^{-1} \widetilde{\widetilde{\mathbf{B}}}\underline{x} \tag{2.36}$$

This form of the analysis implicitly assumes zero initial conditions for the difference equation.

Occasionally it is necessary to convert between one form of channel representation for the 2-D multichannel signals and another without performing any specific filtering or signal processing. This would occur for example if the signal $x(n_1, n_2)$ represented a color image with red, green, and blue components and we wanted to convert the signal to NTSC form. If the new signals are defined in terms of the old signals by the transformation

$$x(n_1, n_2) = Tx(n_1, n_2) \tag{2.37}$$

then the index-ordered signal vector would be transformed according to

$$\underline{x} = \mathbf{T}\underline{x} \tag{2.38}$$

where $\mathbf{T}$ is a $N_1 N_2 M$ by $N_1 N_2 M$ block diagonal matrix. This matrix would contain $N_1 N_2$ nonzero blocks all equal to the signal transformation T.

2.2.4 Reversal Notation

In the analysis of 2-D signals using vector representation, it is sometimes necessary to deal with vectors and matrices whose components are ordered corresponding to decreasing values of the signal index rather than increasing values as in Eq. (2.27). While a reordering of the signal values can be represented by a permutation matrix operation, it is much clearer to develop explicit notation. The notation to be used will apply only to index-ordered vectors and matrices. Component-ordered quantities are less frequently used and do not lend themselves readily to the reorderings that are considered here.

The symbol $\sim$ above a vector will correspond to a vector whose first-level partitions have been organized according to decreasing value of the index.

$$\tilde{\underline{x}} = \begin{bmatrix} \underline{x}_{N_1 - 1} \\ \underline{x}_{N_1 - 2} \\ \vdots \\ \underline{x}_0 \end{bmatrix} \qquad (2.39)$$

where the $\underline{x}_n$ are defined by Eq. (2.27b). We call this a first index reversal of the vector. The symbol $\sim$ below a vector will be used to denote a vector whose second level partitions have been organized according to decreasing index values.

$$\underset{\sim}{\underline{x}} = \begin{bmatrix} \tilde{\underline{x}}_0 \\ \tilde{\underline{x}}_1 \\ \vdots \\ \tilde{\underline{x}}_{N_1 - 1} \end{bmatrix} \qquad (2.40)$$

where

$$\underset{\sim}{\underline{x}}_{n_1} = \begin{bmatrix} \underline{x}(n_1, N_2 - 1) \\ \underline{x}(n_1, N_2 - 2) \\ \vdots \\ \underline{x}(n_1, 0) \end{bmatrix} \qquad (2.41)$$

We call this a second index reversal of the vector and is occasionally useful. Most frequently it will be required to use the doubly reversed vector which is denoted by a double$\sim$over the vector:

$$\underset{\sim}{\tilde{\underline{x}}} = \begin{bmatrix} \tilde{\underline{x}}_{N_1 - 1} \\ \tilde{\underline{x}}_{N_1 - 2} \\ \vdots \\ \tilde{\underline{x}}_0 \end{bmatrix} \qquad (2.42)$$

and denotes a vector where both the main blocks and the second level blocks have been reversed.

Since transformation of a reversed vector usually implies generation of a new vector with corresponding order, it is most reasonable to define reversals of a matrix as a reordering about both its rows and columns. Thus a matrix $\tilde{A}$ represents a matrix A whose first level blocks or partitions have been reversed along both rows and columns. Matrices $\underset{\sim}{A}$ and $\underset{\sim}{\tilde{A}}$ are defined similarly with reversals about rows and columns of the inner blocks. Note also that reversal about both rows and columns of a matrix is equivalent to transposition about both the main and reverse diagonals. This preserves certain symmetry such as block Toeplitz structure when it exists.

If reversal notation is used, the LSI transformation of Eq. (2.2) can be represented as

$$\underline{y} = \underset{\sim}{\tilde{H}}\underline{x} \qquad (2.43)$$

– 15–

where the matrix H is now defined by

$$\mathbf{H} = \begin{bmatrix} \mathbf{H}(0) & \mathbf{H}(1) & \cdots & \mathbf{H}(N_1 - 1) \\ \mathbf{H}(-1) & \mathbf{H}(0) & \cdots & \mathbf{H}(N_1 - 2) \\ \vdots & & & \\ \mathbf{H}(-N_1 + 1) & \mathbf{H}(-N_1 + 2) & \cdots & \mathbf{H}(0) \end{bmatrix} \tag{2.44a}$$

with

$$\mathbf{H}(n_1) = \begin{bmatrix} H(n_1, 0) & H(n_1, 1) & \cdots & H(n_1, N_2 - 1) \\ H(n_1, -1) & H(n_1, 0) & \cdots & H(n_1, N_2 - 2) \\ \vdots & & & \\ H(n_1, N_2 - 1) & H(n_1, N_2 - 2) & \cdots & H(n_1, 0) \end{bmatrix} \tag{2.44b}$$

Reversal notation will also prove to be useful in considering signal models in Chapters III and IV.

2.3 Separable Multichannel 2-D Signals and Transformations
2.3.1 Separable Signals

The direct product of an $L \times Q$ matrix B and an $N \times P$ matrix A is an $NL \times PQ$ matrix

$$B \otimes A = \begin{bmatrix} Ba_{11} & Ba_{12} & \cdots & Ba_{1P} \\ Ba_{21} & Ba_{22} & \cdots & Ba_{2P} \\ \vdots & & & \\ Ba_{N1} & Ba_{N2} & \cdots & Ba_{NP} \end{bmatrix} \tag{2.45}$$

In general $B \otimes A$ is not equal to $A \otimes B$. A number of other properties are given in Table 2.1 and in Appendix C.

Table 2.1 - Properties of Direct Product

$(B \otimes A)(D \otimes C)$	$= BD \otimes AC$
$(B \otimes A)^T$	$= B^T \otimes A^T$
$(B \otimes A)^{-1}$	$= B^{-1} \otimes A^{-1}$

Consider for the moment a single channel 2-D random signal that has the separable form

$$\mathbf{x}(n_1, n_2) = \mathbf{x}_A(n_1) \cdot \mathbf{x}_B(n_2) \tag{2.46}$$

Then if $\underline{\mathbf{x}}_A$ and $\underline{\mathbf{x}}_B$ are the vector representations of the signals $\mathbf{x}_A(n_1)$ and $\mathbf{x}_B(n_2)$, a vector representation of the 2-D signal is given by

$$\underline{\mathbf{x}} = \underline{\mathbf{x}}_B \otimes \underline{\mathbf{x}}_A \tag{2.47}$$

Now if $\mathbf{x}_A(n_1)$ and $\mathbf{x}_B(n_2)$ are <u>independent</u> random processes with correlation matrices $\mathbf{R}_A$ and $\mathbf{R}_B$ the correlation matrix for the 2-D signal vector is

$$
\begin{aligned}
E\left[\underline{\mathbf{x}}\underline{\mathbf{x}}^T\right] &= E\left[(\underline{\mathbf{x}}_B \otimes \underline{\mathbf{x}}_A)(\underline{\mathbf{x}}_B \otimes \underline{\mathbf{x}}_A)^T\right] \\
&= E\left[(\underline{\mathbf{x}}_B \underline{\mathbf{x}}_B^T)\right] \otimes E\left[(\underline{\mathbf{x}}_A \underline{\mathbf{x}}_A^T)\right] \\
&= \mathbf{R}_B \otimes \mathbf{R}_A
\end{aligned}
\tag{2.48}
$$

A similar direct product relation holds for the mean vector and the covariance matrix.

Multichannel 2-D random processes can be separable along the index (n_1, n_2) directions, between channels, or both. Various cases of separable signals and their correlation matrices are given in Table 2.2 assuming index ordering. The specific structure of the matrices can be envisioned by comparisons with the matrices in Fig. 2.3.

<div align="center">Table 2.2 - <u>Separable Forms for Multichannel 2-D Signals</u></div>

Form of Signal	Description	Form of Correlation
$\mathbf{x}(n_1, n_2) = \mathbf{x}_A(n_1) \cdot \mathbf{x}_B(n_2)$	Product of a 1-D single-channel signal and a 1-D multichannel signal	$\mathbf{R}_{\underline{\mathbf{x}}} = \mathbf{R}_B \otimes \mathbf{R}_A$
$\mathbf{x}(n_1, n_2) = x(n_1, n_2) \cdot \underline{c}$	Product of a 2-D single channel signal and a M-dimensional random vector	$\mathbf{R}_{\underline{\mathbf{x}}} = \mathbf{R}_c \otimes \mathbf{R}_x$
$\mathbf{x}(n_1, n_2) = x_A(n_1) \cdot x_B(n_2) \cdot \underline{c}$	Product of two 1- D single channel signals and a random vector	$\mathbf{R}_{\underline{\mathbf{x}}} = \mathbf{R}_c \otimes \mathbf{R}_B \otimes \mathbf{R}_A$

Separable structure for the signals when it exists leads to simplifications in the analysis. For example 2-D problems can be reduced to a pair of 1-D problems. The implications of separability for linear prediction are described in Chapter III.

2.3.2 Separable transformations

If a linear transformation for a multichannel 2-D signal is completely separable it can be represented as the direct product of three matrices

$$
T = W \otimes V \otimes U
\tag{2.49}
$$

where U is a $N_1 \times N_1$ matrix representing transformation along the n_1 direction, V is an $N_2 \times N_2$ matrix representing transformation along the n_2 direction and W is an $M \times M$ matrix representing transformation between channels. If the signal is correspondingly separable as

$$\underline{x} = \underline{c} \otimes \underline{x}_B \otimes \underline{x}_A \tag{2.50}$$

then the processing of the signal is greatly simplified since

$$T\underline{x} = (W\underline{c}) \otimes (V\underline{x}_B) \otimes (U\underline{x}_A) \tag{2.51}$$

However separable transformations are advantageous even if the signal is not separable. Common examples of separable transformations are the DFT, Hadamard and Walsh transforms, and the singular value decomposition.

A convenient relation exists between index-ordered and component-ordered separable linear transformations. In particular, if the index-ordered transformation is given by (2.49) then the component-ordered transformation is given by

$$T' = V \otimes U \otimes W \tag{2.52}$$

A somewhat more concise representation for separable transformations exists. This involves first representing the multichannel 2-D signal in yet another form, as a $N_1 M \times N_2$ matrix

$$X = \begin{bmatrix} X_1 \\ X_2 \\ \vdots \\ X_M \end{bmatrix} \tag{2.53}$$

where X_m is a $N_1 \times N_2$ submatrix whose elements are the signal $x_m(n_1, n_2)$ in channel m. It can be verified that with this representation, a separable transformation of the form

$$\underline{y} = (W \otimes V \otimes U)\underline{x} \tag{2.54}$$

leads to a matrix representation Y with blocks

$$Y_m = \sum_{\ell=1}^{M} w_{m\ell} U X_\ell V^T \tag{2.55}$$

$$m = 1, 2, \ldots, M$$

where $w_{m\ell}$ are the elements of W. This can be written in a single matrix equation as

$$Y = (I \otimes W) \cdot U X V^T \tag{2.56}$$

III. Linear Prediction for Multichannel 2-D Random Processes

3.1 Linear Prediction

3.1.1 Problem Statement

Let $x(n_1, n_2)$ represent a zero-mean stationary multichannel 2-D random signal. The linear prediction problem is concerned with forming a linear estimate of the signal at the point (n_1, n_2) from other values of the signal in a region α. Specifically we form the estimate

$$\hat{x}(n_1, n_2) = - \sum_{\substack{(i_1, i_2) \in \alpha \\ (i_1, i_2) \neq (0,0)}} A_{i_1 i_2}^T x(n_1 - i_1, n_2 - i_2) \qquad (3.1)$$

and the prediction error is defined as

$$\epsilon(n_1, n_2) = x(n_1, n_2) - \hat{x}(n_1, n_2) \qquad (3.2)$$

The matrix coefficients $A_{i_1 i_2}^T$ are chosen to minimize the mean-squared error $E\left[|\epsilon(n_1, n_2)|^2\right]$.

The error is generated from the data by the FIR prediction error filter. From Eqs. (3.1) and (3.2) the difference equation for the filter is

$$\epsilon(n_1, n_2) = \sum_{(i_1, i_2) \in \alpha} A_{i_1 i_2}^T x(n_1 - i_1, n_2 - i_2) \qquad (3.3)$$

with $A_{00} = I$. Since the filter is FIR, the terms $A_{i_1 i_2}^T$ also represent the impulse response and α is the impulse response region of support (see Eq. 2.2a). The correlation function of the error evaluated at lag (0,0) is the $M \times M$ prediction error covariance matrix Σ_ϵ. That is

$$\Sigma_\epsilon = E\left[\epsilon(n_1, n_2)\epsilon^T(n_1, n_2)\right] = R_\epsilon(0,0) \qquad (3.4)$$

The mean-squared error $\mathcal{E}$ is given by

$$\mathcal{E} = E\left[|\epsilon(n_1, n_2)|^2\right] = E\left[\epsilon^T(n_1, n_2)\epsilon(n_1, n_2)\right] = tr\Sigma_\epsilon \qquad (3.5)$$

These quantities are important for the analysis that follows.

3.1.2 Normal Equations

The prediction error filter coefficients and the prediction error covariance are formed by solving a set of Normal equations. These linear equations follow directly from the orthogonality principle [4] which states that the error must be orthogonal to the signal values used in prediction.

19

$$E\left[\mathbf{x}(n_1 - i_1, n_2 - i_2)\epsilon^T(n_1, n_2)\right] = [\mathbf{O}]$$
$$(i_1, i_2) \in \alpha, \quad (i_1, i_2) \neq (0,0) \tag{3.6a}$$

It further follows from Eqs. (3.3), (3.4) and (3.6a)

$$E\left[\mathbf{x}(n_1, n_2)\epsilon^T(n_1, n_2)\right] = E\left[\epsilon(n_1, n_2)\epsilon^T(n_1, n_2)\right] = \Sigma_\epsilon \tag{3.6b}$$

These last two equations can thus be written more concisely as

$$E\left[\mathbf{x}(n_1 - i_1, n_2 - i_2)\epsilon^T(n_1, n_2)\right] = \Sigma_\epsilon \delta(i_1)\delta(i_2)$$
$$(i_1, i_2) \in \alpha \tag{3.7}$$

3.1.2.1 Rectangular Support

The Normal equations will be developed by using an index-ordered vector representation for the signal. At first let α be the rectangular region shown in Fig. 3.1. The size of α is $P_1 \times P_2$ points and L_1 and L_2 can be any values in the range $-P_1 < L_1 \leq 0$, $-P_2 < L_2 \leq 0$. Then an index-ordered representation for the signal data that occurs in Eq. (3.3) is needed.

To make the analysis clear, consider the case where $L_1 = L_2 = 0$. This is the quarter plane or first quadrant predictor. The signal data needed in Eq. (3.3) is in the range $n_1 - P_1 + 1$ to n_1 and $n_2 - P_2 + 1$ to n_2 (see Fig. 3.2). Form a vector $\mathbf{x}_{n_1 n_2}$ as follows

$$\mathbf{x}_{n_1 n_2} = \begin{bmatrix} \underline{\mathbf{x}}_{n_1 - P_1 + 1} \\ \underline{\mathbf{x}}_{n_1 - P_1 + 2} \\ \vdots \\ \underline{\mathbf{x}}_{n_1} \end{bmatrix} \tag{3.8a}$$

$$\mathbf{x}_{n_1 - P_1 + i} = \begin{bmatrix} x(n_1 - P_1 + i, n_2 - P_2 + 1) \\ \mathbf{x}(n_1 - P_1 + i, n_2 - P_2 + 2) \\ \vdots \\ \mathbf{x}(n_1 - P_1 + i, n_2) \end{bmatrix} \tag{3.8b}$$

Then Eq. (3.3) can be written in matrix form as

$$\epsilon(n_1, n_2) = A^T \widetilde{\underline{\underline{\mathbf{x}}}}_{n_1 n_2} \tag{3.9}$$

where

$$A = \begin{bmatrix} A^{(0)} \\ A^{(1)} \\ \vdots \\ A^{(P_1 - 1)} \end{bmatrix} \tag{3.10a}$$

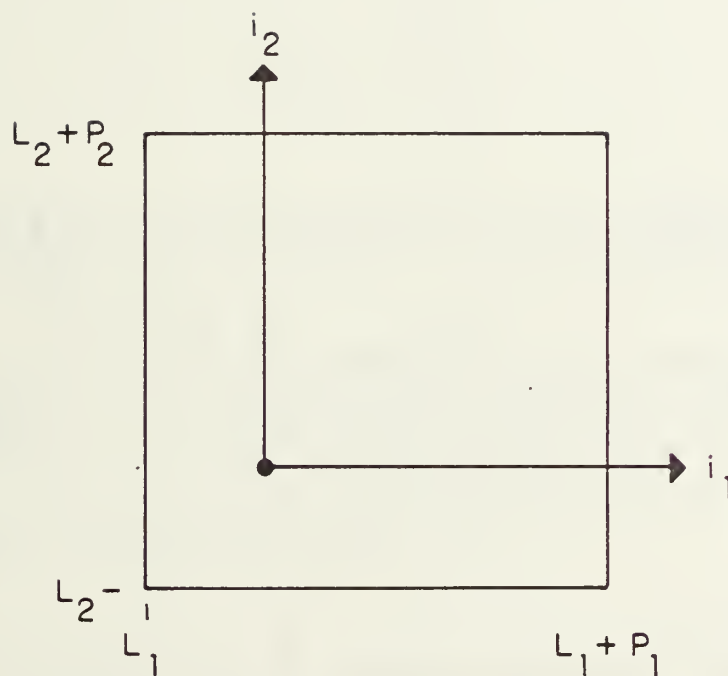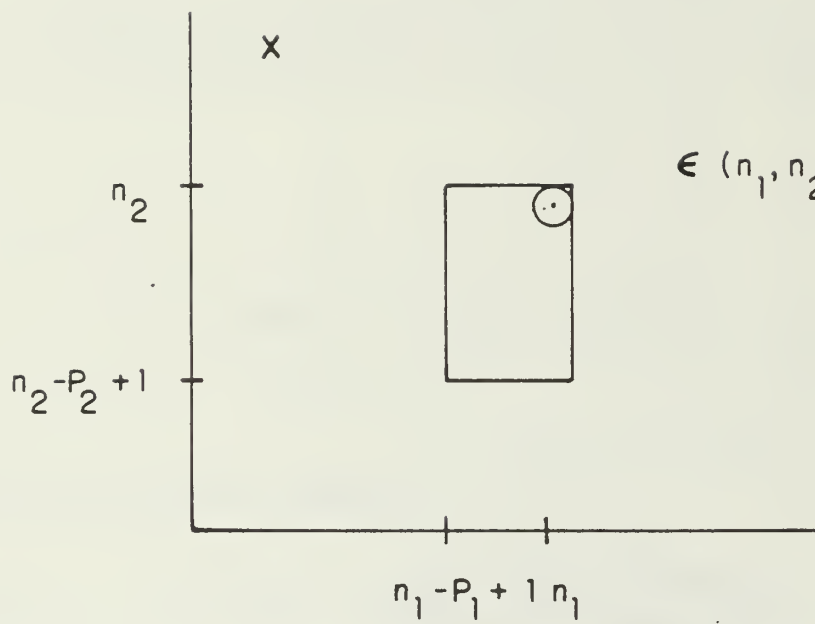$$A^{(i)} = \begin{bmatrix} A_{i0} \\ A_{i1} \\ \vdots \\ A_{i, P_2 - 1} \end{bmatrix} \tag{3.10b}$$

20

Figure 3.1 A general rectangular region of support α for the prediction error filter.

$$\epsilon\,(n_1,n_2) = \sum_{\substack{i_1 = 0 \\ i_2 = 0}}^{\substack{P_2 - 1 \\ P_1 - 1}} A_{i_1 i_2}^{\mathsf{T}}\, \mathbf{x}(n_1 - i_1, n_2$$

Figure 3.2 First quadrant predictor.

22

The Normal equations then follow directly. From Eqs. (3.7) through (3.9) we have

$$E\left[\tilde{\underset{\sim}{\mathbf{x}}}_{n_1 n_2}\, \epsilon^T(n_1, n_2)\right] = E\left[\tilde{\underset{\sim}{\mathbf{x}}}_{n_1 n_2}\, \tilde{\underset{\sim}{\mathbf{x}}}^T_{n_1 n_2}\, \mathbf{A}\right]$$

$$= E\left[\tilde{\underset{\sim}{\mathbf{x}}}_{n_1 n_2}\, \tilde{\underset{\sim}{\mathbf{x}}}^T_{n_1 n_2}\right]\mathbf{A} = \mathbf{S} \tag{3.11}$$

or

$$\tilde{\underset{\sim}{\mathbf{R}}}\mathbf{A} = \mathbf{S} \tag{3.12}$$

where

$$\mathbf{S} = \begin{bmatrix} \mathbf{S}^{(0)} \\ 0 \\ \vdots \\ 0 \end{bmatrix} \tag{3.13a}$$

$$\mathbf{S}^{(0)} = \begin{bmatrix} \Sigma_\epsilon \\ 0 \\ \vdots \\ 0 \end{bmatrix} \tag{3.13b}$$

and the partitioning in Eqs. (3.13) corresponds to that of Eqs. (3.8) and (3.10). Eq. (3.12) represents the Normal equations. The results for a first quadrant multichannel predictor are summarized in Fig. 3.3.

Observe that the correlation matrix that occurs when the Normal equations are written in the standard form (3.12) is the reverse matrix $\tilde{\underset{\sim}{\mathbf{R}}}$ and not $\mathbf{R}$ (compare Figs. 2.3 and 3.3). This point is not usually appreciated or discussed in the literature on linear prediction. For the single channel case $\mathbf{R}$ and $\tilde{\underset{\sim}{\mathbf{R}}}$ are both the same; for our multichannel case it is important to make the distinction.

When L_1 and L_2 of Fig. 3.1 are not equal to zero a similar analysis again leads to Eq. (3.12). The correlation matrix $\tilde{\underset{\sim}{\mathbf{R}}}$ is identical to the one for the previous case but the matrix of filter parameters is defined by

$$\mathbf{A} = \begin{bmatrix} A^{(L_1)} \\ \vdots \\ A^{(L_1 + P_1 - 1)} \end{bmatrix} \tag{3.14a}$$

$$\mathbf{A}^{(i)} = \begin{bmatrix} A_{i, L_2} \\ \vdots \\ A_{i,0} \\ \vdots \\ A_{i, L_2 + P_2 - 1} \end{bmatrix} \tag{3.14b}$$

23

Prediction Equation

$$\hat{\mathbf{x}}(n_1, n_2) = \sum_{i_1=0}^{P_1-1} \sum_{i_2=0}^{P_2-1} A_{i_1 i_2}^{T} \mathbf{x}(n_1 - i_1, n_2 - i_2) \qquad (i_1, i_2) \neq (0,0)$$

Normal Equations

$$
\begin{bmatrix}
\mathbf{R}(0) & \mathbf{R}(-1) & \ldots & \mathbf{R}(-P_1-1) \\
\mathbf{R}(1) & \mathbf{R}(0) & \ldots & \mathbf{R}(-P_1-2) \\
\cdot & \cdot & & \cdot \\
\cdot & & & \cdot \\
& & & \cdot \\
\mathbf{R}(P_1-1) & \mathbf{R}(P_1-2) & \ldots & \mathbf{R}(0)
\end{bmatrix}
\begin{bmatrix}
\mathbf{A}^{(0)} \\
\mathbf{A}^{(1)} \\
\cdot \\
\cdot \\
\cdot \\
\mathbf{A}^{(P_1-1)}
\end{bmatrix}
=
\begin{bmatrix}
\mathbf{S}^{(0)} \\
0 \\
\cdot \\
\cdot \\
\cdot \\
0
\end{bmatrix}
$$

where

$$
\mathbf{R}(k) = \mathbf{R}^{T}(-k) =
\begin{bmatrix}
R(k,0) & R(k,-1) & \ldots & R(k,-P_2-1) \\
R(k,1) & R(k,0) & \ldots & R(k,-P_2-2) \\
\cdot & \cdot & & \cdot \\
\cdot & \cdot & & \cdot \\
& & & \cdot \\
R(k,P_2-1) & R(k,P_2-2) & \ldots & R(k,0)
\end{bmatrix}
\qquad
\mathbf{A}^{(k)} =
\begin{bmatrix}
A_{k,0} \\
A_{k,1} \\
\cdot \\
\cdot \\
\cdot \\
A_{k,P_2-1}
\end{bmatrix}
\qquad
\mathbf{S}^{(0)} =
\begin{bmatrix}
\Sigma_\epsilon \\
0 \\
\cdot \\
\cdot \\
\cdot \\
0
\end{bmatrix}
$$

where

$$R(k_1, k_2) = R^{T}(-k_1, -k_2) = E[\mathbf{x}(n_1, n_2)\mathbf{x}^{T}(n_1 - k_1, n_2 - k_2)] \qquad A_{0,0} = \mathbf{I} \qquad \Sigma_\epsilon = E[(\mathbf{x} - \hat{\mathbf{x}})(\mathbf{x} - \hat{\mathbf{x}})^{T}]$$

Fig. 3.3 Equations of linear prediction for first quadrant support.

The matrix $\mathbf{S}$ is similar to Eq. (3.13) but the non-zero block Σ_ϵ appears in a position corresponding to the location of the coefficient A_{00} in the matrix $\mathbf{A}$.

3.1.2.2 Special Forms

The Normal equations for rectangular support can be viewed in the following way. We have a set of $P_1 \times P_2$ points as shown in Fig. 3.4(a). A correlation matrix $\widetilde{\mathbf{R}}$ is formed for the $P_1 P_2$ points. The terms of the correlation function appearing in this matrix are shown in Fig. 3.4(b). The Normal equations for predicting various points in the array all involve this same matrix $\widetilde{\mathbf{R}}$. They differ only in the indexing of the filter coefficients and in the position of the terms A_{00} and Σ_ϵ in the arrays $\mathbf{A}$ and $\mathbf{S}$.

The filters for predicting the upper right and upper left points in a rectangular region of support are called the first quadrant and second quadrant filters. The first quadrant filter was discussed in detail in the previous subsection. By using properties of the reversal operation the second quadrant Normal equations can be put in the form of Fig. 3.3. When this is done it can be observed that the equations although similar have their second level blocks transposed. Thus the filter coefficients for the first and second quadrant predictors are not the same. The third and forth quadrant filters for predicting the bottom left and bottom right points are also distinct. Their Normal equations differ from the Normal equations of the first and second quadrant filters in that the innermost blocks $R(k_1, k_2)$ are replaced by their transposes. *This is a difference from the single channel 2-D case* where the first and third and the second and fourth quadrant filters are identical.

A very important form of predictor is the nonsymmetric half plane filter. Although this filter clearly has non-rectangular support the form of the Normal equations can be derived from those already considered. The linear prediction problem is depicted in Fig. 3.5. One can think of the NSHP support region as a rectangular region where $|L_2|$ points (marked with x's in Fig. 3.5(a) are missing. The circled point is the one predicted. The Normal equations for the NSHP can be obtained by starting with the equations for rectangular support. One then simply drops out filter coefficients corresponding to the "missing" points and eliminates corresponding rows and columns of the correlation matrix. The required terms of the correlation function are shown in Fig. 3.5(c). The detailed form of the Normal equations is given in Fig. 3.6.

A companion NSHP prediction problem is shown in Fig. 3.5(b). While in Fig. 3.5(a) data is processed from lower left to upper right, in Fig. 3.5(b) data is processed in the opposite direction. We refer to Fig. 3.5(a) as <u>forward</u> prediction and Fig. 3.5(b) as <u>backward</u> prediction. The Normal equations for the backward problem can be obtained in the same manner discussed for the forward problem. If the equations are permuted and put in the form of Fig. 3.6, they will differ only in that the inner blocks $R(k_1, k_2)$ appear transposed.
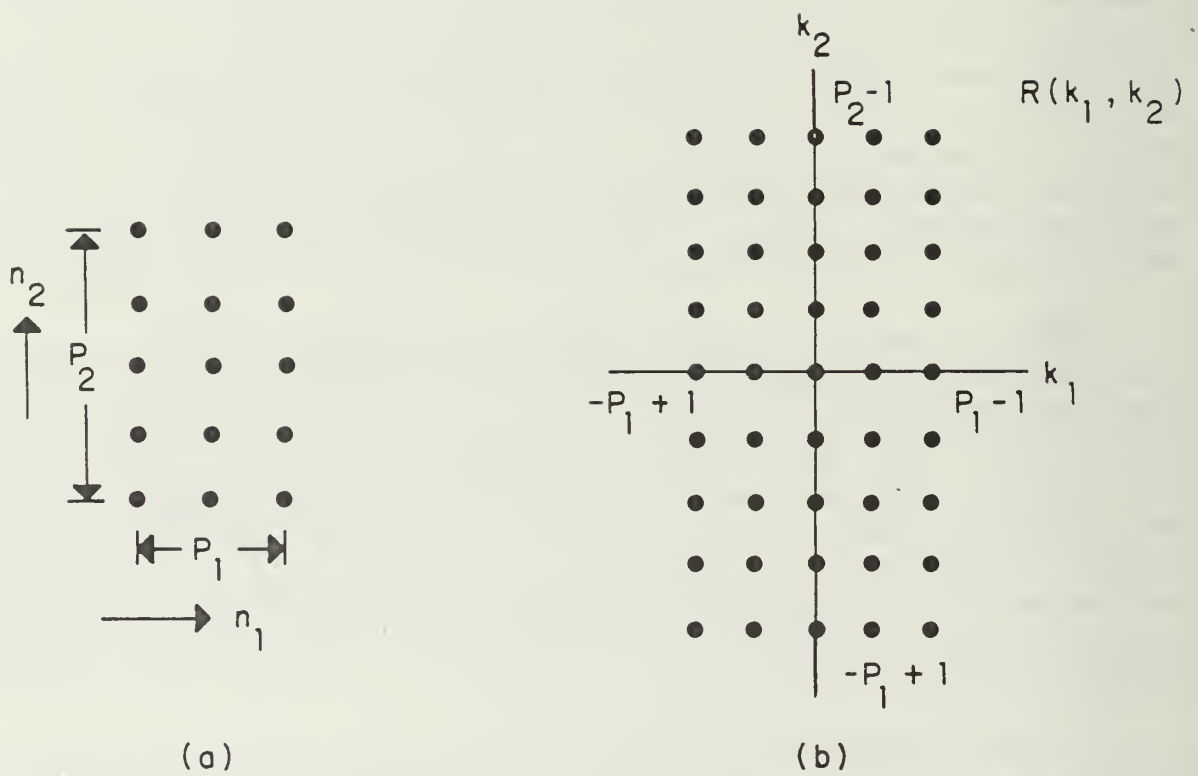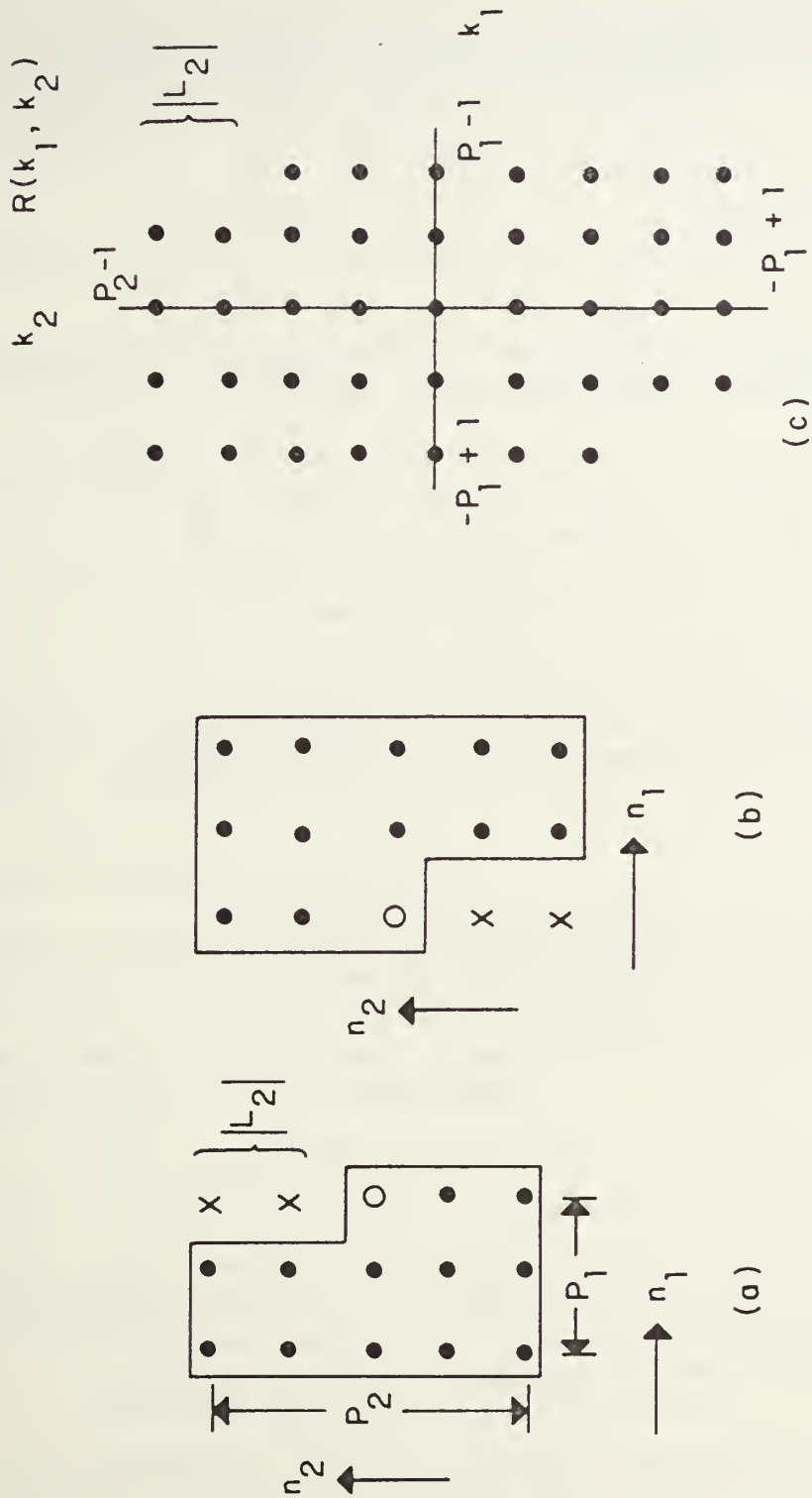
Figure 3.4 Linear prediction with rectangular support.

Note: L_2 is a negative number

Figure 3.5 Linear prediction with NSHP support.

27

Prediction Equation

$$\hat{x}(n_1,n_2) = \sum_{i_2=0}^{i_2-P_2-1} A_{0i_2}^T x(n_1,n_2-i_2) - \sum_{i_1=1}^{P_1-1} \sum_{i_2=L_2}^{L_2-P_2-1} A_{i_1i_2}^T x(n_1-i_1,n_2-i_2)$$

Normal Equations

$$\begin{bmatrix} \mathbf{R}'(0) & \mathbf{R}'(-1) & \cdots & \mathbf{R}'(-P_1+1) \\ \mathbf{R}'(1) & \mathbf{R}(0) & \cdots & \mathbf{R}(-P_1+2) \\ \cdot & \cdot & & \cdot \\ \cdot & \cdot & & \cdot \\ \cdot & \cdot & & \cdot \\ \mathbf{R}'(P_1-1) & \mathbf{R}(P_1-2) & \cdots & \mathbf{R}(0) \end{bmatrix} \begin{bmatrix} \mathbf{A}'^{(0)} \\ \mathbf{A}^{(1)} \\ \cdot \\ \cdot \\ \cdot \\ \mathbf{A}^{(P_1-1)} \end{bmatrix} = \begin{bmatrix} \mathbf{S}'^{(0)} \\ 0 \\ \cdot \\ \cdot \\ \cdot \\ 0 \end{bmatrix}$$

where

$$\mathbf{R}'(k) = \mathbf{R}'^T(-k) = \begin{bmatrix} R(k,-L_2) & R(k,-L_2-1) & \cdot & \cdot & R(k,-L_2-P_2+1) \\ R(k,-L_2+1) & R(k,-L_2) & \cdots & R(k,-L_2-P_2+2) \\ \cdot & \cdot & & \cdot \\ \cdot & \cdot & & \cdot \\ R(k,-L_2-P_2-1) & R(k,-L_2+P_2-2) & \cdots & R(k,0) \end{bmatrix} \quad \mathbf{A}^{(k)} = \begin{bmatrix} A_{k,L_2} \\ A_{k,L_2+1} \\ \cdot \\ \cdot \\ \cdot \\ A_{k,L_2-P_2-1} \end{bmatrix} \quad k \neq 0$$

and

$$\mathbf{R}'(0) = \begin{bmatrix} R(0,0) & R(0,-1) & \cdots & R(0,-L_2-P_2-1) \\ R(0,1) & R(0,0) & \cdots & R(0,-L_2-L_2-P_2+2) \\ \cdot & \cdot & & \cdot \\ \cdot & \cdot & & \cdot \\ \cdot & \cdot & & \cdot \\ R(0,L_2-P_2-1) & R(0,L_2-P_2-2) & \cdots & R(0,0) \end{bmatrix} \quad \mathbf{A}'^{(0)} = \begin{bmatrix} A_{0,0} \\ A_{0,1} \\ \cdot \\ \cdot \\ \cdot \\ A_{0,L_2-P_2-1} \end{bmatrix} \quad \mathbf{S}'^{(0)} = \begin{bmatrix} \Sigma_\epsilon \\ 0 \\ \cdot \\ \cdot \\ \cdot \\ 0 \end{bmatrix}$$

and where all other quantities are defined as in Fig. 3.3.

Fig. 3.6 Equations of linear prediction for NSHP support (forward predictor).

28

3.2 Autoregressive Models

If the error process $\epsilon(n_1, n_2)$ produced by linear prediction were white then one could obtain the original random process by inverse filtering. Specifically, by replacing $\epsilon(n_1, n_2)$ by a white noise $\mathbf{w}$ and solving Eq. (3.3) for $\mathbf{x}(n_1, n_2)$ we have

$$\mathbf{x}(n_1, n_2) = - \sum_{\substack{(i_1, i_2) \in \alpha \\ (i_1, i_2) \neq (0,0)}} A_{i_1 i_2}^T \underline{\mathbf{x}}(n_1 - i_1, n_2 - i_2) + \mathbf{w}(n_1, n_2) \qquad (3.15)$$

This is the multichannel 2-D autoregressive (AR) model. The white noise has a covariance

$$\Sigma_w = E\left[\mathbf{w}(n_1, n_2)\mathbf{w}^T(n_1, n_2)\right] \qquad (3.16)$$

Fig. 3.7 illustrates the relation between linear prediction and autoregressive modeling. While linear prediction uses an FIR filter, AR modeling employs a recursive or IIR filter.

Since the filter coefficients in an AR model satisfy Normal equations identical to those for linear prediction, there is a temptation to equate the two concepts. The distinction lies in the fact that linear prediction does not usually produce white noise. When one uses an AR model to represent an arbitrary random process and sets up Normal equations to solve for the filter coefficients, one is essentially ignoring the distinction. The justification for the white noise AR model can lie only in the belief that an AR model of some order is a close approximation to the true process. For a model with NSHP support it is true that the AR model becomes a close approximation to any given random process if the order becomes sufficiently large. This argument follows by generalization of results in Refs. 5 and 6 to the multichannel case.

3.3 Linear Prediction for Separable Problems

When the 2-D multichannel random process is separable, various simplifications result in the linear prediction problem. Because the correlation matrix is separable (see Section 2.3), the Normal equations (3.12) for linear prediction problems with rectangular support reduce to a set of lower-dimensional Normal equations. The results for a predictor with support in the first quadrant are summarized here.

When the correlation *within* channels is separable from the correlation *between* channels the covariance matrix $\widetilde{\widetilde{\mathbf{R}}}$ in (3.12) can be represented as the direct product of a between-channel covariance matrix $\mathbf{R}_c$ and a within-channel covariance matrix $\widetilde{\widetilde{\mathbf{R}}}_x$. In this case we can postulate a separable form for the matrices $\mathbf{A}$ and $\mathbf{S}$ and show that they provide a solution to the original Normal equations. In particular, we can write

$$(\mathbf{R}_c \otimes \widetilde{\widetilde{\mathbf{R}}}_x)(\mathbf{I}_M \otimes \mathbf{a}_x) = \left(\frac{1}{\sigma_x^2}\Sigma_\epsilon\right) \otimes \sigma_x^2 \iota_{N_1 N_2} \qquad (3.17)$$
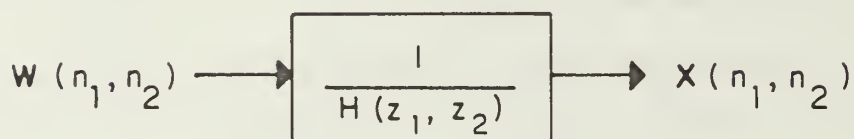
where $\mathbf{I}_M$ is the $M \times M$ identity matrix, $\mathbf{a}_x$ is an $N_1 N_2$-dimensional vector whose first component is 1, and $\iota_{N_1 N_2}$ is the $N_1 N_2$-dimensional vector $(1, 0, 0 \ldots, 0)^T$. Then (3.17) implies the two relations

$$\widetilde{\widetilde{\mathbf{R}}}_x \mathbf{a}_x = \sigma_x^2 \iota_{N_1 N_2} \qquad (3.18a)$$

29

$$X(n_1, n_2) \longrightarrow \boxed{H(z_1, z_2)} \longrightarrow \epsilon(n_1, n_2)$$
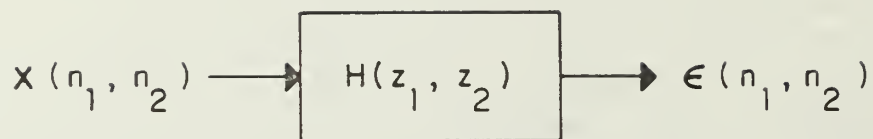
$$H(z_1, z_2) = \sum_{(i_1, i_2) \in \alpha} A^T_{i_1 i_2} z_1^{-i_1} z_2^{-i_2}$$

(a) Linear prediction

$$W(n_1, n_2) \longrightarrow \boxed{\frac{1}{H(z_1, z_2)}} \longrightarrow X(n_1, n_2)$$

(b) AR modeling

Figure 3.7   Linear prediction and AR modeling.

$$\Sigma_\epsilon = \sigma_x^2 \mathbf{R}_c \qquad (3.18b)$$

Since the solution of (3.12) is unique, this shows that it can be found from (3.18). The form of (3.17) indicates that each channel has the same filter coefficients $\mathbf{a}_x$ and that there are no between-channel terms. The parameters $\mathbf{a}_x$ and σ_x^2 are obtained by solving the Normal equations (3.18a) pertaining to a single channel 2-D problem. Then from (3.18b), the prediction error covariance for the 2-D multichannel problem is a scaled version of the between-channel covariance. The scale factor is the single channel prediction error variance.

Similar results can be obtained if the correlation matrix is separable along the n_1 and n_2 directions. In this case the correlation matrix can be represented by the direct product of a matrix $\mathbf{R}_B$ which relates to a 1-D multichannel process along the n_2 direction and a matrix $\mathbf{R}_A$ representing a 1-D single channel process along the n_1 direction (see Table 2.2). The postulated solution is of the form

$$(\widetilde{\mathbf{R}}_B \otimes \widetilde{\mathbf{R}}_A)(\mathbf{A}_B \otimes \mathbf{a}_A) = \left(\frac{1}{\sigma_A^2} \mathbf{S}^{(0)} \right) \otimes \sigma_A^2 \, \iota_{N_2} \qquad (3.19)$$

which implies

$$\widetilde{\mathbf{R}}_B \, \mathbf{A}_B = \frac{1}{\sigma_A} \mathbf{S}^{(0)} = \begin{bmatrix} \mathbf{E}_{P_1} \\ 0 \\ \vdots \\ 0 \end{bmatrix} \qquad (3.20a)$$

$$\widetilde{\mathbf{R}}_A \, \mathbf{a}_A = \sigma_A^2 \, \iota_{N_1} \qquad (3.20b)$$

Equation (3.20a) is a set of Normal equations for a 1-D multichannel problem which we solve for the prediction matrices $\mathbf{A}_B$ and the prediction error covariance $\mathbf{E}_{P_1}$. Equation (3.20b) represents Normal equations for a 1-D single channel problem that we solve for the filter parameters $\mathbf{a}_A$ and the prediction error variance σ_A^2. The solution of these two sets of Normal equations then allows us to compute the filter coefficients as $\mathbf{A}_B \otimes \mathbf{a}_A$ and the error covariance as

$$\Sigma_\epsilon = \sigma_A^2 \, \mathbf{E}_{P_1} \qquad (3.21)$$

In the case where the covariance matrix in (3.12) is completely separable, along rows and columns and between channels, we have $\widetilde{\widetilde{\mathbf{R}}} = \mathbf{R}_C \otimes \widetilde{\mathbf{R}}_B \otimes \widetilde{\mathbf{R}}_A$. Then we are led to the two 1-D single channel subproblems

$$\widetilde{\mathbf{R}}_A \, \mathbf{a}_A = \sigma_A^2 \, \iota_{N_1} \qquad (3.22a)$$

$$\widetilde{\mathbf{R}}_B \, \mathbf{a}_B = \sigma_B^2 \, \iota_{N_2} \qquad (3.22b)$$

and the 2-D multichannel parameters are computed from

$$\mathbf{A} = \mathbf{I}_M \otimes \mathbf{a}_B \otimes \mathbf{a}_A \qquad (3.23a)$$

$$\Sigma_\epsilon = \sigma_A^2 \, \sigma_B^2 \, \mathbf{R}_C \qquad (3.23b)$$

31

The decomposition into lower-order linear prediction problems discussed here would seem to be restricted to the case where the multichannel 2-D random process is separable. In actuality, a decomposition of the multichannel 2-D linear prediction problem into lower-order problems exits in general where there is no separability. This is discussed in the next section. A difference arises however in that the lower-order subproblem for the general case involves an expanded multichannel problem. In addition, we are guaranteed in the separable case, that if the correlation matrix in (3.12) has doubly block Toeplitz structure, the correlation matrices of each of the subproblems will have Toeplitz or block Toeplitz structure. In the general case the Normal equations for the subproblems do *not* all involve correlation matrices with Teoplitz structure, even if the matrix in (3.12) has the required doubly block Toeplitz form.

3.4 Relation Between Multidimensional and Multichannel Linear Prediction

There is a close relation between single channel 2-D linear prediction problems and multichannel 1-D linear prediction problems [7]. More general results exist that show that multidimensional linear prediction problems of any dimension can be decomposed into a series of 1-D multichannel and single channel linear prediction problems [8]. Some specific results will be discussed here that show how 2-D multichannel problems relate to higher order 1-D multichannel problems. These results will be used in the next section to formulate a method for estimation of the 2-D multichannel model parameters without explicit prior estimation of the correlation function.

Fig. 3.8 illustrates a multichannel 2-D linear prediction problem with first quadrant support (a) and the corresponding multichannel 1-D linear prediction problem (b). The Normal equations for the multichannel 2-D problem are given by Eqs. (3.12), (3.13) and (3.10). The structure of the equations is further detailed in Fig. 3.3.

In Fig. 3.8(b) the data is regarded as an array of $P_2 M$ channels of 1-D signals evolving along the n_1 direction. The term $\underline{x}_n$ used in the index-ordered representation of the 2-D data corresponds to the signals in this array of channels. The 1-D $P_2 M$-channel linear prediction problem can then be written as

$$\hat{\underline{x}}_n = - \sum_{i=1}^{P_1 - 1} \left(\alpha^{(i)} \right)^T \underline{x}_{n-1} \tag{3.24}$$

where $\underline{x}_n$ is the $P_2 M$-dimensional data vector and $\hat{\underline{x}}_n$ is its estimate. The coefficients $\alpha^{(i)}$ have the form

$$\alpha^{(i)} = \begin{bmatrix} \alpha_{00}^{(i)} & \alpha_{01}^{(i)} & \cdots & \alpha_{0,P_2-1}^{(i)} \\ \alpha_{10}^{(i)} & \alpha_{11}^{(i)} & \cdots & \alpha_{1,P_2-1}^{(n)} \\ \vdots & \vdots & & \vdots \\ \alpha_{P_2-1,0}^{(i)} & a_{P_2-1,1}^{(i)} & \cdots & \alpha_{P_2-1,P_2-1}^{(i)} \end{bmatrix} \tag{3.25}$$

(a)   2-D data

1st prediction direction

2nd prediction direction
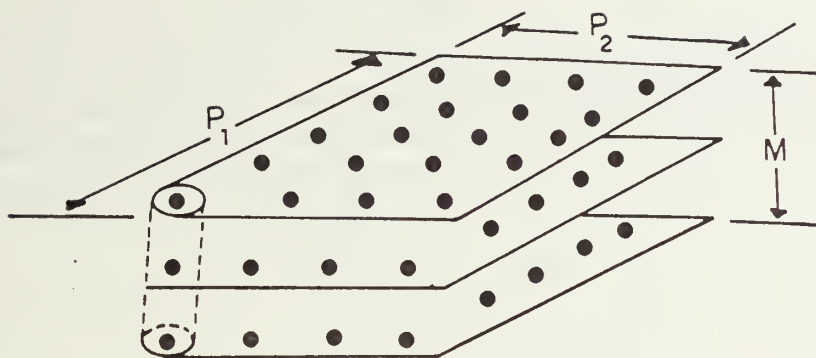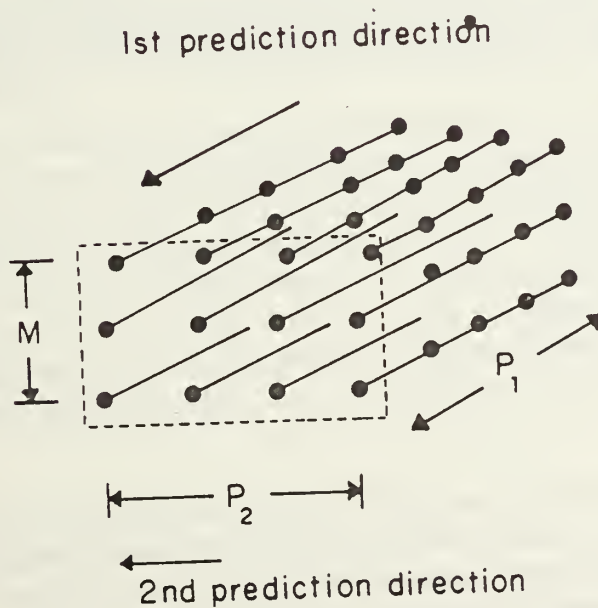
(b)   Multichannel data

Figure 3.8   Multichannel 2-D linear prediction and related multichannel 1-D problem.

33

where each block $\alpha_{kl}^{(i)}$ is of size $M \times M$. The $\alpha^{(n)}$ are found by solving the equation

$$\tilde{\tilde{R}} \, \alpha_{P_1} = \tilde{\tilde{R}} \begin{bmatrix} I \\ \alpha^{(1)} \\ \vdots \\ \alpha^{(P_1-1)} \end{bmatrix} = \begin{bmatrix} E_{P_1} \\ 0 \\ \vdots \\ 0 \end{bmatrix} \tag{3.26}$$

where E_{P_1} is the $P_2 M \times P_2 M$ prediction error covariance and where the correlation matrix appearing on the left side of (3.26) is the same as that in (3.12). Now post mulitply both sides of Eq. (3.26) by the term $A^{(0)}$ and compare the result to Eq. (3.12). In view of Eqs (3.10) and (3.13), Eq. (3.26) will be identical to Eq. (3.12) if we require

$$E_{P_1} A^{(0)} = S^{(0)} \tag{3.27}$$

and

$$A^{(i)} = \alpha^{(i)} A^{(0)} \quad ; \; i = 0, 1, \ldots, P_1 - 1 \tag{3.28}$$

The foregoing equations show that the multichannel 2-D Normal equations can be solved by the following steps. First solve the $P_2 M$-dimensional 1-D multichannel problem (3.26). Since this problem is 1-D, the multichannel Levinson recursion can be employed to find the coefficient matrices $\alpha^{(n)}$ and the prediction error covariance matrix E_{P_1}. Next solve (3.27) for $A^{(0)}$. this is also a set of 1-D Normal equations although the matrix E_{P_1} is not in general Block Teoplitz. Finally find the multichannel 2-D coefficients from (3.28).

Since the multichannel 2-D coefficients are expressed as a product of terms in (3.28), we have the following interpretation of the multichannel 2-D linear prediction problem. The multichannel 2-D prediction error can be computed by first predicting the data along the direction shown in Fig. 3.8(b). This is a 1-D linear prediction problem and results in a $P_2 M$- dimensional prediction error vector corresponding to the array of $P_2 M$ channels shown in the figure. This prediction error is itself filtered in the second direction to compute the M-dimensional prediction error vector for the 2-D problem. The Normal equations solved to obtain the filter coefficients for this second linear prediction problem are represented by (3.27).

This view of multichannel 2-D linear prediction has one further interesting aspect. If the multichannel Levinson recursion is used to solve (3.26), both forward and backward 1-D linear prediction parameters are generated as part of the recursion. By arguments similar to those presented above, the backward 1-D parameters can be shown to relate to the coefficients for the second quadrant 2-D filter. Thus an algorithm based on the multichannel Levinson recursion can be used to solve for both the first and second quadrant filter coefficients simultaneously. This will be shown to be of particular use for the spectrum estimation problem considered in Chapter IV.

3.5 A Direct Method for AR Parameter Estimation

The connection between multidimensional and multichannel linear prediction suggests a method for estimating the AR model parameters. This method will be called a direct method since it does not require prior estimation of the correlation function.

Our method capitalizes on the existance of a direct method for solving the 1-D multichannel linear prediction problem. We will refer to the 1-D method as the multichannel Burg algorithm since it is based on ideas originally suggested by Burg [9]. Details of the method however were developed separately by Nuttal [10] and Strand [11]. The multichannel Burg algorithm is described in Appendix D.

In order to apply the multichannel Burg algorithm to 2-D data, the data is first partitioned into strips along the n_2 direction as shown in Fig. 3.9(a). The strips of width P_2 for an $P_1 \times P_2$ quadrant filter are catenated along the n_1 direction as shown in Fig. 3.9(b). As in the previous section this data is considered to be a 1-D process (in the n_1 direction) with $P_2 M$ channels. The multichannel Burg algorithm is then used to estimate forward and backward linear prediction parameters (including the error covariances). This procedure makes no explicit estimate for the correlation matrix. Discontinuities where the strips were catenated together are ignored since they represent only a small portion of the data. The error covariance matrices that are computed as part of the multichannel Burg procedure are used to form (3.27) and an analogous equation for the backward case. These equations are solved by conventional methods and the multichannel 2-D parameters are computed from (3.28) and its analog for the backward case. This completes the 2-D estimation procedure.
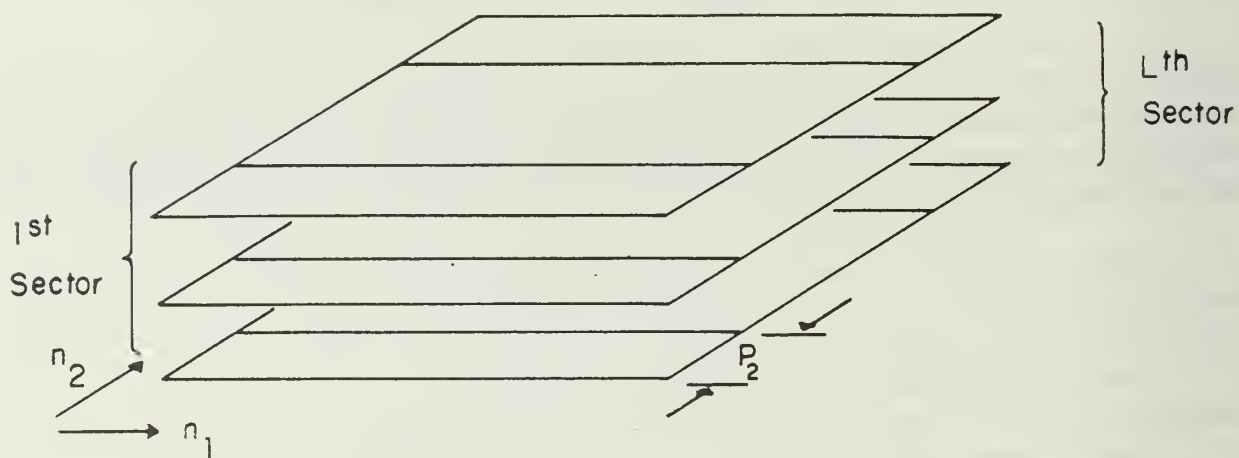
(a) 2-D data organization
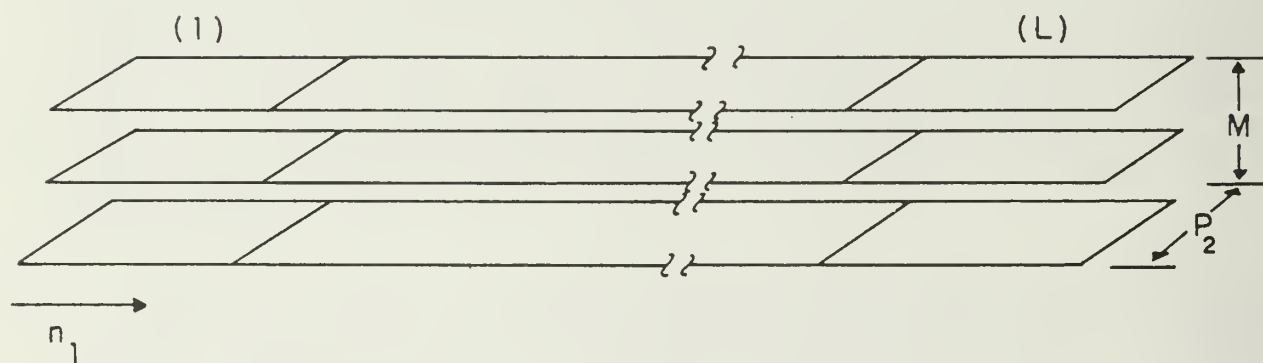
(b) Multichannel data organization

Figure 3.9 Sectioning data for the direct method of AR parameter estimation

IV. Multichannel 2-D Spectrum Analysis

4.1 Spectrum Estimation Models

Parametric or model-based approaches to spectrum estimation are based on a model for the spectrum involving a finite and relatively small number of unknown parameters. These parameters can be estimated from the data and used in a formula that gives the spectrum of the model in terms of the parameters.

Autoregressive modeling is one form of spectrum estimation that will be examined here. A model of the form of Fig. 3.7(b) is used to represent the data. Filter parameters and the white noise covariance are estimated by the techniques described in Chapter III. Since the input spectrum is assumed to be that of white noise, a formula based on Eq. (2.25) can be used to compute the spectrum. If

$$H_z(z_1, z_2) = \sum_{(\ell_1, \ell_2) \in \alpha} A_{\ell_1, \ell_2}^T z_1^{-\ell_1} z_2^{-\ell_2} \tag{4.1}$$

and the output is assumed to be white noise with constant spectral matrix Σ_W, then the spectrum estimate is given by

$$\begin{aligned}
S(\omega_1, \omega_2) &= H_\omega^{-1}(\omega_1, \omega_2) \Sigma_W \, H_\omega^{*T^{-1}}(\omega_1, \omega_2) \\
&= H_z^{-1}(z_1, z_2) \Sigma_W \, H_z^{T^{-1}} \left(z_1^{-1}, z_2^{-1}\right) \big|_{\substack{z_1 = e^{j\omega_1} \\ z_2 = e^{j\omega_2}}}
\end{aligned} \tag{4.2}$$

Note that this results in an estimation of the entire spectrum matrix i.e., all of the auto spectra and cross spectra at once (see Eq. (2.21) and Appendix A). If desired, normalized quantities such as the magnitude squared coherence can be computed from the elements of the spectral matrix (see Eq. (2.22) and Appendix A).

Various spectrum estimates can be obtained by assuming different support for the AR model. These are discussed below.

4.1.1 Non-symmetric Half Plane Models

Non-symmetric half plane models are a suitable choice for the spectrum estimation since arbitrary 2-D spectra can be factored into sections with infinite extent nonsymmetric half plane support [5]. Although any practical algorithm cannot use infinite or even very large support regions, nonsymmetric half plane models of moderate size have proven to give reasonable results for spectrum estimation. An interesting fact is that it is unnecessary to consider the forward and backward predictors of Fig. 3.5(a) and (b) spearately. While these filters have *different* parameters, the white noise covariance is related such that formula (4.2) gives theoretically *identical* spectrum estimates. In subsequent sections of this chapter we examine results of NSHP spectral models of various orders. The definition of order used for NSHP models is depicted in Fig. 4.1.

1st ORDER

4 MATRIX
PARAMETERS

2nd ORDER

12 MATRIX
PARAMETERS
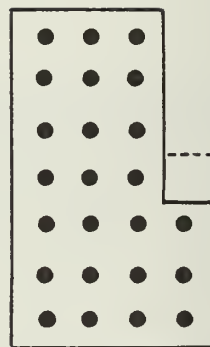
3rd ORDER

24 MATRIX
PARAMETERS

Figure 4.1 Definition of order for NSHP models.

4.1.2 Quadrant Models

AR models with first or second quadrant support are of interest primarily because of their convenience of computation and estimation of the model parameters. The third and fourth quadrant filtes, are also distinct but when they are used in (4.2) with their corresponding white noise covariance they give estimates identical to those of the first and second quadrant filters. A method for estimating the model parameters directly from the data without prior explicit estimation of the covariance function was described in Section 3.5.

It will be seen that first and second quadrant AR models when used individually give poor estimates of the spectrum of many random processes. Features of the spectrum such as peaks tend to be displaced in frequency and elongated in one direction. However a certain combination of the models has proven to give good results for estimation of spectra in 2-D single channel problems [Jackson & Chien [12]]. We propose here a generalization of this method to 2-D multichannel spectrum estimation. A combined spectrum estimate is computed from

$$S(\omega_1, \omega_2) = 2 \left(S_I^{-1}(\omega_1, \omega_2) + S_{II}^{-1}(\omega_1, \omega_2) \right)^{-1} \tag{4.3}$$

where S_I and S_{II} are the spectra corresponding to AR models with first and second quadrant support. From Eqs. (4.3) and (4.2) one can therefore write

$$S(\omega_1, \omega_2) = 2 \left(H_I^{*^T}(\omega_1, \omega_2) \Sigma_{W_I}^{-1} H_I(\omega_1, \omega_2) + H_{II}^{*^T}(\omega_1, \omega_2) \Sigma_{W_{II}}^{-1} H_{II}(\omega_1, \omega_2) \right)^{-1} \tag{4.4}$$

In the special case that the noise is normalized so that $\sum_{W_I} = \sum_{W_{II}} = I$ Eq. (4.4) has the simpler form

$$S(\omega_1, \omega_2) = 2 \left(H_I^{*^T}(\omega_1, \omega_2) H_I(\omega_1, \omega_2) + H_{II}^{*^T}(\omega_1, \omega_2) H_{II}(\omega_1, \omega_2) \right)^{-1} \tag{4.5}$$

This form is analagous to the form proposed by Jackson and Chien for the single channel case.

4.2 Resolution and Phase Estimation Experiments (Sinusoids in Noise Background)

Simulated multichannel 2-D random signals consisting of sinusoids with various relative phases and frequencies in noise backgrounds were generated. This section presents estimated spectra of these random fields.

4.2.1 Comparison of NSHP and Quadrant Modeling

Here we discuss the estimation of a sinusoid in noise background and compare the results of NSHP modeling to quadrant modeling. Three numerical examples are presented which illustrate the results.

Example 1

This example is concerned with the analysis of spectra for a two-channel 2-D single sinusoid signal with different phase in additive noise. The signals generated in channels 1 and 2 were

$$x_1(n_1, n_2) = \cos(n_1\omega_1 + n_2\omega_2) + w_1(n_1, n_2)$$

$$x_2(n_1, n_2) = \cos(n_1\omega_3 + n_2\omega_4 + \phi) + w_2(n_1, n_2)$$

where $w_1(n_1, n_2)$ and $w_2(n_1, n_2)$ are zero-mean independent white noise signals. Spectrum estimation results are given for a data set size of 64 x 64, and a third order NSHP filter. Two cases are considered in this example. In the first case we suppose that, the two channels have the same frequency, but different phase

$$\left(\omega_1 = \omega_2 = \frac{\pi}{2}, \omega_3 = \omega_4 = \frac{\pi}{2} \phi = 1 \text{ radian}\right),$$

while in the second case, we assume two channels with different frequency and different phase:

$$\left(\omega_1 = \omega_2 = \frac{\pi}{2}, \omega_3 = \omega_4 = \frac{\pi}{3} \text{ and } \phi = 1 \text{ rad}\right),$$

Fig. 4.2 shows the results for the components of the 2 x 2 spectrum matrix in the first case. Only the cross term $S_{12}(\omega_1, \omega_2)$ is shown (magnitude and phase) since the term $S_{21}(\omega_1, \omega_2)$ is theoretically and numerically identical. The results show a distinct peak in each of the three components S_{11}, S_{12}, S_{22} corresponding to the location of the sinusoid. The center of the peak is accurately located near $(\pi/2, \pi/2)$. Although the phase of the cross spectrum shows various artifacts around the edge of the region (where the magnitude is small and the phase is that of the noise) the phase at the location of the sinusoid is accurately estimated.

Fig. 4.3 shows $S(\omega_1, \omega_2)$ for the second case (different frequency). The power spectrum estimates of the first and second channels $S_{11}(\omega_1, \omega_2)$ as $S_{22}(\omega_1, \omega_2)$ have a single-peak at the location of the sinusoid. Although the cross spectra should theoretically show no presense of sinusoids some small amount of energy is detectable at those frequencies in the cross spectrum. Similar effects have been observed in 1-D multichannel spectrum estimation and have been attributed to non exact pole-zero cancellations in the estimate for the cross spectrum [13].
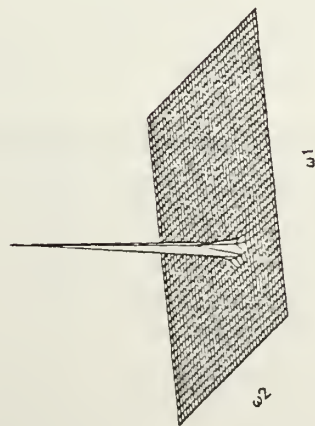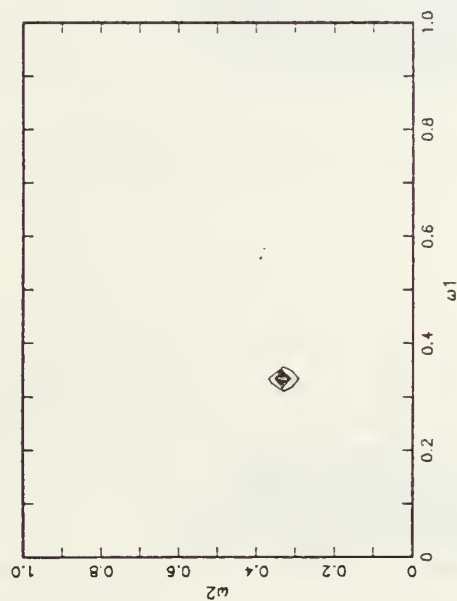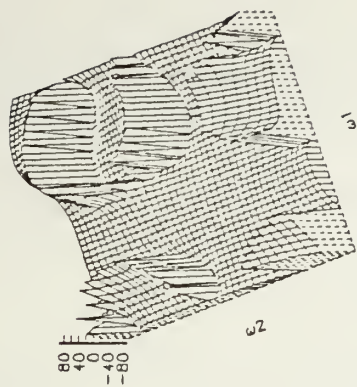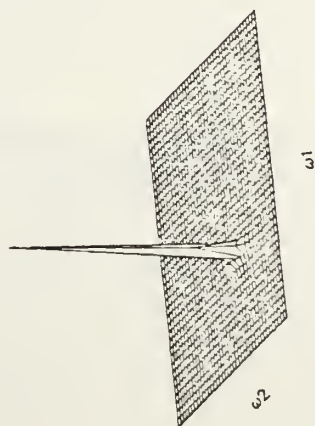
Figure 4.2 Estimate of spectra for sinusoids of same frequency but different phase (NEHP model).
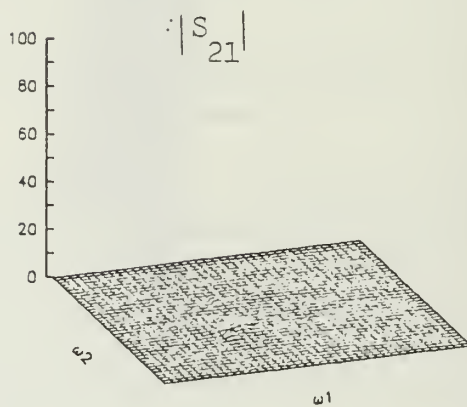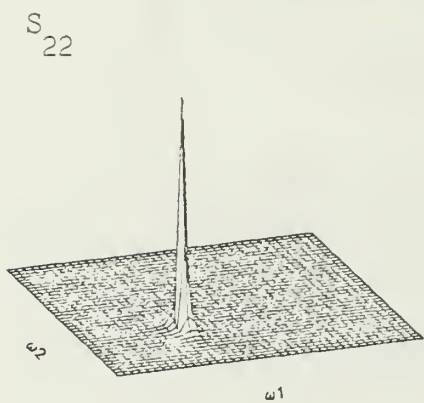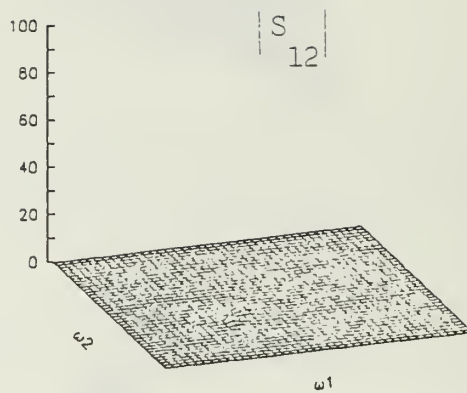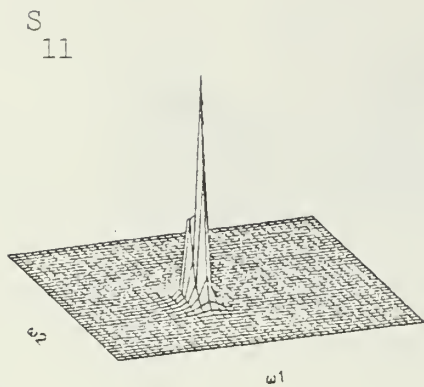
Figure 4.3   Estimate of spectra for sinusoids of different frequency
(NSHP model).

<u>Example 2:</u>

Two-channel 2-D signals with two sinusoids in additive noise are considered in this example. The signals in the channels are defined by

$$x_1(n_1, n_2) = \cos(n_1\omega_1 + n_2\omega_2) + \cos(n_1\omega_3 + n_2\omega_4) + w_1(n_1, n_2)$$
$$x_2(n_1, n_2) = \cos(n_1\omega_1 + n_2\omega_2 + \phi_1) + \cos(n_1\omega_3 + n_2\omega_4 + \phi_2)$$
$$+ w_2(n_1, n_2)$$

The results are presented here for the following data: $w_1(n_1, n_2)$ and $w_2(n_1, n_2)$ are independent zero-mean white noise signals, the frequencies and phases are $\omega_1 = \omega_2 = \frac{\pi}{2}, \omega_3 = \omega_4 = \frac{\pi}{3}$, and $\phi_1 = \phi_2 = 1$ radian and the data set size is 64 x 64.

The power spectrum estimation results for a second order NSHP model are given in Fig. 4.4. The results are close to the theoretical results. $S_{11}(\omega_1, \omega_2)$ and $S_{22}(\omega_1, \omega_2)$ shows that the two sinusoids are easily resolved. The estimated amplitudes are unequal, but this characteristic has been observed in even 1- D AR spectrum estimates. The cross-spectrum $S_{12}(\omega_1, \omega_2)$ shows the sinusoids resolved and the phase estimate is close to the true phase of 1 radian.

<u>Example 3:</u>

Three sinuosids in each channel are considered in this example. The location of the sinusoids is shown in Fig. 4.5. Observe that the phase of the sinusoids in channel 2 differ from those in channel 1 by 1 radian. The sinusoids are imbedded in white noise as in the previous examples. Again a data set of size 64 x 64 was used.

Fig. 4.6 shows the results of spectrum estimation using a fourth order NSHP model. The results show good estimation of the position of the sinusoids in the autospectra and the cross spectra and there is almost no evidence of energy from sinusoids ω_B and ω_D appearing in the spectrum of the opposite channel or in the cross spectrum. The phase of the cross spectrum in the region where the sinusoids are located is nearly constant with a correct value of 1 radian.

Spectrum estimates for Examples 1 and 2 were also computed using quadrant plane models. The estimates were based on 2 x 2 regions of support for the first and second quadrant filters. Fig. 4.7(a) shows the component S_{11} of the spectral matrix. Results for S_{22} are similar. The use of either the first of second quadrant filter alone results in a spreading of the peak in one direction. The combined estimate (Eq. (4.3)) gives a more accurate result similar to that of the NSHP model. Fig. 4.7(b) shows the magnitude and phase estimates for the cross spectrum S_{12}. A similar spreading phenomenon is observed in the magnitude estimate but the estimation of phase is correct for both the individual and the combined spectrum estimates.
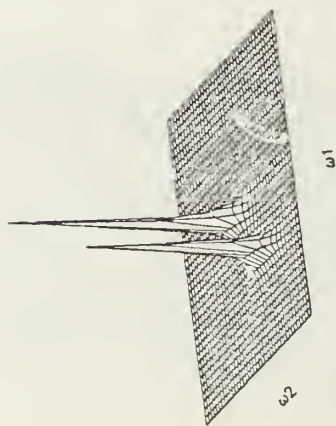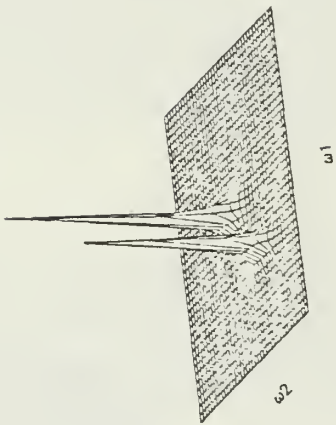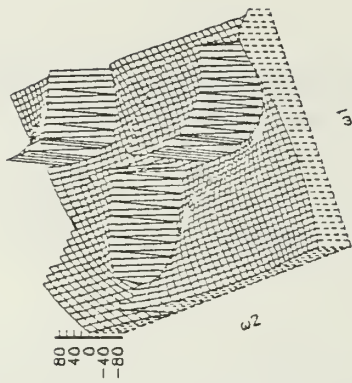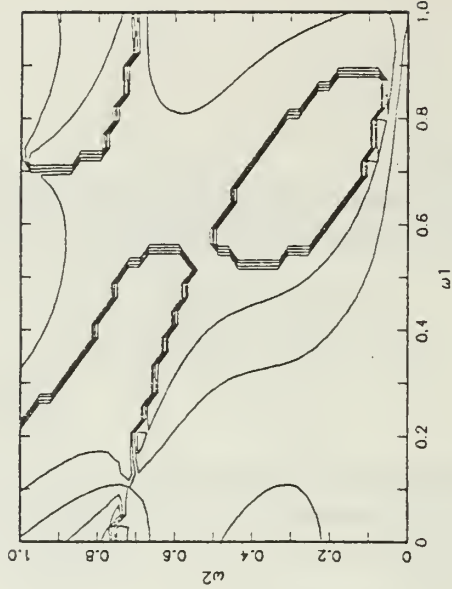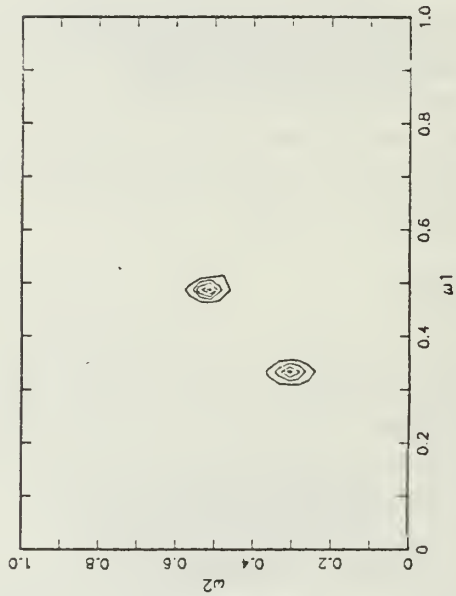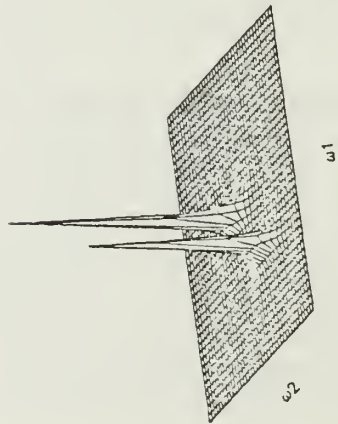
Figure 4.4 Estimation of two sinusoids in white noise (NSHP model).

- 44 -
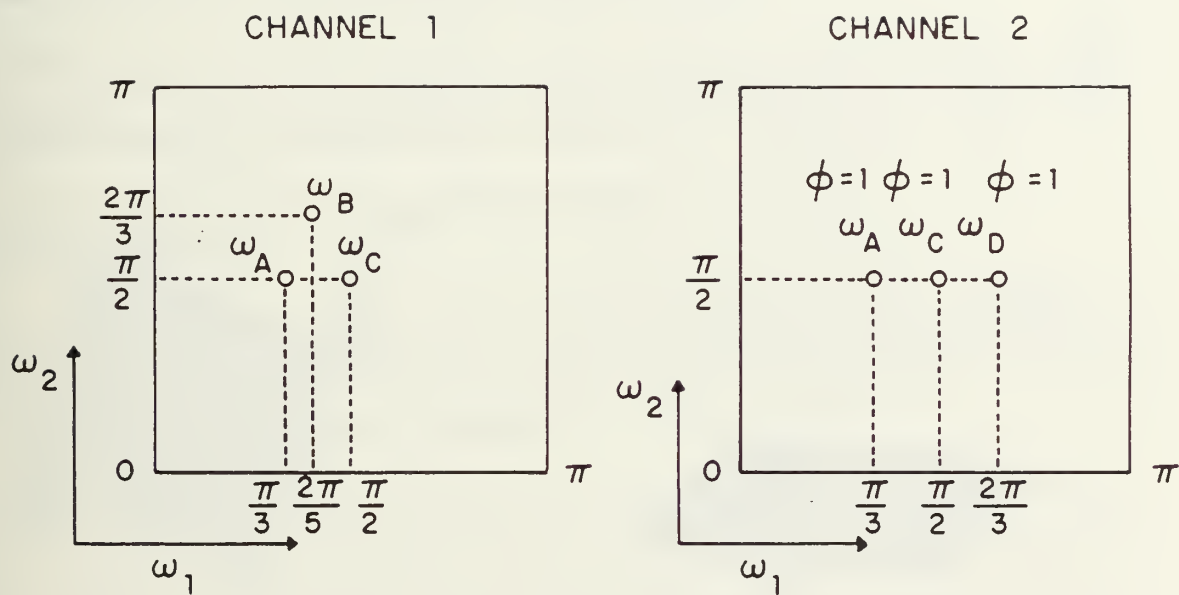
Channel 2 tones have a phase difference of 1 radian with respect to
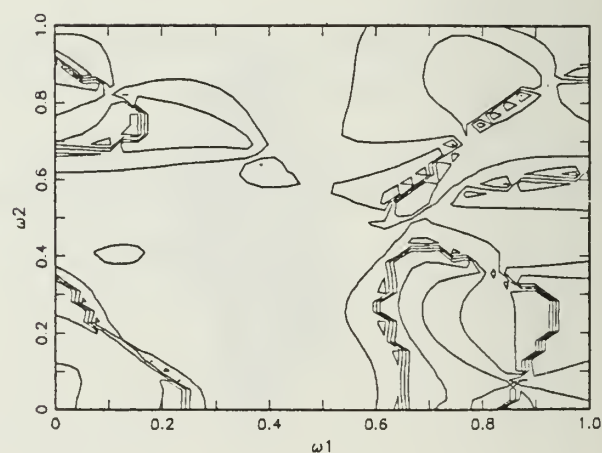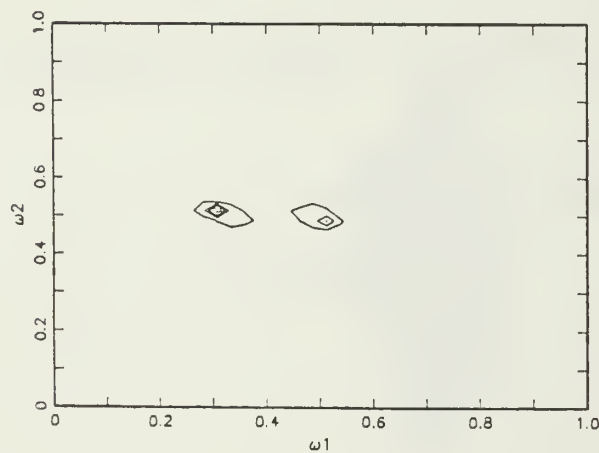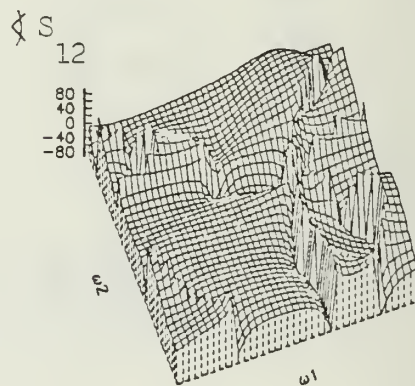Channel 1 tones
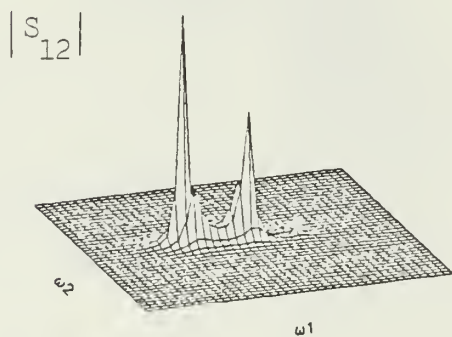
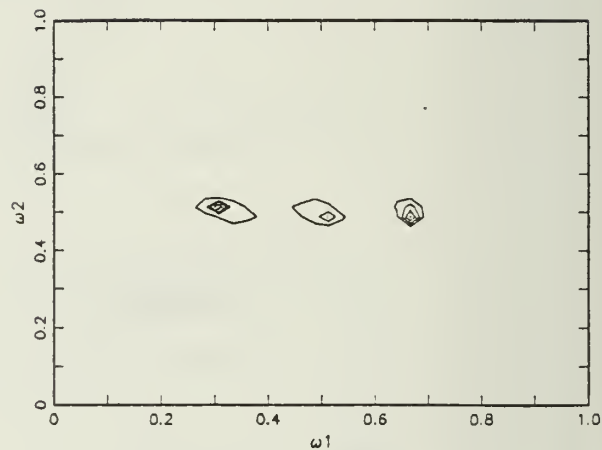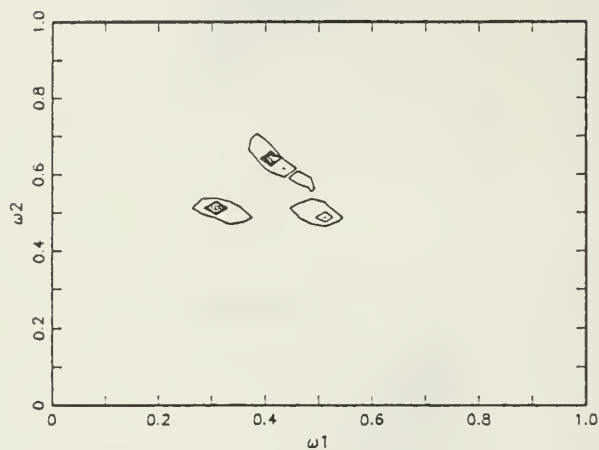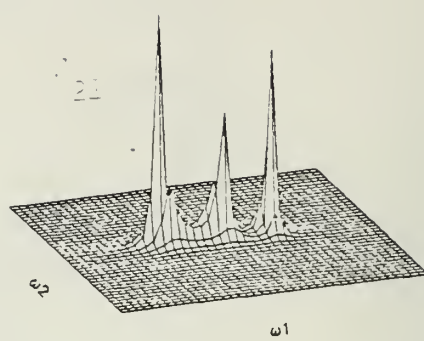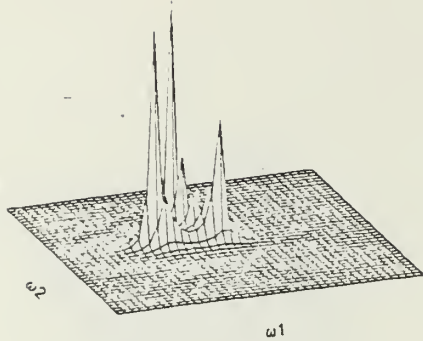Figure 4.5   Location of sinusoids for example 3.

Figure 4.6 Estimation of three sinusoids in noise (NSHP model).

Fig. 4.8 shows the spectrum estimate for two sinusoids in white noise corresponding to Example 2. In this case the phases ϕ_1 and ϕ_2 were taken to be unequal and given values of 1.5 and 0.5 radians respectively. The results of this quadrant based model can be qualitatively compared to the results for the NSHP model of Fig. 4.4. The placement of the sinusoid along a diagonal shows some characteristics of the quadrant models. The first quadrant results show a very significant spreading of the peaks along a direction orthogonal to the line connecting their centers. This is observed in both the autospectral components and the cross spectra. The second quadrant estimates show good resolution with little spreading of the peak. However the combined estimate gives the best results with sharp peaks and with magnitudes more nearly equal than those observed with the NSHP model. The phase in Fig. 4.8(c) is slowly varying in the region of the sinusoids for all of the estimates with a correct values of approximately 1.5 and 0.5 radians at the locations of the sinusoids. (Exact values produced by the combined estimate are 1.42 and 0.57 radians respectively.)

These experiments indicate that the result of spectrum estimation using a single quadrant model is not generally reliable but the estimate resulting from combining the two models according to Eq. (4.3) is quite accurate.

4.2.2 Model order, Data Set Size, and Signal-to-Noise Ratio Experiments

A comprehensive set of experiments was performed to determine performance of the spectrum estimation procedures as a function of model order, data set size, and signal-to-noise ratio. The results are briefly summarized here. More detailed description of the results will be reported separately.

The results of the model order and data set size experiments showed that to some extent the lack of resolution resulting from a small data set size could be compensated for by choosing a larger model order. There is a limit to this trade-off however since a larger model has more parameters and thus should require more data to estimate parameters that are statistically reliable. The experimental observation may be better restated in the following way. When the data set is large a smaller order model can produce results that are comparable to a large model.
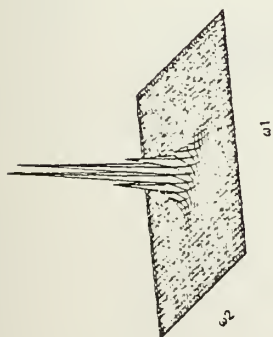
The case of two sinusoids in noise (Example 2) was repeated for smaller size data sets using a NSHP model. For a second order filter the results of spectrum estimation using a 32 × 32 point data set were essentially the same as those using the 64 × 64 point data set reported above. For smaller data sets the results degraded considerably. However the resolution obtained using a second order NSHP filter on a 16 × 16 point data set was similar to that obtained with a third order filter on an 8 × 8 point data set. These results for the cross spectrum are shown in Fig. 4.9. Results for the autospectra are similar. Note in Fig. 4.9 that although the amplitude of the estimate varies in the three cases depicted, the phase remains essentially constant.
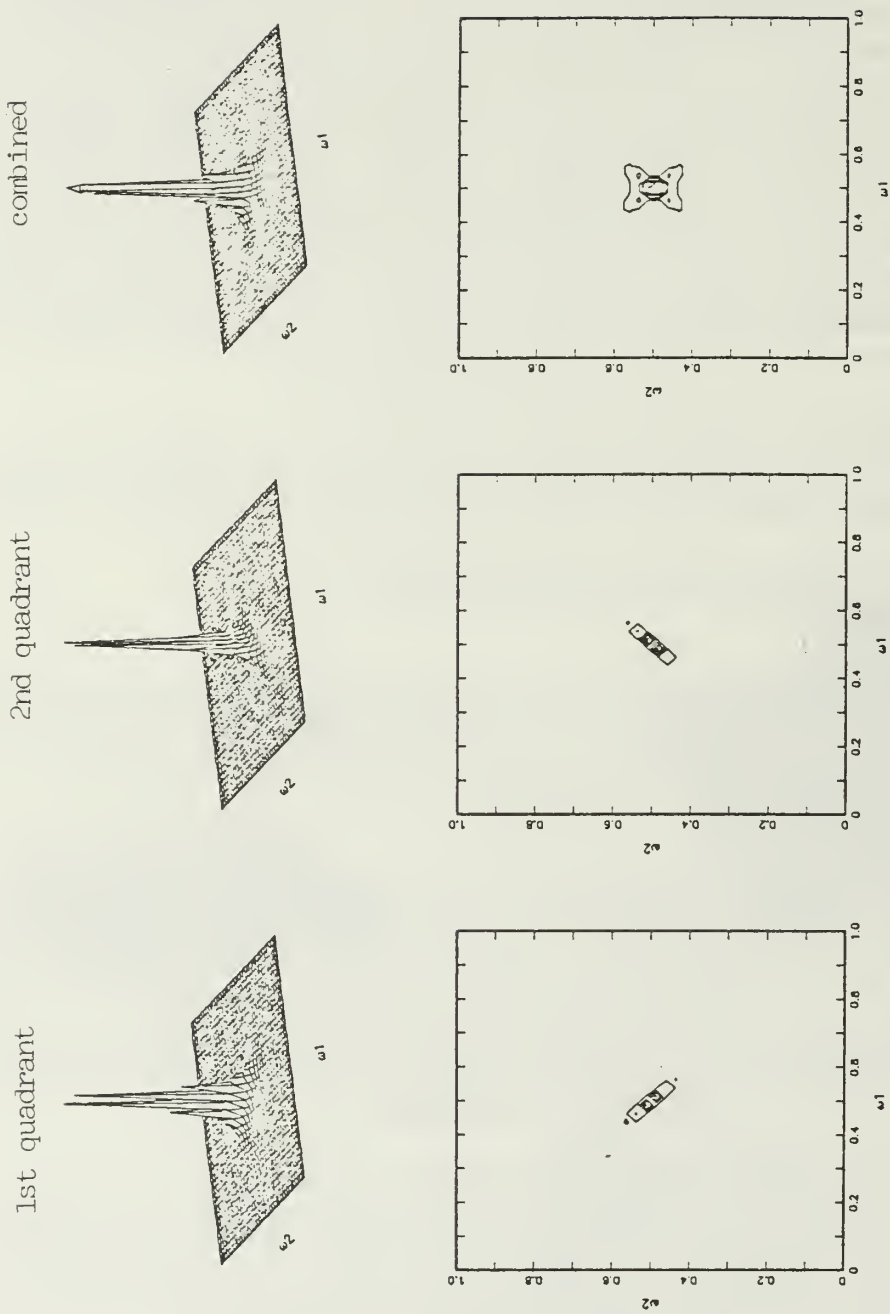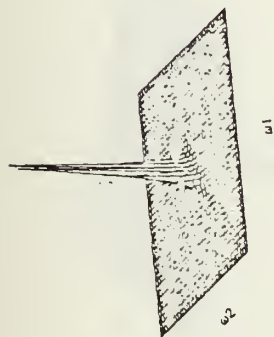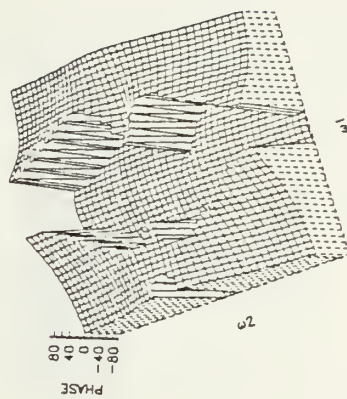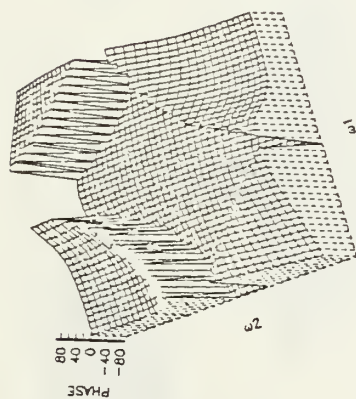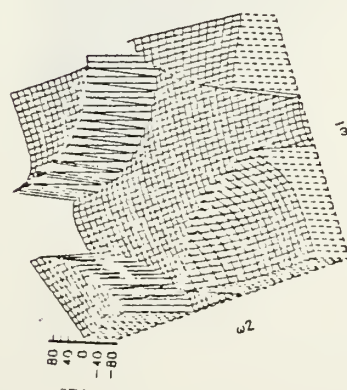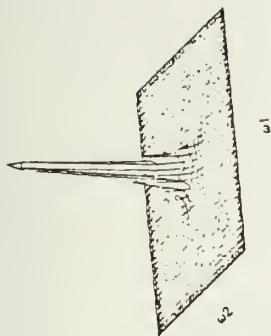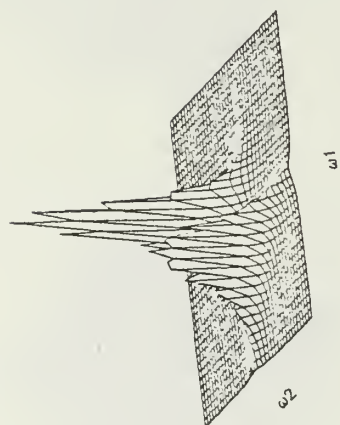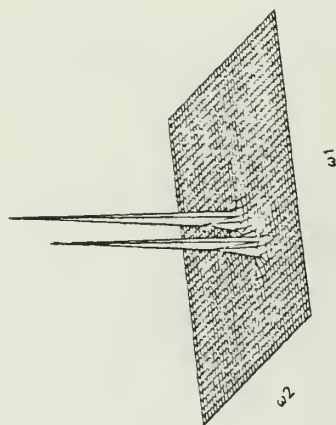
1st quadrant　　2nd quadrant　　combined

(a) S_{11}

Figure 4.7 Estimation of single sinusoid using quadrant models.

combined

2nd quadrant

1st quadrant

amplitude

phase

PHASE 80 40 0 -40 -80

PHASE 80 40 0 -40 -80

80 40 0 -40 -80

ω2

ω2

ω2

ω1

ω1

ω1

ω2

ω2

ω2

ω1

ω1

ω1

(b) S_{12}

Figure 4.7 Estimation of single sinusoid using quadrant models. (cont'd)

SECOND QUADRANT

FIRST QUADRANT

COMB.

ω1

ω2

Figure 4.8 Estimation of two sinusoids using quadrant models.
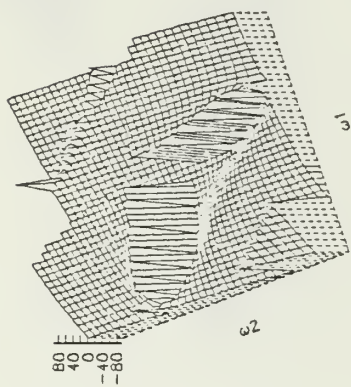
(a) S_{11}

SECOND QUADRANT

FIRST QUADRANT
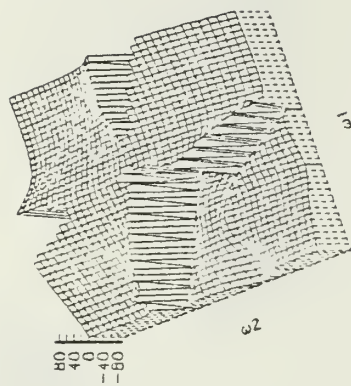
COMB.

$(b) \left| S_{12} \right|$

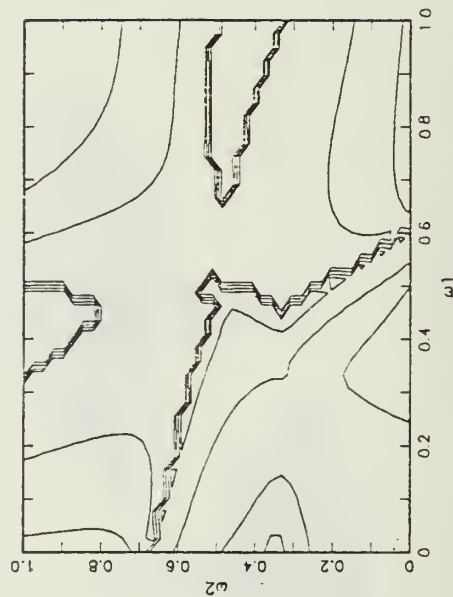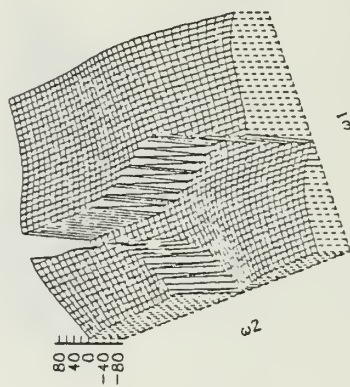Figure 4.8 Estimation of two sinusoids using quadrant models.   (cont'd)

- 51-

COMB

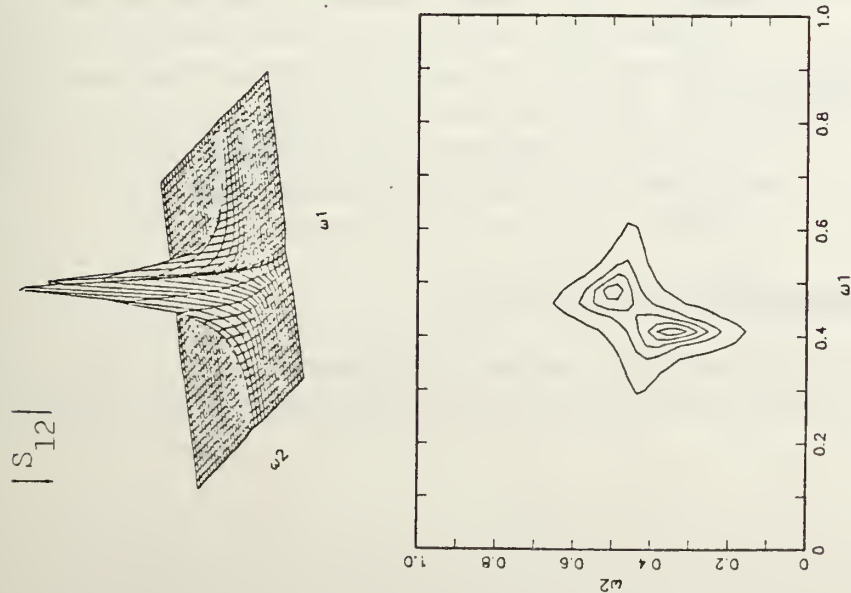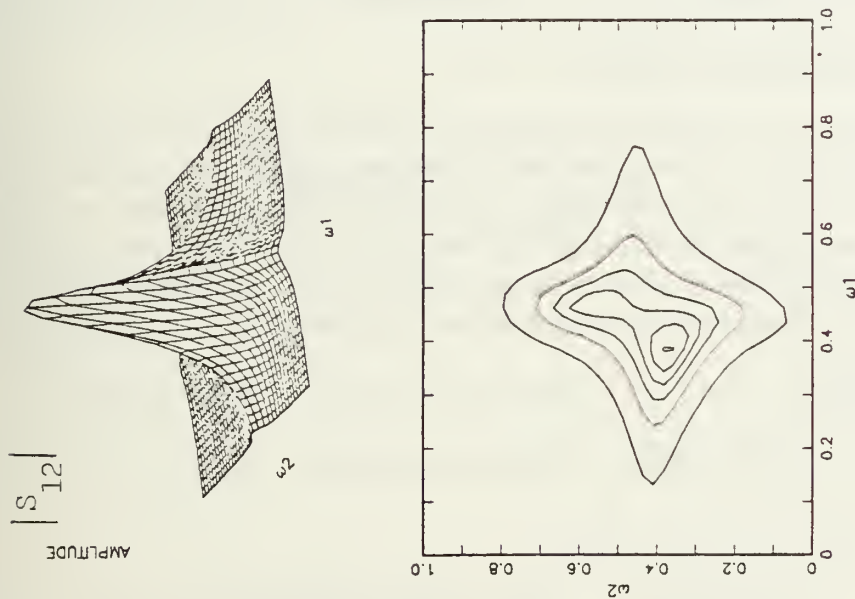FIRST QUADRANT

SECOND QUADRANT
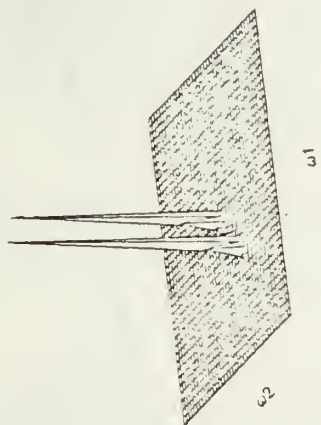
(c) $\hat{S}_{12}$
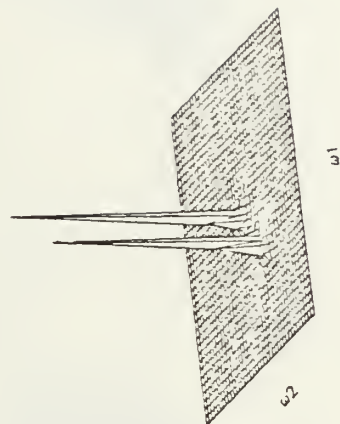
Figure 4.8 Estimation of two sinusoids using quadrant models.   (cont'd)
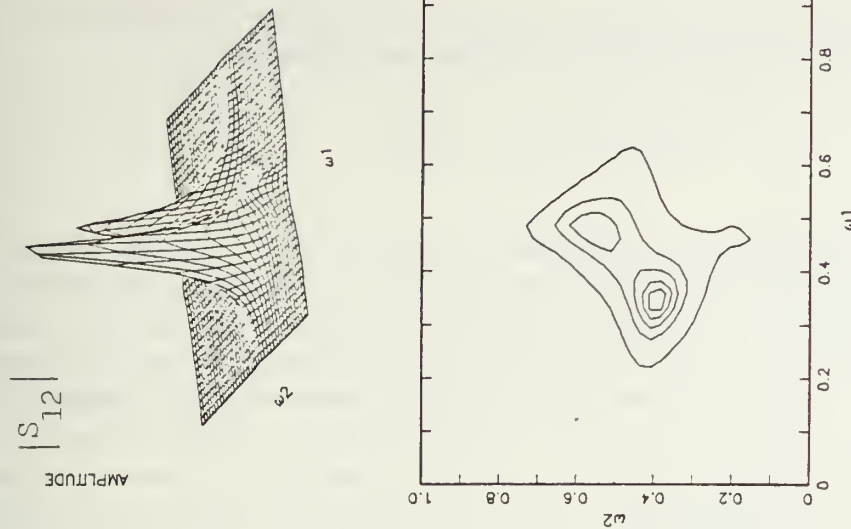
Figure 4.9 Effects of model order and data set size.

10 X 10 2nd ord.   8 X 8 2nd ord.   8 X 8 3rd ord.

$|S_{12}|$ $|S_{12}|$ $|S_{12}|$

$\emptyset_1 = 1.01918$ rad $\emptyset_1 = 0.9586$ rad $\emptyset_1 = 0.9605$ rad

$\emptyset_2 = 0.9723$ rad $\emptyset_2 = 1.0572$ rad $\emptyset_2 = 1.0391$ rad

The signal-to-noise ratio for sinusoids in noise was defined by

$$SNR = 10 \log_{10} \left(\frac{A^2}{\sigma^2} \right) \tag{4.6}$$

where A is the amplitude of each sinusoidal component and σ^2 is the white noise variance (chosen to be the same for each channel). Fig. 4.10 shows results of the cross spectrum estimation for a 64×64 data set with closely spaced sinusoids of frequencies $\omega_1 = \omega_2 = \pi/2$ and $\omega_1 = \omega_2 = \frac{2\pi}{5}$. the model used for these experiments was second order. At a SNR of 12 dB the sinuosids are completely resolved with sharp peaks. At a SNR of 3.5 dB the peaks begin to merge and at 0 dB the peaks become a single ridge making it difficult to predict that there are two sinusoids. The phase obtained by this method however remains essentially constant for all of the signal-to-noise values. A contour plot of the phase is shown for the 0 dB case again illustrating its slowly varying character in the region around the two sinusoids.

4.3 Estimation of More General Spectra

This section contains two additional examples of multichannel 2-D spectrum analysis involving simulated data. These cases were designed to test the accuracy of estimating a linear phase term in the cross spectrum and the ability to estimate parameters of a known 2-D random process from data. The latter is closely related to the 2-D linear system identification problem, since a linear system can be identified by driving it with white noise and then estimating the cross spectrum between input and output.

4.3.1 Estimation of Delay

For this experiment two channels of data were defined by

$$x_1(n_1, n_2) = w_1(n_1, n_2)$$
$$x_2(n_1, n_2) = \beta x_1(n_1 - d_1, n_1 - d_2) + w_2(n_1, n_2)$$

where W_1 and W_2 are two independent white noise processes. Spectrum estimates were generated and the slope of the phase of the cross spectrum was measured to estimate the delays d_1 and d_2. Fig. 4.11 shows the cross spectrum estimate that was obtained using a first order NSHP model for white noise term with unit variance and parameter values of $\beta = 0.5$, $d_1 = d_2 = 1$. The magnitude of the cross spectrum is constant and the phase shows a linear dependence with slope corresponding to $d_1 = d_2 = 1$. Thus the experimental result agrees precisely with the theory.

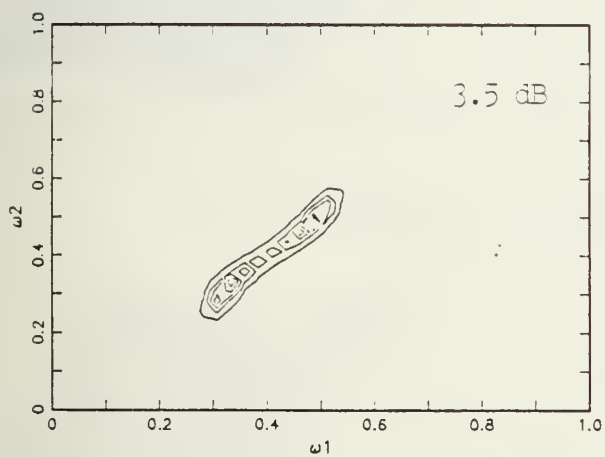### 4.3.2 Estimation of Parameters for a Linear Model

The goal of this experiment was to estimate the parameters of a known linear process from records of data generated by the process. The following multichannel 2-D
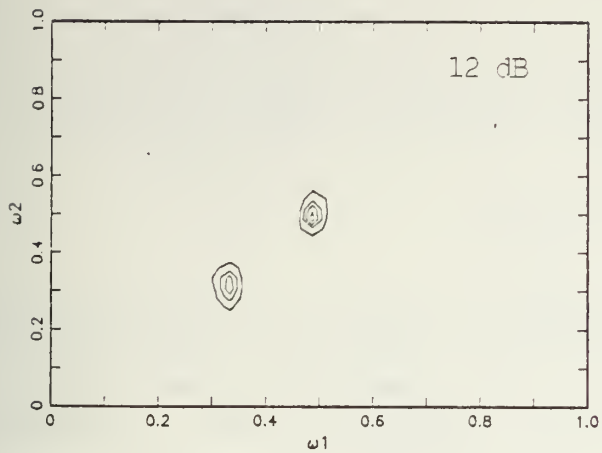
$\emptyset_1 = 1.0108$ rad

$\emptyset_2 = 0.9956$ rad

$\emptyset_1 = 1.0309$ rad

$\emptyset_2 = 0.9861$ rad
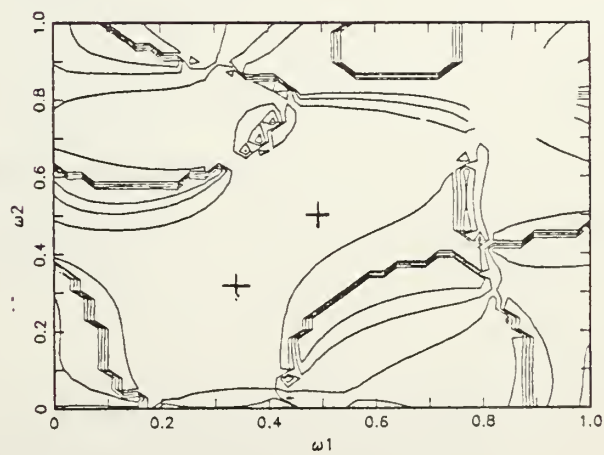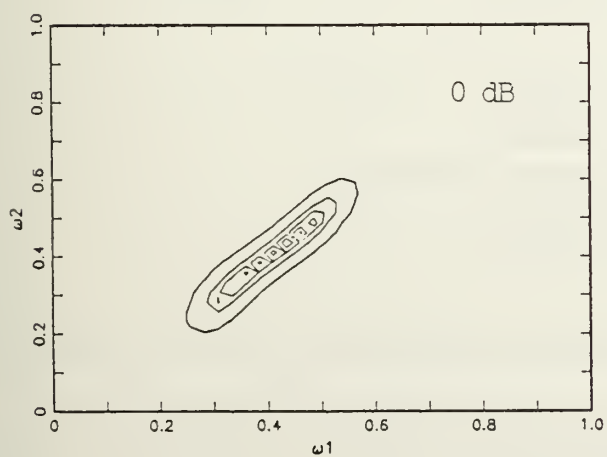
$\emptyset_1 = 1.0449$ rad

$\emptyset_2 = 0.9769$ rad

Figure 4.10   Signal/noise ratio experiments for cross spectrum.

S₁₂

S$_{12}$
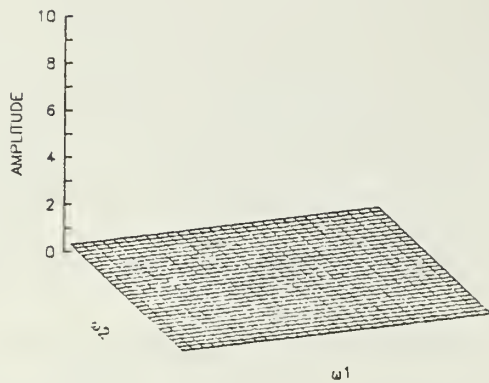
S$_{21}$

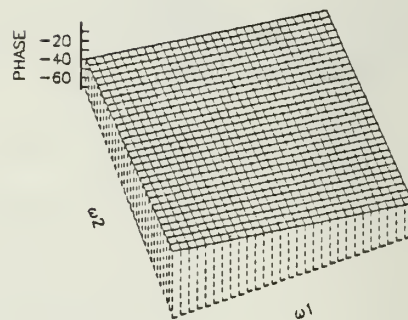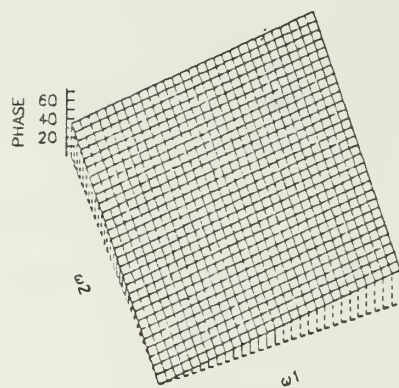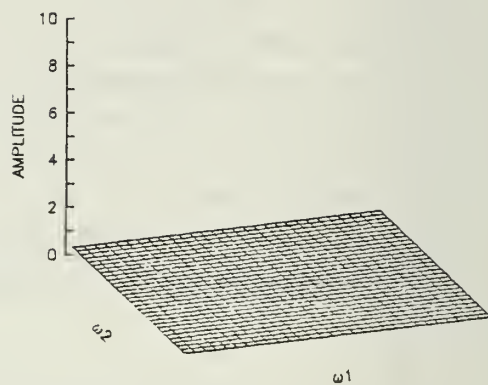Figure 4.11   Linear phase estimation.

process was simulated.

$$\begin{bmatrix} x_1(n_1,n_2) \\ x_2(n_1,n_2) \end{bmatrix} = \begin{bmatrix} 0.6 & 0 \\ 0.5 & 0 \end{bmatrix} \begin{bmatrix} x_1(n_1,n_2-1) \\ x_1(n_1,n_2-1) \end{bmatrix} + \begin{bmatrix} 0 & -0.7 \\ 0 & 0.4 \end{bmatrix} \begin{bmatrix} x_1(n_1-1,n_2) \\ x_2(n_1-1,n_2) \end{bmatrix}$$

$$+ \begin{bmatrix} \omega_1(n_1,n_2) \\ \omega_2(n_1,n_2) \end{bmatrix}$$

where: $w_i(n_1,n_2)$ $(i = 1,2)$ are two independent white noise signals. This process actually has support only in the first quadrant but a first order NSHP model was used to test the estimation procedure. For this problem one would expect the two matrix coefficients $A_{1,-1}$ and A_{11} to be small (near zero).

Table 4.1 shows the result of estimating the parameters with a 64 $\times$ 64 point data set. The estimates for the non-zero parameters of the model are close to the given values, and all of the remaining parameters but one are at least one order of magnitude smaller. The estimated spectrum components for this process are shown in Fig. 4.12. Energy is spread over a wide range of frequencies with concentration near higher values of ω_1 and lower values of ω_2. This is consistent with the signs of the terms in the defining equations for the process.

Table 4.1 Estimated parameters for a 1st order NSHP
model for a linear process.

$A_{0,0}$	1	0
	0	1
$A_{0,1}$	-0.56432	-0.027493
	-0.60426	-0.036813
$A_{1,-1}$	0.014809	-0.14316
	0.00057926	-0.022275
$A_{1,0}$	0.054647	0.58588
	-0.012384	-0.35247
A_{11}	0.017226	0.01443
	-0.0-3484	0.0055484

4.4 Comparison of Direct and Indirect Methods

The results described in the previous sections were based on algorithms that first estimate the 2-D matrix correlation function and then solve Normal equations to determine the AR model parameters. These methods will be called indirect since they
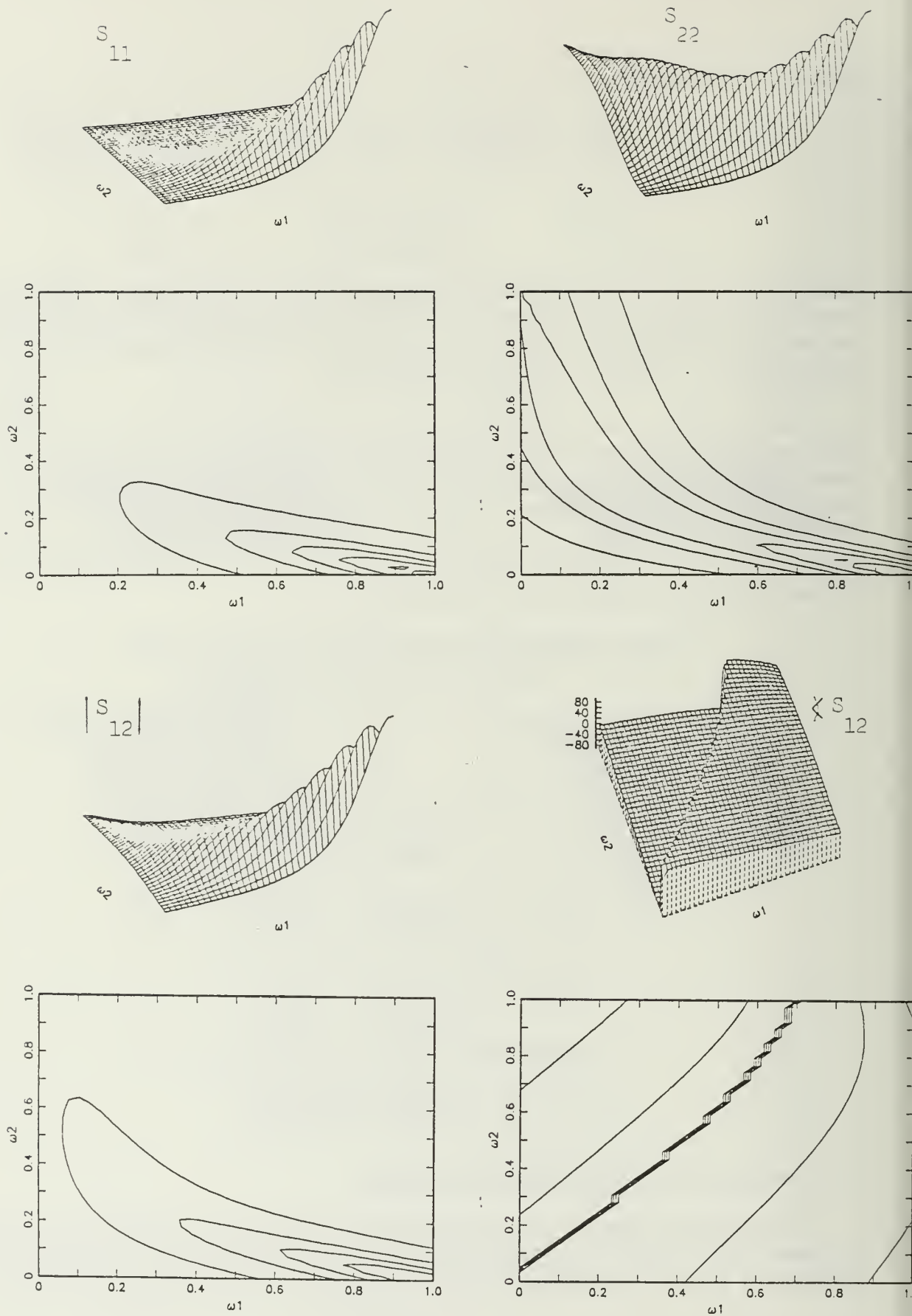
Figure 4.12 Estimated spectra for a multichannel 2-D linear process.

require estimation of the correlation function as a prerequisite to determining the model parameters. A direct method for estimating the model parameters, i.e., a method that estimates the parameters directly from the data was described in section 3.5. This method is very well suited to spectrum estimation using combined first and second quadrant models since it estimates both sets of filter parameters simultaneously. Although the direct method has not been exhaustively tested on all of the cases reported earlier, our initial results indicate that its estimates are at least comparable to and in some cases better than those of the indirect methods.

Figure 4.13 shows the results of estimating a single sinusoid in white noise using combined 2 × 2 point quadrant filters. These results are the same as the combined results shown in Fig. 4.7 but are depicted in a slightly different format. Fig. 4.14 shows the spectrum estimation results for the same data using the direct method of parameter estimation. The direct method yields a sharper peak with somewhat lower sidelobes. Estimates of the one radian phase shift between the channels are 1.05 rad. for the indirect method and 1.03 rad. for the direct method.

Figure 4.15 shows the results for estimating two sinusoids in white noise using combined 3 × 3 point quadrant filters with parameters estimated by the indirect method. These results are the same as those shown earlier in Fig. 4.8. Fig. 4.16 shows the results of the direct method applied to the same data. In this case the results appear to be nearly equivalent. A few minor peaks appear in both cases. For the indirect method these peaks appear closer to the main peak while for the direct method they appear further out. Phase estimates at the peak locations are 1.47 and 0.55 radians for the indirect method and 1.48 and 0.50 radians for the direct method. The values produced by the direct method are slightly closer to the true values of 1.5 and 0.5 radians.
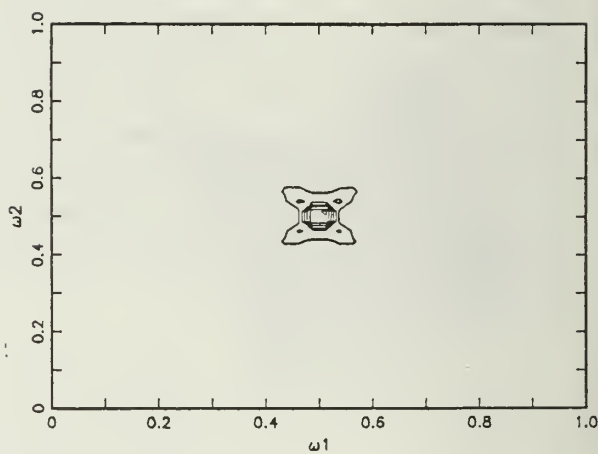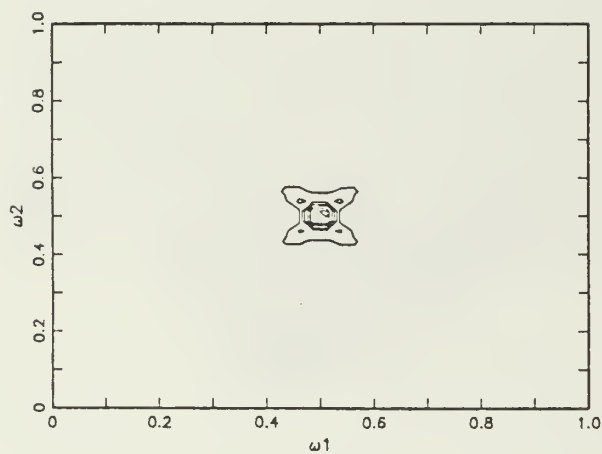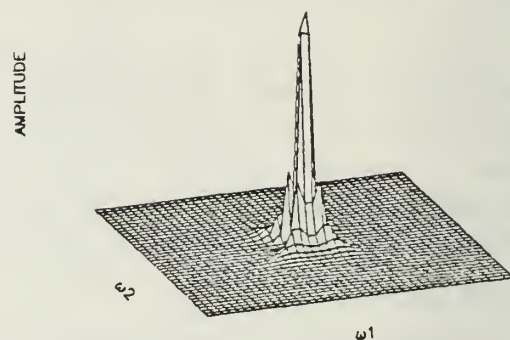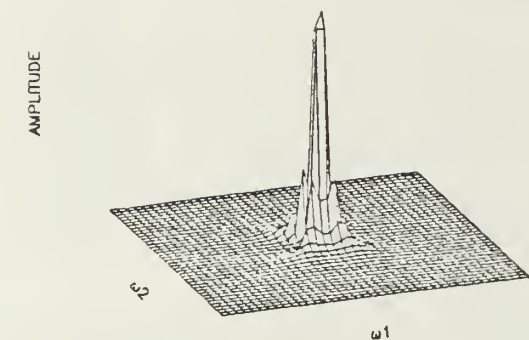
(a) S_{11} (b) S_{22}

Figure 4.13   Estimation of sinusoid in white noise;
indirect parameter estimation.
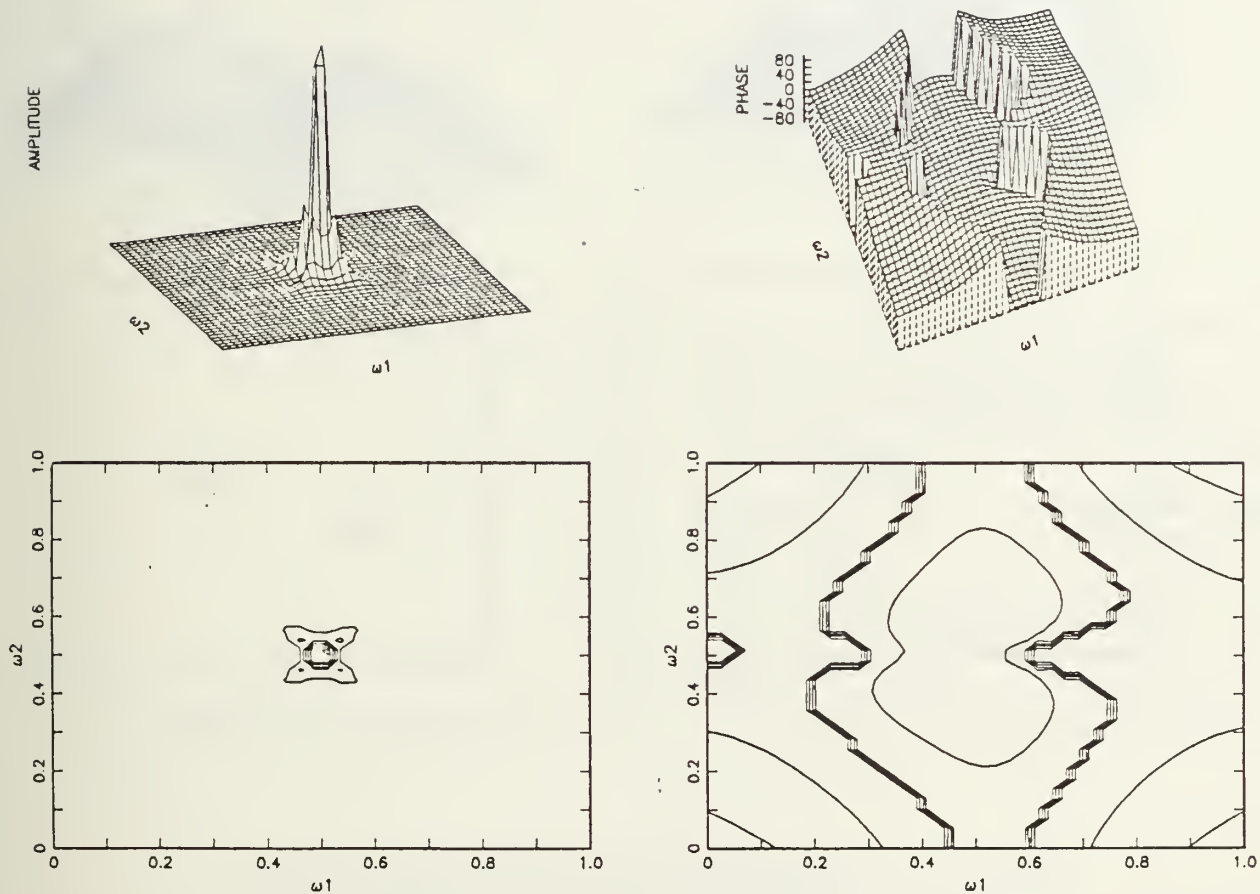
(c) S_{12}

Figure 4.13   Estimation of sinusoid in white noise;
indirect parameter estimation. (cont'd)

Figure 4.14   Estimation of sinusoid in white noise;
direct parameter estimation.

- 62-

(c) S_{12}

Figure 4.14   Estimation of sinusoid in white noise;
direct parameter estimation. (cont'd)

(a) S_{11} (b) S_{22}

Figure 4.15   Estimation of two sinusoids in white noise; indirect parameter estimation.

(c) S_{12}

Figure 4.15   Estimation of two sinusoids in white noise;
              indirect parameter estimation.   (cont'd)

Figure 4.16   Estimation of two sinusoids in white noise;
direct parameter estimation.

(c) S
     12

Figure 4.16   Estimation of two sinusoids in white noise;
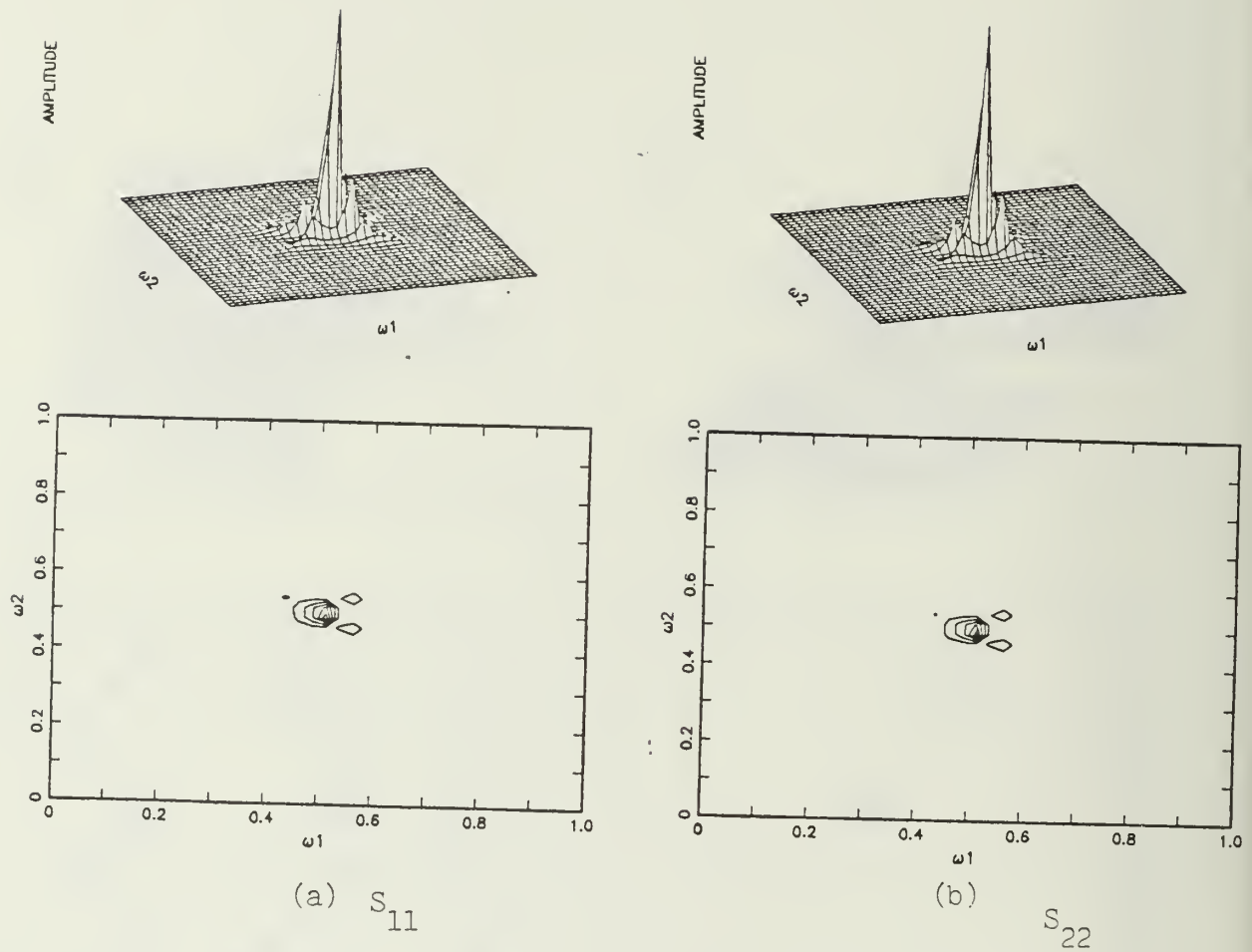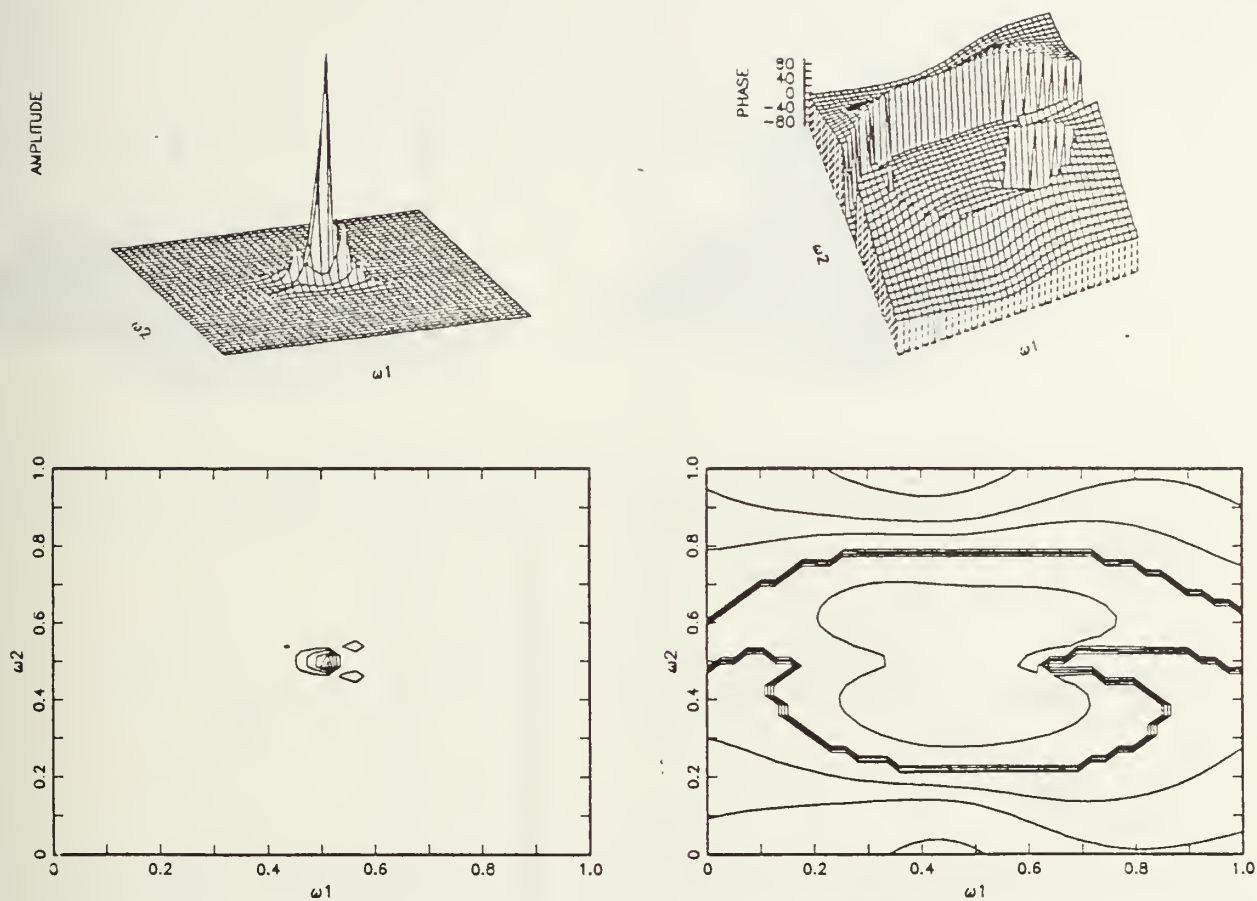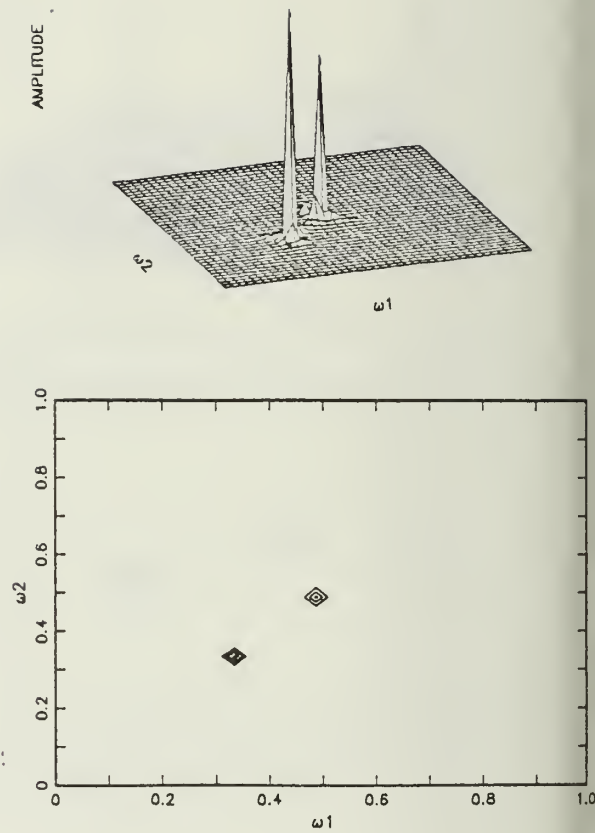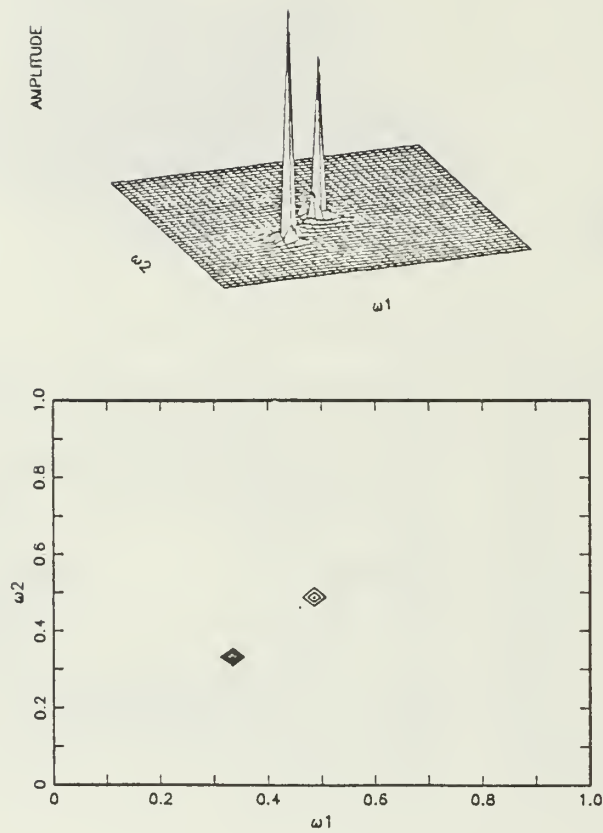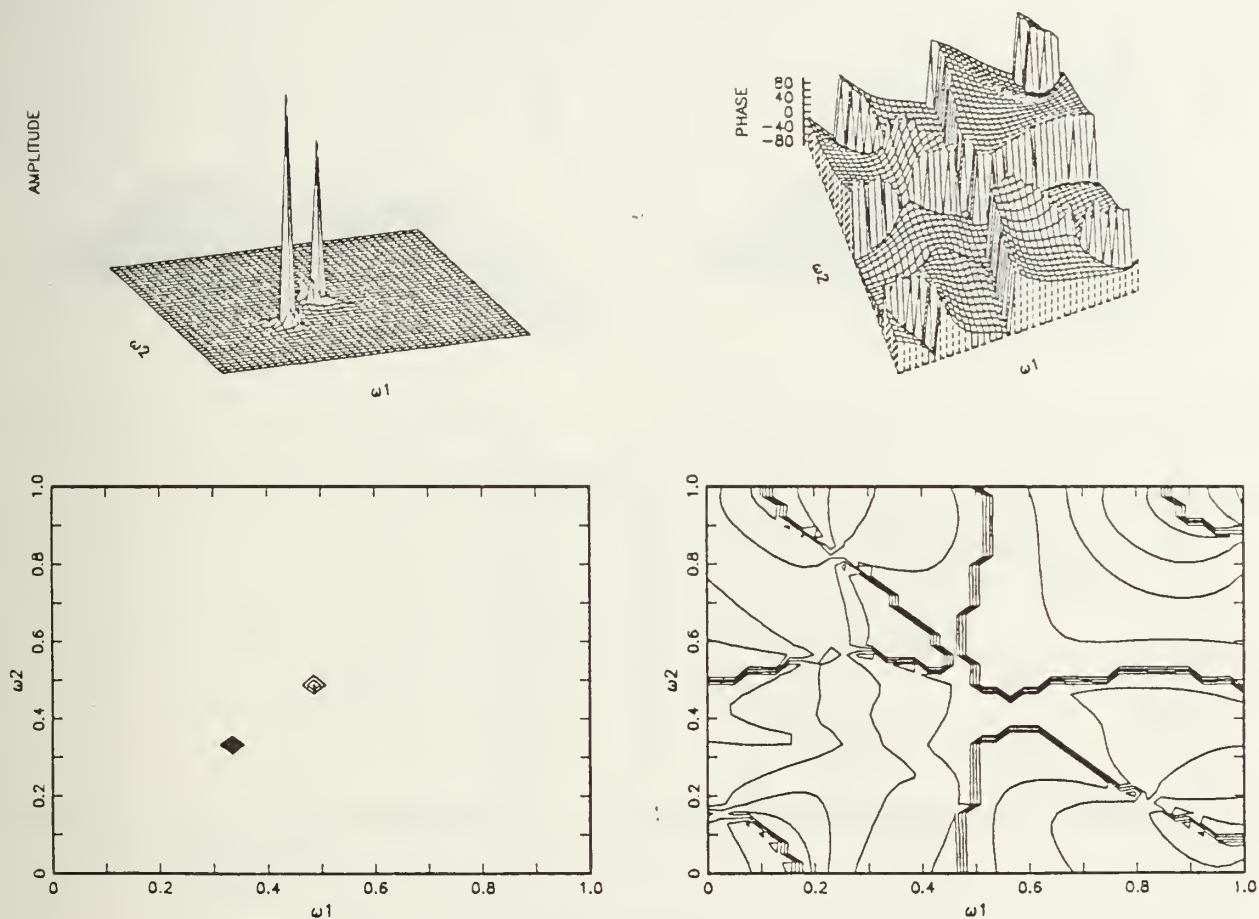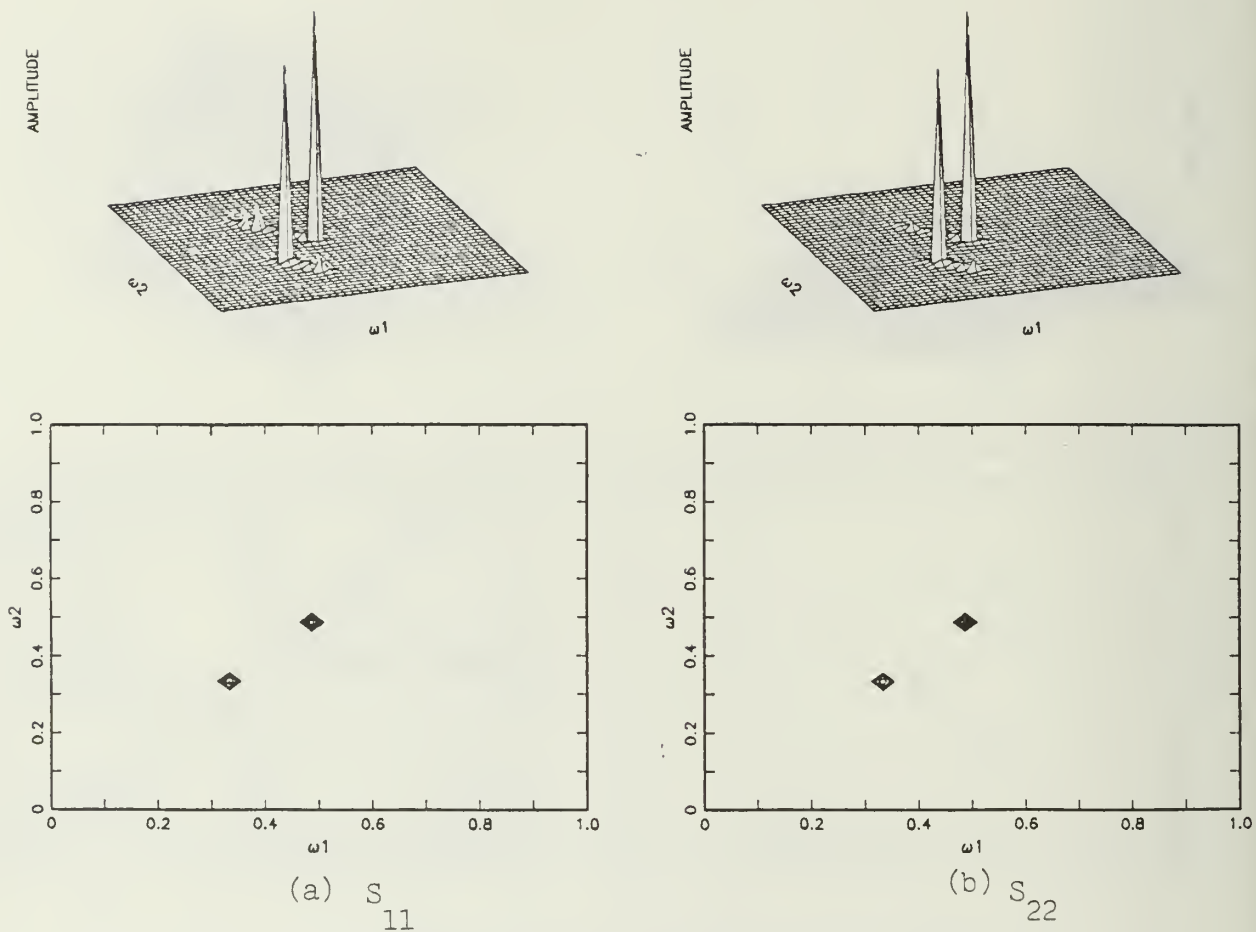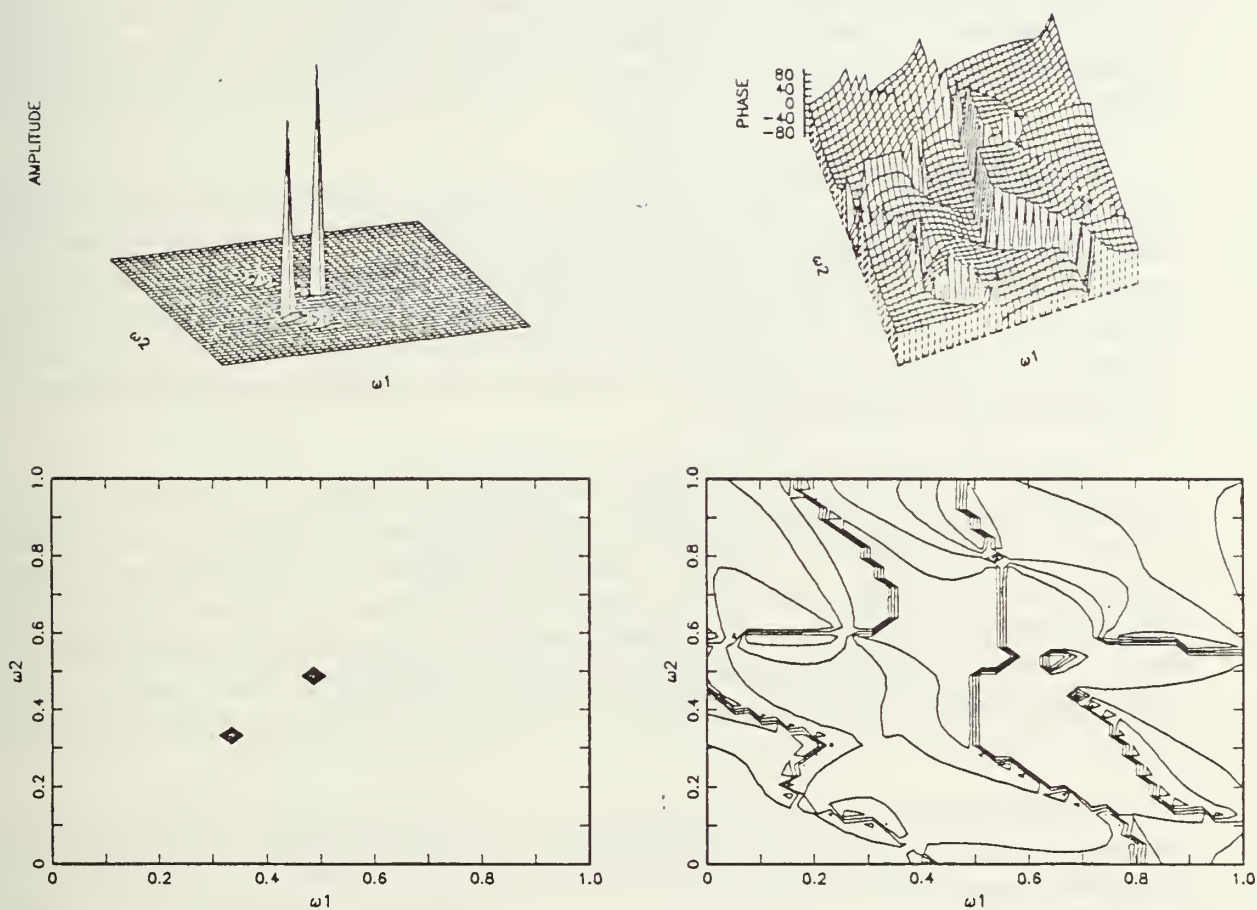   direct parameter estimation.   (cont'd)

V. Image Processing Applications

This chapter deals briefly with application of the theory of multichannel 2-D signals to image processing. Three applications are discussed namely, segmentation of color images, image coding, and image spectrum analysis.

5.1 Image Segmentation

This section describes an algorithm for image segmentation that uses a multichannel 2-D model to represent the images involved. This type of model works best for images involving multiple textures, such as aerial photographs of the ground in rural areas.

The application here will be to color or "false color" images (the latter are derived from images recorded on color infrared film). For these cases the multichannel 2-D signal has three components (M=3) corresponding to the red, green, and blue video signals (see Fig. 5.1). The same methods could be applied to image data from a multispectral scanning satellite that records data on four, seven, or even more IR channels. In this case the number of components M would be equal to the number of channels of scanner data employed.

It is assumed that regions with similar texture are defined by boundaries of corresponding pixels in each of the three color image components and that within each region the texture is described by a multichannel 2-D AR model. A superimposed Markov model characterizes the occurance of regions by specifying a form for the probability that a given pixel belongs to the region given that neighboring pixels belong to the same or other regions. The combination of the two models has been called a doubly stochastic image model in analogy with doubly stochastic models occuring in the study of point processes.

The doubly stochastic image model has been used in conjunction with monochrome images and single-channel AR models. Since many of the details of the algorithms are described in our earlier work [14] for monochrome images our description of the method here will be brief.

5.1.1 Segmentation Algorithm

The image to be segmented is assumed composed of several homogenous regions of texture. The red, green, and blue intensities are represented by the multichannel 2-D signal*

$$\mathbf{F}(n_1, n_2) = \begin{bmatrix} F_1(n_1, n_2) \\ F_2(n_1, n_2) \\ F_3(n_1, n_2) \end{bmatrix} \tag{5.1}$$

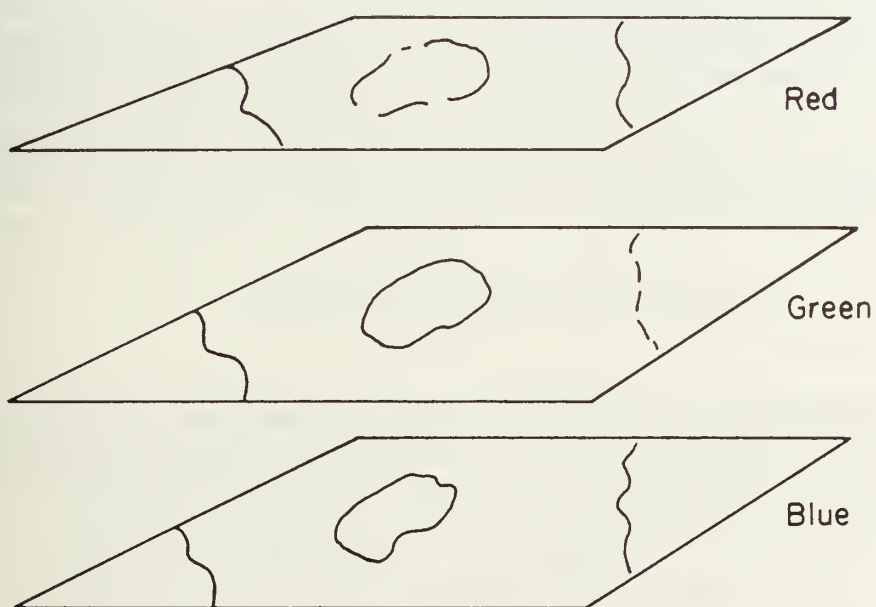* We use the notation $\mathbf{F}$ to represent an image to adhere to previous convention.

Fig. 5.1 Representation of a color image as a 3-channel 2-D random process.

and within a particular region this signal is generated by the AR model

$$\mathbf{F}'(n_1, n_2) = \sum_{i_1 i_2} A_{i_1 i_2} \mathbf{F}'(n_1 - i_1, n_2 - i_2) + \mathbf{W}(n_1, n_2) \qquad (5.2a)$$

$$\mathbf{F}(n_1, n_2) = \mathbf{F}'(n_1, n_2) + \boldsymbol{\mu} \qquad (5.2b)$$

where $\boldsymbol{\mu}$ is a constant mean vector. The white noise $\mathbf{W}(n_1, n_2)$ is described by a 3×3 spatially invariant covariance matrix

$$\Sigma_w = E\left[\mathbf{W}(n_1, n_2)\mathbf{W}^T(n_1, n_2)\right] \qquad (5.3)$$

which in general is not diagonal. A separate model of this type is formed for each of the image regions in which there is a different texture.

The essence of the segmentation algorithm is as follows. Using the models (5.2) and a Gaussian white noise source, we can form a probability density function for the set of all pixels in the color image conditioned on the regions. Assume that there are Q regions $\mathcal{R}_1, \mathcal{R}_2, \ldots, \mathcal{R}_Q$. Since the texture is independent from region to region, this density function can be written as

$$p(\mathbf{F}|\mathcal{R}_1, \mathcal{R}_2, \ldots, \mathcal{R}_Q) = \prod_{i=1}^{Q} p(\mathbf{F}|\mathcal{R}_i) \qquad (5.4)$$

where $p(\mathbf{F}|\mathcal{R}_i)$ represents the joint density for the pixels contained in region $\mathcal{R}_i$. Now assume that there is a way to represent the probability of occurence of a particular set of regions in the image $Pr[\mathcal{R}_1, \mathcal{R}_2, \ldots, \mathcal{R}_Q]$. Then Bayes's rule states that

$$Pr[\mathcal{R}_1, \mathcal{R}_2, \ldots, \mathcal{R}_Q|\mathbf{F}] = \frac{p(\mathbf{F}|\mathcal{R}_1\mathcal{R}_2, \ldots, \mathcal{R}_Q)\, Pr[\mathcal{R}_1, \mathcal{R}_2, \ldots \mathcal{R}_Q]}{p(\mathbf{F})}$$

Thus a maximum a posteriori (MAP) estimate for the regions can be obtained if the $\mathcal{R}_i$ are chosen to maximize

$$p(\mathbf{F}|\mathcal{R}_1, \mathcal{R}_2, \ldots \mathcal{R}_Q)\, Pr[\mathcal{R}_1, \mathcal{R}_2, \ldots \mathcal{R}_Q] \qquad (5.5)$$

Since the form of the probability density function for the white noise is known, the form of the density function for pixels within a given region can be obtained by transformation. The resulting image probability density function is most conveniently represented in terms of the errors of linear prediction which can be written as

$$\mathbf{E}(n_1, n_2) = \mathbf{F}'(n_1, n_2) - \sum_{i_1, i_2} A_{i_1 i_2} \mathbf{F}'(n_1 - i_1, n_2 - i_2) \qquad (5.6)$$

where the assumed constant mean level is subtracted out prior to applying (5.6). By using the linear model, the density function for pixels within a region $\mathcal{R}_i$ can be represented as

$$p\left(\mathbf{F}|\mathcal{R}_i\right) = \prod_{(n_1,n_2) \in R_i} p_{w_{k_i}}\left(\mathbf{E}(n_1,n_2)\right) \tag{5.7}$$

where $p_{w_{k_i}}$ is the probability density function for the white noise source of type k_i within region $\mathcal{R}_i$.

Now, suppose that an image has many regions, but that each region contains only one or another of two texture types. Then choosing a set of regions for the image is equivalent to labeling the pixels with labels 0 and 1. If an appropriate statistical model for the labels of the pixels exists then the prior probability $Pr\left[\mathcal{R}_1, \mathcal{R}_2, \ldots \mathcal{R}_Q\right]$ can be computed. This is the other ingredient needed to form the MAP estimate. An appropriate statistical model is one that represents a particular class of 2-D Markov processes [14, 15]. This model permits calculations of the desired prior probabilities.

Combination of the linear filtering model with the Markov model results in an algorithm to obtain a MAP region estimate. Since the resulting equations are of high dimension and nonlinear, a (possibly suboptimal) solution is obtained by iterating the conditions

$$\left[\mathbf{E}^{(0)}\left(n_1,n_2\right)\right]^T \left[\Sigma_{w_0}\right]^{-1} \mathbf{E}^{(0)}\left(n_1,n_2\right)$$

$$+ ln\left|\Sigma_{w_0}\right| - 2lnPr\left[0|S_{(n_1,n_2)}\right] \quad \begin{array}{c} 0 \\ < \\ > \\ 1 \end{array}$$

$$\left[\mathbf{E}^{(1)}\left(n_1,n_2\right)\right]^T \left[\Sigma_{w_1}\right]^{-1} \mathbf{E}^{(1)}\left(n_1,n_2\right)$$

$$+ ln\left|\Sigma_{w_1}\right| - 2lnPr\left[1|S_{(n_1,n_2)}\right] \tag{5.8}$$

which are derived from (5.4) through (5.7) and the Gaussian form of the density function. The terms $\mathbf{E}^{(0)}\left(n_1,n_2\right)$ and $\mathbf{E}^{(1)}\left(n_1,n_2\right)$ are the error terms at pixel (n_1,n_2) computed using the filters of type 0 and 1 respectively and Σ_{w_i} is the corresponding white noise covariance. The terms $Pr\left[0|S_{(n_1,n_2)}\right]$ and $Pr\left[1|S_{(n_1,n_2)}\right]$ are Markov transition probabilities representing the probability that the pixel at location (n_1,n_2) has label 0 or 1 given that a set of other pixels $S_{(n_1,n_2)}$ in the neighborhood has a prespecified set of labels. The inequality provides a rule for assigning pixel labels individually based on labels obtained at a previous iteration; the two expressions in (5.8) are evaluated and the pixel is given a label corresponding to the sense of the inequality.

5.1.2 Experimental Results

Results of applying the segmentation to color images are given here. Fig. 5.2(a) shows a 128 × 128-pixel color image representing an aerial photograph of the ground
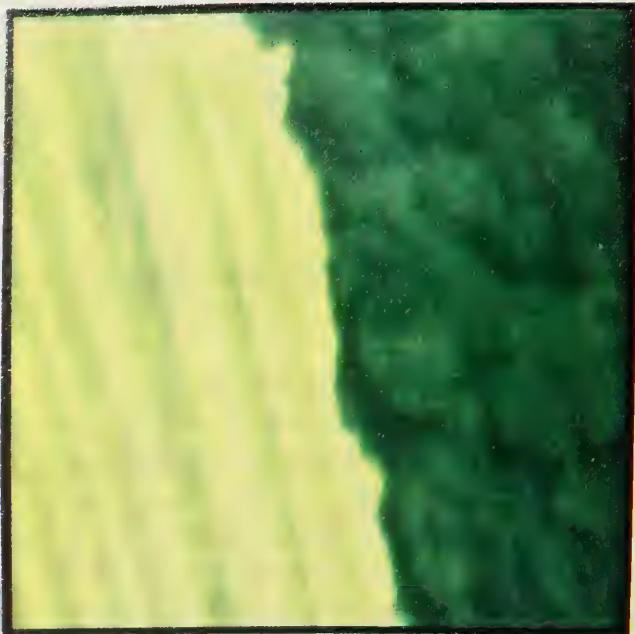
(a) color image

(b) red component

(c) green component

(d) blue component

Figure 5.2   Color image of trees and field.

in a rural area.* The green textured area is a grove of trees and the predominantly yellow area is a field with tall grass. Figs. 5.2(b) and (c) and (d) show the red, green, and blue components of the image. (The blue component is very dark and may not reproduce well.)

Figure 5.3 shows the results of segmentation of this image. The algorithm used 3-channel 2×2 first quadrant models for each of the two terrain types. The Markov model used a neighborhood size of 5×5. Note that attempts to segment this image based on color would have failed because the fields contain large linear patterns of green. The linear filtering models however match the colored texture in the image and result in a segmentation, that except for a few isolated pixels, is very accurate.

Figure 5.4(a) shows another color image of trees and a field. This image is somewhat more difficult to segment because the areas of green in the field do not appear as a linear pattern but are mixed in more homogeneously. Figure 5.4(b) shows the results of segmentation using image models similar to those used in the other example. Again, with the exception of some small areas the segmentation is quite accurate.

5.2 Image Coding

The models developed in this report can be applied to the coding of color or other multichannel images for purposes of storage or transmission. In this application, a model is formed for the image, the parameters of the model are stored or transmittted, and the model is used to reproduce the image. Two general schemes appear to be practical.

The first scheme is applicable when portions of an image each have a homogenous texture and one is concerned about reproducing only the general character of the texture and not the specific gray levels at each pixel. In this case a white noise-driven linear model can serve to characterize the image sufficiently so that only the parameters of the model need to be retained. This is analogous to the analysis-synthesis method for speech encoding [16]. In a practical application of the method, the image would first be segmented and the boundaries of the regions would be coded and retained. Within each region, a linear model could be formed for the image and the parameters (filter coefficients and noise covariance) would be estimated and retained. The image would be "decoded" by driving the filter for each region with white noise having the specified covariance and thus reproducing the image texture within that region.

The second scheme is quite general and would apply to any image. It is analogous to differential pulse code modulation (DPCM) in speech. A linear predictive filter is derived and applied to the image. The coefficients for the filter and the actual error residuals are retained and coded. Since there is usually great redundancy in a multichannel image the error residuals will tend to have low dynamic range and can

---

* Data courtesy of Rome Air Development Center, Griffiss AFB, N. Y.
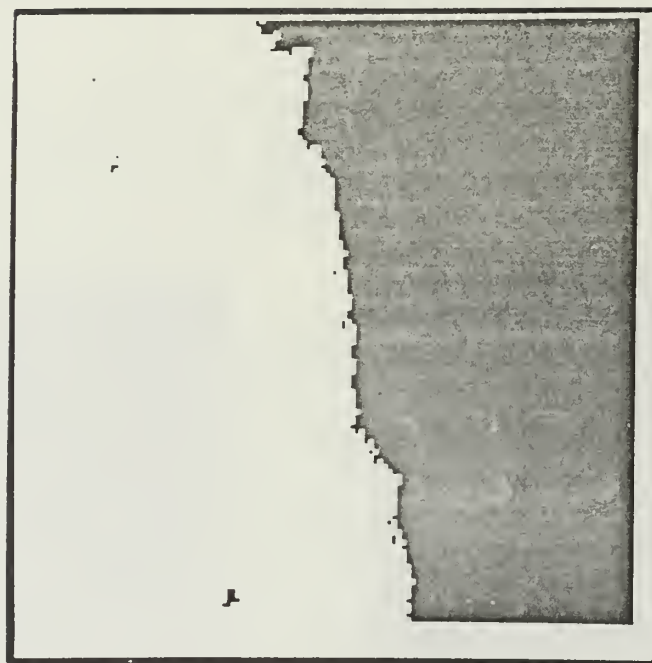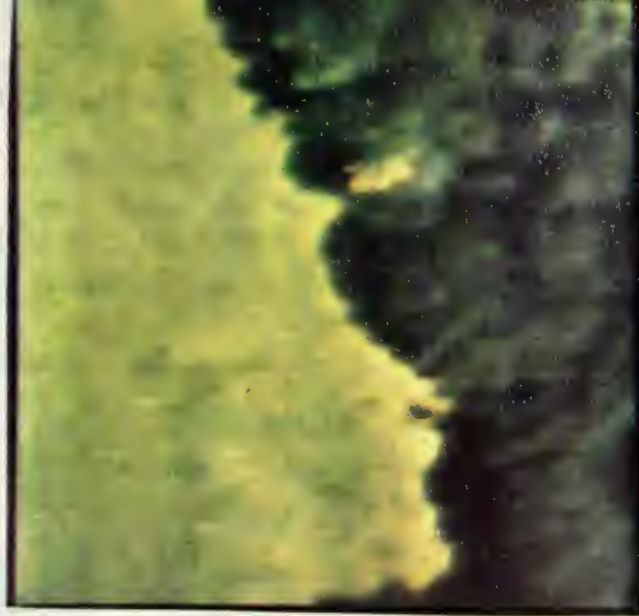
Figure 5.3   Segmentation of the tree-field color image.

(a) original color image

(b) segmentation

Figure 5.4 Color image of another area of
trees and field and segmentation.

therefore be coded with a fewer number of bits than the original image. The image is reproduced by inverse filtering using the decoded error residual as input to the filter.

The method just described is most effective when the linear predictive filter is well matched to the image being coded. Since one cannot expect that large general images will be well-represented by a linear filtering model, it is advisable to divide the image into small rectangular blocks and develop separate linear predictive filters for each block. Since the image within each block is usually more homogenous, one can expect that lower error residuals will be produced, resulting in more efficient coding.

DPCM methods have been developed and used in the coding of single images and image sequences. Their use for multichannel images using the linear predictive models discussed in this report would seem to be particularly effective.
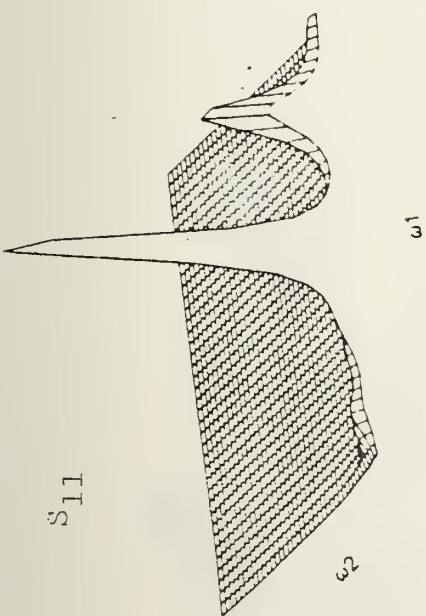
5.3 Image Spectrum Analysis

Spectra for portions of the color image of Fig. 5.2 were computed using the methods of Chapter IV. Only the red and green components were analyzed; these were designated as channel 1 and and channel 2 respectively.

Two portions of the image were selected: a 64×64-pixel section (one quarter of the image) in the lower left representing the field and a 64×64-pixel section in the upper right representing the trees. The signal index n_1 was taken as the horizontal direction and n_2 was taken as the vertical direction. The images showed distinct differences in their spectra which could be used as a basis for discrimination.
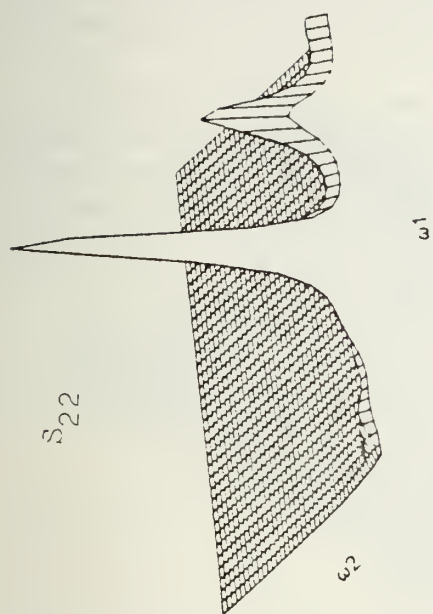
Fig. 5.5 shows the 2-D spectral components of the fields. The red, green, and magnitude of the cross spectrum appear to be very similar. Power is distributed in the middle and higher frequency ranges in the ω_1 direction and around zero frequency in the ω_2 direction. This power distribution can be attributed to the somewhat evenly spaced lines of green (perhaps some kind of plants) appearing in rows in the field. The phase of the cross spectrum seems to oscillate between approximately 10° and -40° in a more-or-less regular fashion.

Fig. 5.6 shows the estimated spectral component for the trees. Again, the red, green, and magnitude of the cross spectrum are very similar. The power tends to concentrate in a lower region of the ω_1 scale than the power for the fields with a peak occuring around $\pi/6$ corresponding to the spatial placement of the trees. The phase of the cross spectrum again varies between $+10^\circ$ and -40° but with somewhat milder oscillations.

The concentration of power around $\omega_2 = 0$ in the tree spectra at first seemed strange. One would expect that the tree image would show similar intensity variations in the horizontal and vertical directions and so the spectra should be more-or-less similar in the ω_1 and ω_2 directions. On closer examination it was found that the

S_{22}

(b) green spectrum

$\angle S_{12}$

(c) cross spectrum

S_{11}

(a) red spectrum

$|S_{12}|$
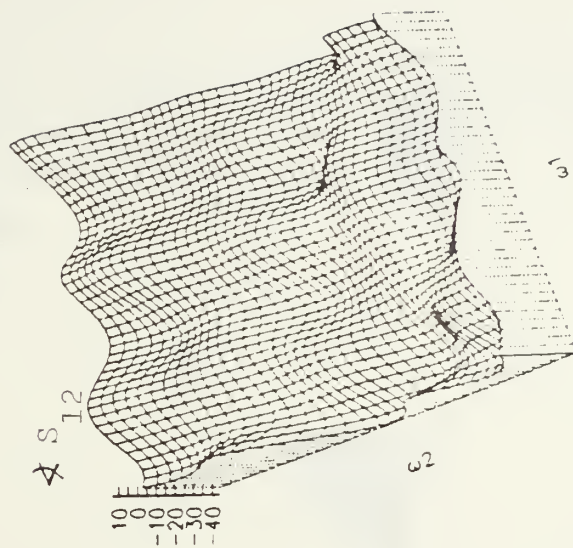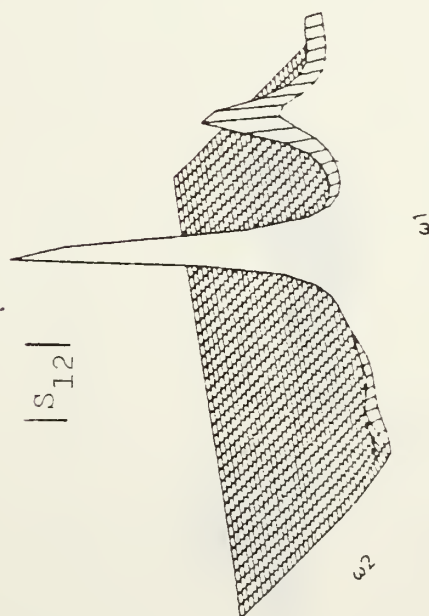
Fig. 5.5 Spectra for red and green components of the fields image.

S_{22}

(b) green spectrum

$\angle S_{12}$

$|S_{12}|$

S_{11}
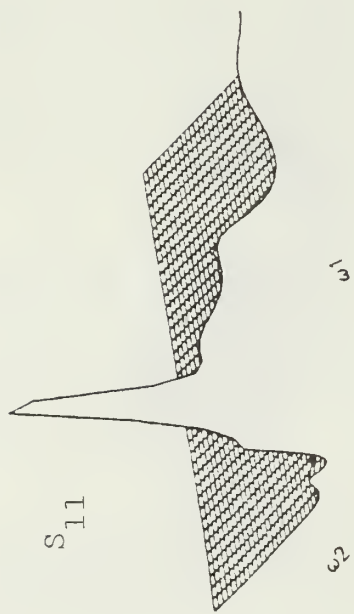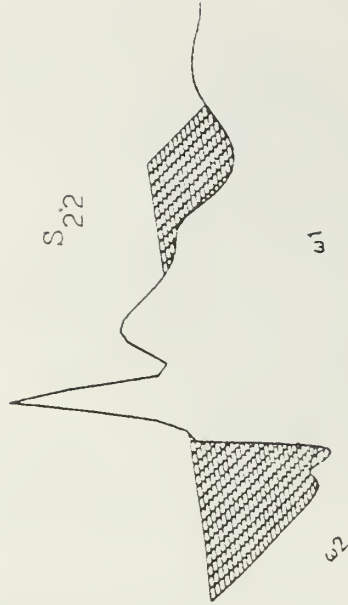
(a) red spectrum
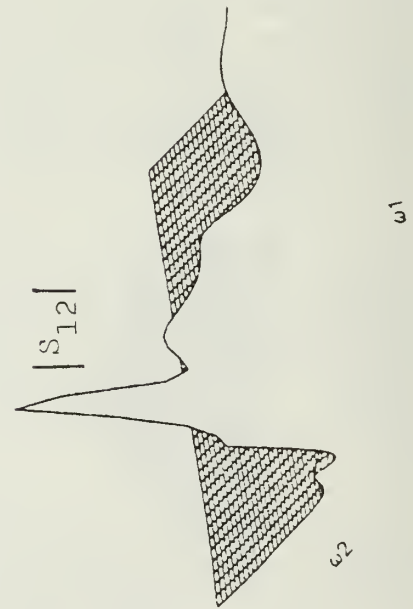
(c) cross spectrum

Fig. 5.6 Spectra for red and green components of the trees image.

image intensity variations for this data are <u>not</u> the same in both horizontal and vertical directions. Fig. 5.7 shows typical slices of the image in the n_1 and n_2 directions (we have examined several). The intensity exhibits rapid changes in the n_1 (horizontal) direction but shows a very slow change in the n_2 (vertical) direction. This accounts for the energy in the spectra being concentrated around $\omega_2 = 0$.

We can only guess a reason for this lack of symmetry in the tree image data. A plausible explanation is that a slight blurring of the image occurred due to the motion of the aircraft during the time at which the photograph was taken. This would have resulted in a lack of higher frequency detail in the direction of motion.

Fig. 5.7 Spatial variation of intensity in the trees image.

Image Intensity

VI. Conclusions

This report developed analysis methods for multichannel 2-D random signals. Although these signals could be considered as a special case of three-dimensional signals, the multichannel nature of their origin provides them with special properties that are not shared by multidimensional signals in general. A good example of this is the concept of phase of the cro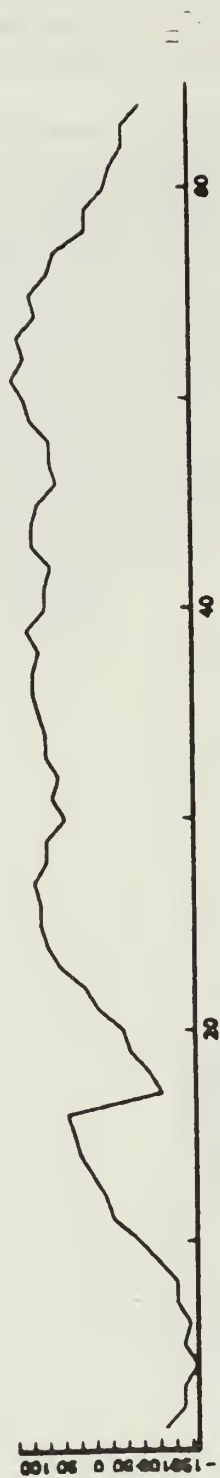ss spectrum. This idea seems natural when considering a multichannel 2-D signal but would have no counterpart in a 3-D analysis. While there has been a large body of research for two and three-dimensional signals, analysis methods specifically for multichannel 2-D signals have not heretofore been given much consideration.

A substantial part of the work in this report concentrated on 2-D linear prediction and autoregressive modeling. Concepts from the analysis of both single channel 2-D signals and multichannel 1-D signals were generalized in this development.

An important application of the signal modeling arises in spectrum analysis. The methods described in Chapter IV of this report showed how autoregressive models could be used to estimate the entire spectral matrix for multiple 2-D signals. Estimates are developed simultaneously for the autospectrum of each signal and the magnitude and phase of the cross spectra between the signals in each channel. Spectrum estimation for multichannel 2-D signals is the topic of a separate investigation [17] and many results in addition to those reported here have already been developed.

The application of the analysis methods to image processing was discussed briefly. Methods for image segmentation, image coding, and spectrum analysis were discussed in this report. Many further image processing applications such as enhancement filtering, target detection [18], and others seem possible.

While the report represents the results of a serious effort to develop and apply the theory of multiple 2-D random signals, the work is by no means complete. Several applications to image processing have already been mentioned and should be developed. In addition, the analysis of some types of radar and array data seem to be important applications of the spectrum analysis and modeling. Special sensors such as the laser radar [19] where the data collected represents intensity, range, and doppler in two-dimensions offer further opportunities for research.

By concentrating on linear prediction and AR modeling, we have looked at only a single (although rich) aspect of the analysis of multichannel 2-D signals. Other more general methods of modeling and estimation including pole-zero and noncausal modeling were not fully developed. Representation of the signals in other 'coordinate' systems by applying transformations between channels may lead to data reduction or other advantages in various applications. We hope not only to continue our work in this area but also, by publication of this report, to stimulate interest in the further analysis of multichannel two-dimensional signals.

Appendix A

Spectral Representation of Multichannel 2-D Random Processes

A stationary multichannel 2-D random process can be characterized in the frequency domain by a 2-D spectral matrix. The spectral matrix is defined by Eq. (2.20) of Chapter II and has the specific form

$$S_x(\omega_1,\omega_2) = \begin{bmatrix} S_{11}(\omega_1,\omega_2) & S_{12}(\omega_1,\omega_2) & \dots & S_{1M}(\omega_1,\omega_2) \\ \vdots & & & \\ S_{M1}(\omega_1,\omega_2) & S_{M2}(\omega_1,\omega_2) & \dots & S_{MM}(\omega_1,\omega_2) \end{bmatrix} \qquad (A.1)$$

where $S_{ij}(\omega_1,\omega_2)$ is the 2-D Fourier transform of $R_{ij}(k_1,k_2)$ the cross correlation between channels i and j. The spectral matrix is a periodic function of ω_1 and ω_2 with period 2π in each dimension and so it needs only to be considered only on the interval $-\pi \le \omega_1 \le \pi$ and $-\pi \le \omega_2 \le \pi$.

It follows from Eqs. (2.7a) and (2.11) that

$$S_x(\omega_1,\omega_2) = S_x^{*T}(\omega_1,\omega_2)$$

and thus the spectral matrix is Hermitian symmetric. In addition, since the components $R_{ii}(k_1,k_2)$ are positive definite functions, the diagonal terms $S_{ii}(\omega_1,\omega_2)$ which represent the 2-D power spectrum of each channel are non-negative. Cross spectral terms $S_{ij}(\omega_1,\omega_2)$ for $i \ne j$ are complex in general. However, since $R_{ij}(k_1,k_2)$ is <u>real</u> the magnitude of S_{ij} is an <u>even</u> function and the phase is an <u>odd</u> function of ω_1 and ω_2.

It is sometimes convenient to write the matrix of the squared magnitudes of the terms of S_x as

$$\begin{bmatrix} S_{11} & \dots & 0 \\ & \ddots & \\ 0 & \dots & S_{MM} \end{bmatrix} \begin{bmatrix} 1 & \kappa_{12}^2 & \dots & \kappa_{1M}^2 \\ \vdots & \vdots & & \vdots \\ \kappa_{M1}^2 & \kappa_{M2}^2 & \dots & 1 \end{bmatrix} \begin{bmatrix} S_{11} & \dots & 0 \\ & \ddots & \\ 0 & \dots & S_{MM} \end{bmatrix}$$

where the middle quantity is called the squared coherency matrix. It's elements are the <u>magnitude squared coherency</u> (MSC) between the ith and j^{th} channels and are defined as

$$\kappa_{ij}^2(\omega_1,\omega_2) = \frac{|S_{ij}(\omega_1,\omega_2)|^2}{S_{ii}(\omega_1,\omega_2)S_{jj}(\omega_1,\omega_2)} \qquad (A.2)$$

It follows from the properties discussed above that the matrix is real and symmetric, that is, $\kappa_{ij}(\omega_1,\omega_2) = \kappa_{ji}(\omega_1,\omega_2)$. The MSC measures the correlation between the the signals in channels i and j at frequencies ω_1 and ω_2. It is insensitive to spatial shifts between the signals in the two channels. These effects are manifested as phase in the cross spectrum.

Appendix B
Examples of Correlation Matrices

This appendix gives examples of the correlation matrices

$$\mathbf{R} = E\left[\underline{x}\,\underline{x}^T\right]$$

and

$$\mathbf{R}' = E\left[\underline{x}'\underline{x}'^T\right]$$

for index-ordered and component-ordered representations of a stationary multichannel 2-D signal. The examples are given for $N_1 = 3, N_2 = 4$, and $M = 2$. The terms $r_{ij}^{k\ell}$ appearing in the matrices are defined by

$$r_{ij}^{k\ell} = E\left[x_i(n_1, n_2)x_j(n_1 - k, n_2 - \ell)\right]$$

That is, $r_{ij}^{k\ell}$ is the element in the ith row and the jth column of the matrix correlation function $R(k, \ell)$ (see Eq. 2.6a).

$$R =$$

Note: $r_{ij}^{k\ell} = r_{ji}^{-k-\ell}$

The matrix is: Block Toeplitz but not block symmetric, has block Toeplitz (but not block symmetric) blocks. The sub-blocks are symmetric but not Toeplitz in general.

Figure B.1   Index-ordered correlation matrix $N_1 = 3$, $N_2 = 4$, $M = 2$.

$$R' =$$

Block (1,1), top-left:

$$
\begin{array}{cccc|cc}
r_{11}^{00} & r_{11}^{0-1} & r_{11}^{0-2} & r_{11}^{0-3} & r_{11}^{10} & r_{11}^{1-1} \cdots \\
r_{11}^{01} & r_{11}^{00} & r_{11}^{0-1} & r_{11}^{0-2} & r_{11}^{11} & r_{11}^{10} \\
r_{11}^{02} & r_{11}^{01} & r_{11}^{00} & r_{11}^{0-1} & \vdots \\
r_{11}^{03} & r_{11}^{02} & r_{11}^{01} & r_{11}^{00} &
\end{array}
$$

Block (1,2), upper-right:

$$
\begin{array}{cc}
r_{12}^{00} & r_{12}^{0-1} \\
r_{12}^{01} & r_{12}^{00} \\
& \ddots
\end{array}
$$

Second row of major blocks:

$$
\begin{array}{cccc|cccc}
r_{11}^{10} & r_{11}^{1-1} & r_{11}^{1-2} & r_{11}^{1-3} & r_{11}^{00} & r_{11}^{0-1} & r_{11}^{0-2} & r_{11}^{0-3} \\
r_{11}^{11} & r_{11}^{10} & r_{11}^{1-1} & r_{11}^{1-2} & r_{11}^{01} & r_{11}^{00} & r_{11}^{0-1} & r_{11}^{0-2} \\
r_{11}^{12} & r_{11}^{11} & r_{11}^{10} & r_{11}^{1-1} & r_{11}^{02} & r_{11}^{01} & r_{11}^{00} & r_{11}^{0-1} \\
r_{11}^{13} & r_{11}^{12} & r_{11}^{11} & r_{11}^{10} & r_{11}^{03} & r_{11}^{02} & r_{11}^{01} & r_{11}^{00}
\end{array}
$$

Third block:

$$
\begin{array}{cccc}
r_{11}^{10} & r_{11}^{1-1} & r_{11}^{1-2} & r_{11}^{1-3} \\
r_{11}^{11} & r_{11}^{10} & r_{11}^{1-1} & r_{11}^{1-2} \\
r_{11}^{12} & r_{11}^{11} & r_{11}^{10} & r_{11}^{1-1} \\
r_{11}^{13} & r_{11}^{12} & r_{11}^{11} & r_{11}^{10}
\end{array}
$$

Lower-left block (2,1):

$$
\begin{array}{cc}
r_{21}^{00} & r_{21}^{0-1} \\
r_{21}^{01} & r_{21}^{00} \\
& \ddots
\end{array}
$$

Lower-right block (2,2):

$$
\begin{array}{cc}
r_{22}^{00} & r_{22}^{0-1} \\
r_{22}^{01} & r_{22}^{00} \\
& \ddots
\end{array}
$$

Note: $r_{ij}^{k\ell} = r_{ji}^{-k-\ell}$

Each major block is identical except for underlined subscripts on r. The overall matrix is neither block Toeplitz nor block symmetric. Major blocks are block Toeplitz (but not block symmetric) with Toeplitz blocks.

Figure B.2   Component-ordered correlation matrix $N_1 = 3$, $N_2 = 4$, $M = 2$.

Appendix C
Direct Product of Matrices

The direct product or Kronecker product of matrices is an important notational operation in dealing with multidimensional signals. This appendix summarizes the most important properties of the direct product without proof. For a more thorough discussion see Ref. [20].

Given two matrices

$$A = \begin{bmatrix} a_{11} & a_{12} & \cdots & a_{1P} \\ \vdots & & & \\ a_{N1} & a_{N2} & & a_{NP} \end{bmatrix} \tag{C.1}$$

and

$$B = \begin{bmatrix} b_{11} & b_{12} & \cdots & b_{1Q} \\ \vdots & & & \\ b_{L1} & b_{L2} & \cdots & b_{LQ} \end{bmatrix} \tag{C.2}$$

the direct product $B \otimes A$ is defined as the partitioned matrix

$$B \otimes A = \begin{bmatrix} Ab_{11} & Ab_{12} & \cdots & Ab_{1Q} \\ \vdots & & & \\ Ab_{L1} & Ab_{L2} & \cdots & Ab_{LQ} \end{bmatrix} \tag{C.3}$$

If matrices A, C and B, D are conformable then some properties are as follows.

$$(B \otimes A)(D \otimes C) = BD \otimes AC \tag{C.4}$$

If A and B are square matrices $(N = P, L = Q)$ then

$$(B \otimes A)T = B^T \otimes A^T \tag{C.5}$$
$$tr(B \otimes A) = tr(B)tr(A) \tag{C.6}$$
$$|B \otimes A| = |B|^N |A|^L \tag{C.7}$$

Further if A and B are nonsingular then the direct product is nonsingular and

$$(B \otimes A)^{-1} = B^{-1} \otimes A^{-1} \tag{C.8}$$

Some further useful properties follow from the preceeding ones. If $\mathbf{\Lambda}, \mathbf{\Phi}$ and $\Theta, \mathbf{\Psi}$ are the eigenvalue and eigenvector matrices for B and A respectively, then $\mathbf{\Lambda} \otimes \Theta, \mathbf{\Phi} \otimes \mathbf{\Psi}$ are the eigenvalue and eigenvector matrices for $B \otimes A$. That is

$$(B \otimes A)(\mathbf{\Phi} \otimes \mathbf{\Psi}) = (\mathbf{\Phi} \otimes \mathbf{\Psi})(\mathbf{\Lambda} \otimes \Theta) \tag{C.9}$$

To state this another way, if ϕ_1 and ψ_j are eigenvectors of B and A corresponding to eigenvalues λ_i and θ_j then $\phi_i \otimes \psi_j$ is an eigenvector of $B \otimes A$ corresponding to eigenvalue $\lambda_i \theta_j$. That is,

$$(B \otimes A) \cdot (\phi_i \otimes \psi_j) = \lambda_i \theta_j (\phi_i \otimes \psi_j) \qquad (C.10)$$

In addition if A and B are symmetric with a modified Cholesky decomposition

$$A = GDG^T$$

and

$$B = G'D'G'^T$$

where G and G' and unit lower triangular and D and D' are diagonal, then

$$(B \otimes A) = (G' \otimes G)(D' \otimes D)(G' \otimes G')^T \qquad (C.11)$$

Some further fundamental properties and cautions should be observed. It is clear from the definition that the direct product is associative, i.e.,

$$(C \otimes B) \otimes A = C \otimes (B \otimes A) \qquad (C.12)$$

In addition, the operation is distributive over addition:

$$(B + C) \otimes A = B \otimes A + C \otimes A \qquad (C.13)$$
$$A \otimes (B + C) = A \otimes B + A \otimes C \qquad (C.14)$$

However, the direct product is <u>not</u> commutative (in general $B \otimes A \neq A \otimes B$) and it is not distributive over ordinary matrix multiplication.

Appendix D

Multichannel Levinson Recursion and Burg Algorithm

Multichannel Levinson Recursion (1-D)

The multichannel Levinson recursion (also called the Levinson-Wiggins-Robinson (LWR) algorithm) deals with a linear prediction problem of the form (3.24) and solves the Normal equations (3.26). The associated backward prediction problem is

$$\hat{x}'_{n-N_1+1} = -\sum_{i=1}^{N_1-1} \left(\alpha^{(i)'}\right)^T \underline{x}_{n-N_1+1+i} \tag{3.24}'$$

and leads to the Normal equations*

$$\underset{\sim}{R}\alpha'P_1 = \underset{\sim}{R}\begin{bmatrix} I \\ \alpha^{(1)'} \\ \vdots \\ \alpha^{(P_1-1)'} \end{bmatrix} = \begin{bmatrix} E'_{P_1} \\ 0 \\ \vdots \\ 0 \end{bmatrix} \tag{3.26}'$$

where $\alpha^{(i)'}$ has a form analogous to (3.25). The recursion is specified by the following set of equations.

$$\Delta_i = [R^T(1) \quad R^T(2) \quad \ldots \quad R^T(i)]\,\tilde{\alpha}_{i-1} \tag{D.1a}$$

$$\Delta'_i = \Delta_i^T = [R(1) \quad R(2) \quad \ldots \quad R(i)]\,\tilde{\alpha}'_{i-1} \tag{D.1b}$$

$$\Gamma_i = \left(E'_{i-1}\right)^{-1}\Delta_i \tag{D.2a}$$

$$\Gamma'_i = E_{i-1}^{-1}\Delta_i^T \tag{D.2b}$$

$$\alpha_i = \begin{bmatrix} \alpha_{i-1} \\ \ldots \\ 0 \end{bmatrix} - \begin{bmatrix} 0 \\ \ldots \\ \tilde{\alpha}'_{i-1} \end{bmatrix}\Gamma_i \tag{D.3a}$$

$$\alpha'_i = \begin{bmatrix} \alpha'_{i-1} \\ \ldots \\ 0 \end{bmatrix} - \begin{bmatrix} 0 \\ \ldots \\ \tilde{\alpha}_{i-1} \end{bmatrix}\Gamma'_i \tag{D.3b}$$

$$E_i = E_{i-1}\left(I - \Gamma'_i\Gamma_i\right) \tag{D.4a}$$

$$E'_i = E'_{i-1}\left(I - \Gamma_i\Gamma'_i\right) \tag{D.4b}$$

---

* Note that $\sim$ denotes second level block reversal.

The terms $\mathbf{\Gamma}_i$ and $\mathbf{\Gamma}'_i$ are the forward and backward reflection coefficient or partial correlation matrices. The term $\mathbf{\Delta}_i$ ($\mathbf{\Delta}'_i$) can be interpreted as a cross correlation between the forward (backward) prediction error and the one unit delayed, backward (forward) prediction error. Eqs. (D.1) – (D.4) are applied recursively beginning with $i = 1$ and ending with $i = P_1 - 1$.

Multichannel Burg Algorithm

This multichannel form of the Burg algorithm was developed by Nuttal [10] and Strand [11]. The procedure centers around estimating the terms $\mathbf{\Delta}_i$ and $\mathbf{\Delta}'_i$ of the multichannel Levinson recursion directly from the data. Then the rest of the equations (D.2) – (D.4) can be applied without modification.

Define the forward and backward error terms for the 1-D multichannel linear prediction problem as

$$\underline{e}_n^{(i)} = \underline{x}_n - \hat{\underline{x}}_n = \alpha_i^T \tilde{\underline{x}} \qquad (D.5a)$$

$$\underline{e}_n''^{(i)} = \underline{x}_{n-i+1} - \hat{\underline{x}}'_{n-i+1} = \alpha_i'^T \underline{x} \qquad (D.5b)$$

From these definitions and Eqs. (D.3) it can be seen that the errors satisfy the recursion

$$\underline{e}_n^{(i)} = \underline{e}_n^{(i-1)} - \mathbf{\Gamma}_i^T \underline{e}_n'^{(i-1)} \qquad (D.6a)$$

$$\underline{e}_n'^{(i)} = \underline{e}_{n+1}'^{(i)} - \mathbf{\Gamma}_i'^T \underline{e}_{n+1}^{(i)} \qquad (D.66)$$

The recursion is sustained by defining

$$\mathbf{D} = \frac{1}{N_P} \sum_{n=1}^{N_P} \underline{e}_n^{(i)} \left(\underline{e}_n^{(i)} \right)^T \qquad (D.7a)$$

$$\mathbf{B} = \frac{1}{N_P} \sum_{n=1}^{N_P} \underline{e}_n'^{(i)} \left(\underline{e}'^{(i)} \right)^T \qquad (D.7b)$$

$$\mathbf{G} = \frac{1}{N_P} \sum_{n=1}^{N_P} \underline{e}_n''^{(i)} \left(\underline{e}_n^{(i)} \right)^T \qquad (D.7c)$$

where N_P is the number of points in the data record minus the length of the filter. The matrix $\mathbf{\Delta}_i$ is then obtained as the solution of the bilinear equation

$$\mathbf{C}_1 \mathbf{\Delta}_i + \mathbf{\Delta}_i \mathbf{C}_2 = \mathbf{C}_3 \qquad (D.8)$$

where

$$\mathbf{C}_1 = (\mathbf{E}'_i)^{-1} \mathbf{B} \qquad (D.9a)$$

$$\mathbf{C}_2 = (\mathbf{E}_i)^{-1} \mathbf{D} \qquad (D.9b)$$

$$\mathbf{C}_3 = -2\mathbf{G} \qquad (D.9c)$$

There are several approaches to solving (D.8). One approach is to transform Δ_i into an equivalent vector representation by concatenating rows of the matrix into the MN_1-dimensional vector δ. The matrix C_3 is likewise transformed to a vector c_3. Equation (D.8) can then be written as

$$Q\delta = c_3 \qquad (D.10)$$

where

$$Q = C_1 \otimes I_M + I_M \otimes C_2^T \qquad (D.11)$$

where I_M is the $M \times M$ identity matrix. Eq. (D.10) can then be solved for δ.

References

[1] R.M. Haralick and G.L. Kelly, "Pattern Recognition with Measurement Space Spatial Clustering for Multiple Images," *Proceedings of the IEEE*, Vol. 57, No. 4, April 1969.

[2] B.R. Hunt and O. Kubler, "Karhunen-Loève Multispectral Image Restoration, Part I," *IEEE Trans. Acoustics, Speech, and Signal Processing*, Vol. ASSP-32, No. 3, June 1984.

[3] D.E. Dudgeon and R.M. Mersereau, *Multidimensional Digital Signal Processing* (Prentice-Hall, Englewood Cliffs, NJ, 1984).

[4] A. Papoulis, *Probablity, Random Variables and Stochastic Processes* (McGraw-Hill, New York, 1965).

[5] M.P. Ekstrom and J.W. Woods, "Two-Dimensional Spectral Factorization with Applications in Recursive Digital Filtering," *IEEE Trans. Acoustics, Speech, and Signal Processing*, Vol. ASSP-24, No. 2, pp. 115-128, April 1976.

[6] T.L. Marzetta, "A Linear Prediction Approach to Two- Dimensional Spectral Factorization and Spectral Estimation," Ph.D. Thesis, Dept. of Electrical Engineering and Computer Science, M.I.T. (Feb. 1978).

[7] C.W. Therrien, "Relations Between 2-D and Multichannel Linear Prediction," *IEEE Trans. Acoustics, Speech, and Signal Processing*, Vol. ASSP-29, No. 3, June 1981.

[8] C.W. Therrien, "Linear prediction for 2-D Vector Random Fields," Proc. 19th Asilomar Conference on Circuits, Systems, and Computers, Pacific Grove, CA., November 1985.

[9] J.P. Burg, "Maximum Entropy Spectral Analysis," Ph.D. Thesis, Dept. of Geophysics, Stanford University (May 1975).

[10] A.H. Nuttall, "Multivariate Linear Predictive Spectral Analysis Employing Weighted Forward and Backward Averaging: A Generalization of Burg's Algorithm," Naval Underwater System Center, New London, CT, NUSC Tech. Rep. 5501, Oct 1976.

[11] O.N. Strand, "Multichannel Complex Maximum Entropy (Autoregressive) Spectral Analysis," *IEEE Trans. on Automatic Control*, Vol. AC-22, No. 4, pp. 634-640, Aug. 1977.

[12] L.B. Jackson and H.C. Chien, "Frequency and Bearing Estimation by Two-Dimensional Linear Prediction," Proceedings 1st Int. Conf. on Accoustics, Speech and Signal Processing, Washington, DC, April 2-4, 1979, pp. 665-668.

[13] S.L. Marple and A.H. Nuttal, "Experimental Comparison of Three Multichannel Linear Prediction Spectral Estimators," *IEE Proc.*, Vol. 130, No. 3 (April 1983).

[14] C.W. Therrien, "An Estimation-Theoretic Approach to Terrain Image Segmentation," *Computer Vision, Graphics and Image Processing*, Vol. 22, No. 3, June 1983.

[15] J. Besag, "Spatial Interaction and Statistical Analysis of Lattice Systems," *Jo. Royal Statistical Society Ser. B*, Vol. 36, No. 2, pp. 192-236, 1974.

[16] M.L. Honig and D.G. Messerschmitt, *Adaptive Filters: Structures, Algorithms, and Applications*, (Kluwer, Boston, 1984).

[17] H. El Shaer, Dept. of Electrical and Computer Engineering, Naval Postgraduate School, Private Communication.

[18] C.W. Therrien, T.F. Quatieri, and D.E. Dudgeon, "Statistical Signal Models and Algorithms for Image Analysis," *Proc. IEEE*, Vol. 74, No. 4, pp 532-551, April, 1986.

[19] R.C. Harney and R.J. Hull, "Compact Infrared Radar Technology," Proc. Society of Photo-Optical Instrumentation Engineers, Vol. 227 - CO_2 Laser Devices and Applications, pp. 162- 168, Washington, D.C., April 1980.

[20] C.W. Therrien and K. Fukunaga "Properties of Separable Covariance Matrices and Their Associated Gaussian Random Processes, " *IEEE Trans. Pattern Anal. and Machine Intelligence*, Vol. PAMI-6, No.5, September 1984.

Principal Symbols

$\mathbf{x}(n_1, n_2)$	Multichannel 2-D signal
$x_m(n_1, n_2)$	Signal component
$\underline{x}, \underline{x}_n$	Signal vectors - index ordering
$\underline{x}', \underline{x}^m, \underline{x}_n^m$	Signal vectors - component ordering
$\mathbf{X}, \mathbf{X}_m$	Signal matrices
$A_{i_1 i_2}^T, B_{l_1 l_2}^T$	Coefficients of difference equation, filter coefficients
$H(l_1, l_2)$	Impulse response
$H_z(z_1, z_2)$	System function (z transform of impulse) response
$H_w(\omega_1, \omega_2)$	Frequency response (Fourier transform of impulse response)
$\mathbf{H}, \mathbf{H}(n_1)$	Matrix representation of impulse response
M	number of channels
$\mathbf{m}$	Mean for signal $\mathbf{x}$
$R_x(k_1, k_2)$, $R_{xy}(k_1, k_2)$	Correlation functions
$K_x(k_1, k_2), K_{xy}(k_1, k_2)$	Covariance functions
$S_x(\omega_1, \omega_2), S_{xy}(\omega_1, w_2)$	Power density spectra
$\kappa_x(\omega_1, \omega_2)$	Coherence function
$\underline{m}$	Mean vector , index ordering
$\underline{m}'$	Mean vector, component ordering
$\mathbf{R}, \mathbf{R}(n)$	Correlation matrix index ordering
$R', R_{n_1 n_2}, R_k^{n_1 n_2}$	Correlation matrix, component ordering
Σ_ϵ	Multichannel 2-D prediction error covariance matrix

DISTRIBUTION LIST

Mr. Fred Rahrig   1
Rome Air Development Ctr.
Griffiss AFB, NY 13441
Attn: IRRE

Dr. George Carayannopoulos   1
MIT Lincoln Laboratory
Room L-128
244 Wood Street
Lexington, MA 02173-0073

Dr. Dan Dudgeon   1
MIT Lincoln Laboratory
Group 21
244 Wood St.
Lexington, MA 02173-0073

Dr. Tom Quatieri   1
Room B-356
MIT Lincoln Lab.
Lexington, MA 02173-0073

Prof. Jae Lim   1
Dept. of Electrical Engineering
& Computer Science
Room 36-653
MIT
Cambridge, MA 02139

Prof. Bobby Hunt   1
Digital Image Analysis Lab
Dept. Computer & Electrical Engineering
University of Arizona
Tucson, AZ 85721

Dr. Steve Lang   1
Mail Stop MER-24-1583C
Sanders Associates
Nashua, NH 03061-2034

Dr. Larry Marple   1
Schlumberger Well Services
5000 Gulf Freeway
Houston, TX 77210-4594

Dr. Lonnie Wilson   1
Sig-Pro Systems, Inc.
22560 Murietta Rd.
Salinas, CA 93943

Dr. Phillip Fishman   1
MIT Lincoln Lab
Lexington, MA 02173-0073

Prof. John Diamesis   1
Meledron 4
Chalandri
Athens 15233 Greece

Dr. A. Nuttal   1
New London Lab
Naval Underwater Systems Center
New London, CT 06320

Dr. Tom Marzetta   1
Schlumberger-Doll Research
Old Quarry Road
P.O. Box 307
Ridgefield, CT 06877

Hamdy El-Shaer   1
Naval Postgraduate School
Code 62
Monterey, CA 93943

T. Kupeli   1
Naval Postgraduate School
Code 62
Monterey, CA 93943

Dr. S. R. Parker   1
Naval Postgraduate School
Code 62Px
Monterey, CA 93943

Dr. Paul Moose   1
Naval Postgraduate School
Code 62Me
Monterey, CA 939343

Prof. Peter Lewis   1
Naval Postgraduate School
Code 55Lw
Monterey, CA 93943

Prof. R. Cristi   1
Naval Postgraduate School
Code 62Cx
Monterey, CA 93943

Prof. R. Hippenstiel   1
Naval Postgraduate School
Code 62Hi
Monterey, CA 93943

Prof. H. Rigas   1
Naval Postgraduate School
Code 62Rr
Monterey, CA 93943

Prof. D. Kirk   1
Naval Postgraduate School
Code 62Ki
Monterey, CA 93943

Dr. Charles Therrien   20
Naval Postgraduate School
Code 62Ti
Monterey, CA 93943